MTL TR 90-21

AD

PROCESSING AND CHARACTERIZATION OF HIGH STRENGTH, HIGH DUCTILITY HADFIELD STEEL

JOHN F. CHINELLA
METALS RESEARCH BRANCH

April 1990

US ARMY
LABORATORY COMMAND
MATERIALS TECHNOLOGY LABORATORY

U.S. ARMY MATERIALS TECHNOLOGY LABORATORY
Watertown, Massachusetts 02172-0001

The findings in this report are not to be construed as an official Department of the Army position, unless so designated by other authorized documents.

Mention of any trade names or manufacturers in this report shall not be construed as advertising nor as an official indorsement or approval of such products or companies by the United States Government.

DISPOSITION INSTRUCTIONS

Destroy this report when it is no longer needed.
Do not return it to the originator.

UNCLASSIFIED

SECURITY CLASSIFICATION OF THIS PAGE (When Data Entered)

REPORT DOCUMENTATION PAGE		READ INSTRUCTIONS BEFORE COMPLETING FORM
1. REPORT NUMBER MTL TR 90-21	2. GOVT ACCESSION NO.	3. RECIPIENT'S CATALOG NUMBER
4. TITLE (and Subtitle) PROCESSING AND CHARACTERIZATION OF HIGH STRENGTH, HIGH DUCTILITY HADFIELD STEEL		5. TYPE OF REPORT & PERIOD COVERED Final Report 6. PERFORMING ORG. REPORT NUMBER
7. AUTHOR(s) John F. Chinella		8. CONTRACT OR GRANT NUMBER(s)
9. PERFORMING ORGANIZATION NAME AND ADDRESS U.S. Army Materials Technology Laboratory, Watertown, Massachusetts 02172-0001 SLCMT-EMM		10. PROGRAM ELEMENT, PROJECT, TASK AREA & WORK UNIT NUMBERS
11. CONTROLLING OFFICE NAME AND ADDRESS U.S. Army Laboratory Command 2800 Powder Mill Road Adelphi, Maryland 20783-1145		12. REPORT DATE April 1990 13. NUMBER OF PAGES 132
14. MONITORING AGENCY NAME & ADDRESS(if different from Controlling Office)		15. SECURITY CLASS. (of this report) Unclassified 15a. DECLASSIFICATION/DOWNGRADING SCHEDULE

16. DISTRIBUTION STATEMENT (of this Report)

Approved for public release; distribution unlimited.

17. DISTRIBUTION STATEMENT (of the abstract entered in Block 20, if different from Report)

18. SUPPLEMENTARY NOTES

Thesis submitted to Worcester Polytechnic Institute, Worcester, Massachusetts, in partial fulfillment of the requirements for the Degree of Master of Science in Materials Engineering, August 1989.

19. KEY WORDS (Continue on reverse side if necessary and identify by block number)

Austenitic steels, Stress-strain rate, Strain hardening,
Plastic flow, Microstructure, Deformation twins,
Yield strength, Thermomechanical processing,

20. ABSTRACT (Continue on reverse side if necessary and identify by block number)

(SEE REVERSE SIDE)

DD FORM 1 JAN 73 1473 EDITION OF 1 NOV 65 IS OBSOLETE

UNCLASSIFIED

SECURITY CLASSIFICATION OF THIS PAGE (When Data Entered)

Block No. 20

ABSTRACT

Hadfield steel plastic flow behavior is known by strain hardening without necking to high levels of strength and strain, and is described by upward curvature strain hardening with near-constant, near-linear strain hardening rates over large ranges of deformation temperature. This plastic flow behavior is valued for severe service applications, but Hadfield steel yield stress is low.

The purpose of this experimental study is to warm roll solution treated, Fe-12.5Mn-2.01Mo-1.15C Hadfield steel to high yield strength and to retain the valued characteristics of Hadfield steel plastic flow behavior. The objective of the study is to determine the effects of warm rolling on plastic flow behavior and microstructure of Hadfield steel.

Experimental plastic flow behavior is evaluated in tension from both engineering and true stress-strain behavior. The purpose of the study is met by material thermomechanically processed to provide high yield stress, moderate rates of increasing load or strain hardening, high true uniform strain and ultra-high true uniform stress.

The experimental stress-strain curves and microstructures suggest an influence of Hadfield steel deformation twins on plastic flow.

Preface

The study plan concept and general approach of processing was suggested by G.B. Olson, formerly a consultant at the U.S. Army Materials Technology Laboratory, Watertown, Massachusetts. Continuous cast ingot material was provided by M.R. Staker of the U. S. Army Materials Technology Laboratory.

This study is part of a present research-development effort by John F. Chinella, in progress at the U.S. Army Materials Technology Laboratory, Watertown MA. The purpose of the research effort is to increase strength and retain properties of strain hardening known in the solution treated condition of Hadfield steel.

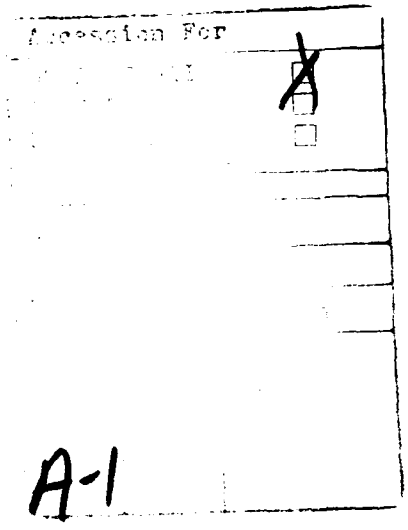

Table of Contents

APPENDIX

List Of Tables

List of Figures

1.0 Introduction

1.1 Purpose and Objective

Metastable, austenitic, Fe-Mn-C Hadfield steel in the soft solution treated condition, is known for its high toughness and high rate of strain hardening during deformation to high values of stress and strain [1,2]. Because strain hardening behavior of Hadfield steel is also distinguished by near-linear plastic strain hardening ($d\sigma/d\varepsilon$) rates that are nearly constant in slope at temperatures from -100 °C to +250 °C, the plastic flow behavior of Hadfield steel may be called temperature insensitive [3,4]. In severe service conditions, Hadfield steel's properties of high toughness and high ductility, combined with a high strain hardening rate of low temperature sensitivity, has enabled one of the first discovered steel alloys to remain competitive with many recently developed, modern alternative alloys.

The plastic flow behavior of Hadfield steel, described by high strain hardening to high levels of strength and strains, with near constant rates of strain hardening over large ranges of deformation temperature, is appropriate for many severe service applications. One disadvantage of Hadfield steel however, is low yield stress in the soft solution treated condition.

The purpose of this research is to warm roll Hadfield steel to high values of yield strength, and retain the desireable plastic flow characteristics of soft, low strength, solution treated Hadfield steel. The study objective is to determine the effects of warm rolling on plastic flow behavior and microstructure of Hadfield steel.

1.2 Characteristics of Solution Treated Hadfield Steel

Austenitic Fe-Mn-C steel, called Hadfield steel after its inventor, is a tough, non-magnetic alloy useful for severe service against impact and abrasion [1,2]. The standard Hadfield steel processing method of solution treatment includes holding at temperatures between 1000 °C to 1090 °C for 1 to 2 hours, and water quenching to obtain a soft and tough metastable austenitic solid solution alloy that strain hardens during deformation [2]. When processed by the typical method of casting or forging to shape, followed by solution treatment, Hadfield steel typically work hardens as shown in Figure 1, from a yield stress of 40-60 ksi to 100-130 ksi ultimate tensile stress with about 50% uniform elongation before necking and fracture. The normal service temperature of solution treated Hadfield steel includes temperatures of -100 °C to

+205 °C where Hadfield steel has excellent properties of toughness and ductility in comparison to ferritic steels. During impact abrasion, Hadfield steel hardens to resist wear while still retaining high core toughness at small distances from wear surfaces, so that typical applications of Hadfield steels have been in mining, railway, and heavy industry. Military applications have included personnel armor and non-magnetic steel components for naval vessels.

The most common composition range of Hadfield steel includes Fe, 14.00-11.00% Mn and 1.35-1.05% C as specified by ASTM A-128 grade A shown in Table 1. In order to achieve values of high yield and ultimate tensile strengths shown in Table 2 and to resist the embrittlement caused by $(FeMn)_3C$ carbide transformation during welding, modified Hadfield grades that include 1.0-2.1 percent molybdenum have been developed [2,5]. The molybdenum modified grade, ASTM A 128-E2, has been used in this study for achievement of high strength from warm rolling, and for achievement of high ultimate strength in service.

Fe-Mn-C Hadfield steel reaches its optimal properties of combined toughness, strength, abrasion resistance, and ductility at a composition of approximately Fe-12.5Mn-1.2C [2]. The most essential factor that may influence plastic flow behavior and abrasive resistance behavior in metastable, austenitic Hadfield steel [2,5,6], as in many other steels [7], is carbon content. As carbon content is increased above 1.1% it is more difficult to retain carbon in solution during solution treatment and quenching and this can account for reduced ductility and strength from incomplete solution treatment and primary carbides [1,2].

High carbon content in Hadfield steel may contribute high hardening [2,4,5] during deformation and abrasion of solution treated Hadfield steel, but it also provides an opportunity for strain enhanced carbide precipitation and possibly embrittlement during warm rolling [5]. This carbide precipitation occurs initially at grain boundaries during reheating and is enhanced by prior strain. Carbides and inclusions are well known to be related to void coalescence and growth fracture [2,8], and in the case of Hadfield steel, when void nucleation is related to a introduction of a softening mechanism at low strains and fracture, deformation will not fully develop strain hardening at high strains. Solution treatment slack quenching, or warm roll reheating, may initiate grain boundary carbide precipitation in high carbon content Hadfield steel resulting in the introduction of a grain boundary void nucleation softening mechanism leading to plastic instability and mechanical properties of low strain and low strength [1,2].

Not only high, but low carbon contents may cause processing difficulties and poor mechanical behavior and plastic flow properties. Decarburization of surfaces during solution treatments and forging yields metastable austenitic steels of low carbon content that can easily transform to martensite [6], and that have undesirable brittle mechanical properties in comparison to the standard grade Hadfield steel that remains fully austenitic during strain to -196 °C.

Although low ductility and early fracture in Hadfield steel has been related to high carbon content and associated carbide precipitation [1,2,5], several approaches have been successfully used to prevent carbide induced fracture. One approach is to lower carbon content to 1.00-0.80% and sacrifice strength for greater carbon solubility during heat treatment and reheating [2,5]. Another approach that has been used is the addition of 2.00-1.00% Mo with or without a reduced carbon content. The molybdenum modified grades show improved resistance to carbide precipitation, and in low carbon grades the Mo addition can compensate for loss of strength from low carbon content [2,5].

Since carbide precipitation is a thermally activated process dependent on time and temperature, warm rolling techniques that reduce time at temperature could reduce the possibility of strain enhanced carbide formation. In particular, more rapid heatup or quench rates, and high warm roll reductions are some processing techniques that could be used to reduce time at temperature in the experimental approach. High reductions could also be beneficial by favoring elevated temperature, strain-induced defect hardening mechanisms over time-temperature dependent strengthening mechanisms. By using high reductions, warm roll strengthened structures could be inherited directly from strain induced defect structures and little opportunity for thermally activated interface growth or diffusion would be available.

2.0 Background Review

2.1 Strain Hardening Mechanisms in Hadfield steel

The exact mechanism of work hardening that occurs in Hadfield steel has remained controversial for more than one hundred years after its discovery in 1882, only becoming better understood after the advent of electron microscopy allowed phase and microstructural identification possible. After the discovery of fcc deformation twinning (in pure copper) by Blewitt in 1957, research was stimulated in the role of deformation twinning on the plastic flow behavior in fcc alloys [9]. Most recent studies of Hadfield steel [4,10-13] have observed and identified deformation twinned microstructures in Hadfield steel. Many of these studies, most notably Adler, Olson, and Owen [4], have suggested or advocated that Hadfield steel deformation twins influence plastic flow and work hardening behavior in a similar manner as other alloys that deform by fcc combined slip-twinning [9,14-20]. However, some other recent studies by Dastur and Leslie [21], and by Zuidema, Subramanyam, and Leslie [22] have advocated that the principal mechanism of work hardening in Hadfield steel is dynamic strain aging (DSA), caused by a reorientation of Mn-C couples within dislocation cores.

Although a strain induced martensitic transformation has been attributed as the cause of strain hardening in Hadfield steel [23], all recent studies included within this study have conclusively demonstrated that a strain induced martensitic transformation does not occur in Hadfield steel even at liquid nitrogen temperatures. White and Honeycombe [6] showed by high resolution TEM replicas and by X-ray diffraction that previously electropolished specimens had no surface phase relief effects indicative of a phase transformation, and that only Fe-Mn-C alloys of low carbon or low Mn content transformed to martensite. Studies by Roberts [10], Raghavan, Sastri, and Marcinkowski [11], and Dastur and Leslie [21], showed by transmission electron microscopy (TEM) and selected area diffraction (SAD) that no α' martensites were present in deformed Hadfield steel, although Roberts observed that a very small amount of ε martensite was formed in hammered specimens.

Deformation twinning had been proposed by Doepkin in 1952 [3] as a potential contributor to deformation in fcc metastable austenitic Hadfield steel on the basis of circumstantial evidence. Doepkin observed strain markings in two to three directions that were suggested to correlate to {111} twinning planes, and audible clicks were reported to accompany load strain jumps during tensile tests. True stress-strain

curves from -196 C to 100 °C shown in Figure 1 from Doepkin's study indicate a near constant average strain hardening rate $d\sigma/d\varepsilon$. Additional circumstantial evidence for deformation twinning was provided by White and Honeycombe [6], by high resolution TEM replicas of deformation microstructure that showed no signs of cross slip to 300 °C, and by deformed structure described as similar to α brass, now known to deform by combined slip and deformation twinning.

Roberts [10] in 1963 was among the first investigators who provided conclusive experimental evidence of deformation twinning in Hadfield steel by TEM and and SAD. Roberts concluded that Hadfield steel deformed by tension and by explosive shock had deformation twins as the most prominent microstructure, but observed a variety of microstructures dependent on states of deformation through tension, through hammering, or through shock hardening. From the wide variety of microstructures of comparable hardness, Roberts suggested that microstructure hardness was a function of the overall resultant dislocation density, not any specific microstructure.

The importance of carbon to Hadfield steel hardness was suggested by Roberts. This suggestion was by reference to a strengthening of steel review by Cohen [7] that discussed twinned martensite strengthening contributions known in Fe-Ni-C alloys of constant M_S. Three basic types of twinned martensite strengthening contributions were discussed in Cohen's review, (1) twin substructure refinement, (2) carbon induced bct distortion or dipole-dislocation interaction, and (3) all kinds of carbide precipitation. Cohen showed that for Fe-Ni-C alloys of constant M_S with 0.02% to 0.82% carbon, martensitic strength was greatly influenced by carbon content and aging temperature through temperature independent strengthening contributions of carbon dipole distortion hardening and temperature dependent carbon aging precipitation hardening, in addition to the basic, but low hardening contribution provided by temperature independent carbon free twin structure.

Hadfield steel deformation twins reported by Roberts had large twin spacing and an explosive formed, high hardness of 600 DPH compared to Fe-Ni carbon-free twinned martensite of hardness 340 DPH with thin twin spacing. Roberts suggested the larger Hadfield twin thickness material should have a low structural component to hardening, in comparison to the thin twin spacing of Fe-Ni martensite and inferred that carbon may have an important role in contributing to Hadfield steel hardness.

Raghavan [11] in 1969 conducted another TEM and SAD study of deformation work hardening in Hadfield steel by observing microstructures in all stages of compressive deformation. Deformation twins were shown by TEM to act as obstacles to other twins

and to dislocations during deformation. Slip-twin interaction theory was discussed, whereby to pass a slip dislocation through a coherent fcc matrix-twin interface, dislocations generally must be left at twin boundaries. These dislocation interactions required for matrix-twin slip were shown by Raghavan to be unfavorable in terms of energy requirements, so that dislocation pile-up and an increase of stress would be required before slip continued across the twin boundary. The increased stress requirement was therefore suggested by Raghavan to result in dislocation slip strain hardening during deformation twinning in a manner analogous to grain refinement. This Hall-Petch kind of twin structural refinement for dislocation strain hardening also has been suggested to enhance strain hardening in other combined slip-twinning alloys [9.14,15,17].

Dastur and Leslie [21] in 1981 concluded that dynamic strain aging (DSA), and not deformation twinning was the primary or dominant factor leading to high strain hardening in Hadfield steel. Dastur made his conclusion that DSA determined Hadfield steel work hardening behavior on the basis of twinned microstructures that showed a monotonic decrease to zero twin density from -25 °C to 225 °C and on the basis of stress-strain curves of low maximum 0.04 strains and work hardening increments from 0.002 to 0.04 strains in tension, over a temperature range of -25 °C to 300 °C. The absence of DSA below -25 °C, accompanied by low work hardening between low 0.002 and 0.04 strain increments in the presence of profuse twinning, was interpreted by Dastur such that the low work hardening behavior results were determined by the absence of a DSA hardening mechanism, actually responsible for determining the high rates of strain hardening in Hadfield steel from -25 °C to 290 °C.

In a more recent study, shortly after the study by Adler, Olson and Owens [4], Zuidema, Subramanyam and Leslie [22] determined the effect of aluminum on work hardening, toughness, and wear of modified Hadfield steels and concluded that pronounced work hardening without the presence of twinning in a modified Hadfield steel containing 2.7% Al and1.75% C cast doubt on Adler, Olson, and Owen's claim of unusual structural hardening of Hadfield steel associated with deformation twinning.

DSA was not considered by Adler, Olson, and Owen [4] to be a primary influence on plastic flow behavior in Hadfield steel. Adler, Olson, and Owen have provided evidence, through a strain increment study similar to Dastur and Leslie's [21] but within a more extensive range of temperatures and strains, that rather being described by slip controlled power law hardening, the strain hardening behavior in Hadfield steel was determined or influenced over large regions of temperature and strain by both the rate

and extent of twin transformation during combined slip and twinning deformation. This twinning influence on plastic flow behavior was described by a proposed Hadfield steel constitutive flow equation similar to those equations experimentally developed to explain the softening and hardening effects of strain induced martensitic transformation plasticity [25-27] (see Appendix).

Adler et. al. observed that twinned microstructures were observed with little dependence on temperature over the range examined, unlike Dastur and Leslie's observation that twin density decreased monotonically to zero from -25 °C to 225 °C. Other studies have shown that twinning in Hadfield steel occurs in many kinds of deformation states [10,12,13].

Adler's [4] results of low strain hardening at low strains were similar to those obtained by Dastur at deformation temperatures below -25 °C where hardening from low strain increments was low. Dastur had concluded this low strain, low strain hardening was from the absence of DSA. Yet, at this same temperature of -25 °C, Adler observed from high strain increments that work hardening was high in comparison to other deformation temperatures. The unusual strain dependent low and high strain hardening at low temperatures that was observed by Adler was called *anomalous* hardening. Anomalous hardening is uniquely determined by temperature and strain dependent softening and hardening contributions of transformation plasticity [14,24-27].

Adler et. al. [4] concluded that plastic flow behavior of Hadfield steel in uniaxial tension and compression showed σ - ε curve shapes that indicated effects similar to transformation plasticity softening and hardening effects (see Appendix) with curve shapes that correlated with temperature, strain, and the observed extent and rate of twinning. The σ - ε curve average strain hardening rates and associated twinned microstructures were weakly dependent on temperature over the range examined and were consistent with the softening effect of twinning as a parallel deformation mechanism to slip and were consistent with a hardening effect of the twinned microstructure. The combined effect of the softening and hardening were suggested to give temperature dependent upward exponential curvature [26-28] to the σ - ε curves in contrast to downward power law curvature indicative of slip controlled plasticity [28].

Other evidence of twinning influence on plastic flow behavior was provided by higher strain hardening rates observed in compression compared to that in tension. This difference in hardening was found to be consistent with observed texture development

and was found to be consistent with a previous Taylor analysis for combined slip and fcc twinning by Chin, Mammel, and Dolan [28,29].

A computed dependence of stacking fault energy with Mn content at a constant carbon content of 1.15% C, correlated with a previously observed dependence of strain hardening versus percent manganese determined by White and Honeycombe [6]. Adler et. al. suggested the Hadfield composition corresponded to an optimum composition for low stacking fault energy that could provide a maximum rate of deformation twinning at a constant carbon content and hence a maximum rate of deformation hardening.

Adler compared plastic flow behavior of Hadfield steel with Co-33Ni-0.02 C carbon-free combined slip-twinning alloy that had identical twinning kinetics as that of Hadfield steel and compared plastic flow behavior to a Fe-20.6Ni-1.04C alloy that deforms by slip. No differences in strain hardening were observed at low strains, where plastic flow and deformation was described and controlled by slip in all alloys. At large strains, where twinning was observed by microscopy and related to texture effects and plastic flow behavior, upward plastic flow curvature and high strain hardening was observed and associated with Hadfield steel twin formation. Adler et. al. proposed that the unusual hardening in Hadfield steel resulted from a twinning process in a non-random fcc solid solution for which the product is a distorted phase with orthorhombic symmetry [30], somewhat analogous to bct C-induced distortion of martensite [7]. The distorted twins were called *pseudotwins* , and the high hardness of these twins was proposed to account for anomalous and high hardening of Hadfield steel in comparison to the other alloys examined at high levels of strains.

In conclusion, a constitutive flow σ - ε relation [26] amended from martensitic transformation plasticity, was proposed by Adler et. al. that included similar effects of martensitic transformation plasticity softening and hardening [26,31] (see Appendix). Hardening was related to dislocation strain hardening flow stress of constituent austenite that was strain corrected by the twinning contribution to imposed strain, by twin structure Hall-Petch grain refinement interaction with dislocation strain, and by the proposed hardness increase of Hadfield steel pseudotwins. The pseudotwin hardness was proposed to include somewhat similar contributions to hardness as found in twinned martensite, from dipole distortion and carbon aging [7].

Adler superimposed twinning effects of softening as an alternative deformation mechanism to slip on the hardening contribution to flow stress to provide a negative contribution to hardening by a softening or relaxation effect (see Appendix). The softening effect was related to the rate of transformation *during* deformation [26] such

that if increased transformation occurred, increased softening contribution was provided to lower the rate of hardening contributed by constituent dislocation strain hardened austenite, Hall-Petch structure and high hardness psudotwins.

2.2 Thermomechanical Treatment of Metastable Austenitic Steels

The effect of thermomechanical treatment (TMT) or warm rolling on the mechanical behavior of metastable austenitic steels have been studied and it is well known that TMT can result in high strength and improved levels of ductility for Fe-Mn-C alloys [9,20,32,33] and for Fe-Cr-Ni-C alloys [14,24-27]. Despite the differences in these alloy systems, the approach to TMT and the effect on microstructure can be similar.

Both alloy systems may have strain induced transformations of austenite to hcp or bct martensite, or austenite to deformation twins. These strain induced transformations in these alloys are dependent upon temperature and strain [9,14,20,24-26] such that at high temperatures during TMT the strain induced transformation is suppressed or decreased and dislocation slip microstructures are favored.

The mechanical behavior and transformation behavior following TMT is greatly different for the two alloy systems. After TMT to high values of strength and during subsequent deformation at room temperature, the transformation may again be favored by thermodynamics during deformation to influence plastic flow from high values of strength. The result of TMT on many metastable austenitic steels has been increased strength and ductility, and plastic flow and mechanical behavior influenced by a reduced [20,33] or increased [25-27] volume fraction of transformation product, depending on the alloy and transformation mechanism. The rate of transformation as well as the total volume fraction and kind of transformation product is important and can strongly influence resulting mechanical behavior as observed in Fe-Cr-Ni-C steel (Figure 2) [25], and as observed for Fe-15.1Mn-0.41C [33] warm rolled at low strains.

Generally the experimental results of TMT treatments of Fe-Mn-C [20,32,33] alloys have not been as successful as those TMT treatments of Fe-Cr-Ni-C [14,24-27] alloys in terms of the final mechanical properties of strength and ductility. The transformation kinetics in the solution treated condition and TMT response of the Fe-Cr-Ni-C austenitic steels has been known for many years [24] (see Appendix), unlike the Fe-Mn-C martensitic or twinning alloys [9].

Warm rolling results of Drobnjak and Parr [32,33] for Fe-15.1Mn-0.41C and Fe-13.8-0.42C-2.9Mo austenites resulted in increased rates of martensitic

transformation during subsequent tests in tension for low TMT reductions of less than 20%. This more rapid rate of transformation after low TMT reductions at 500 °C resulted in mechanical behavior of increased strength and ductility up to 20% RT but as RT increased, further increases in strength occurred with decreasing ductility. The volume fraction of strain induced transformed martensite in the warm rolled Fe-Mn-C base alloys of Drobnjak and Parr decreased to zero at high roll reductions.

Sipos, Remy, and Pineau [20] demonstrated that in the solution treated condition, Fe-20Mn-4.2Cr-0.5C austenite deforms below room temperatures to mainly a hcp martensitic structure, deforms at 100 °C by deformation twins and stacking faults, and deforms at 500 °C by undissociated dislocations.

This Fe-20Mn-4.2Cr-0.5C alloy demonstrates the temperature dependence of transformations on mechanical behavior. Solution treated condition material had low ductility and elongation associated with the hcp martensitic transformation during deformation at temperatures less than room temperature, but as deformation temperature was increased, the twin and stacking fault structure was associated with high homogeneous elongation and reduction of area. As deformation temperature was increased further to where deformation structures were composed of undissociated dislocations, the uniform elongation again decreased but reduction of area remained high, so that plastic flow became localized.

Fe-20Mn-4.2Cr-0.5C [20] material warm rolled at 100 °C and at 500 °C and tested in tension at room temperature had improved strength and increased ductility in tension by increased reduction of area at low deformation temperatures, but elongation decreased. After TMT the volume fraction of strain induced hcp martensite was reduced for both 100 °C and 500 °C TMT temperatures, with the 500 °C temperature more effective in decreasing transformation.

3.0 Experimental Methodology

3.1 Approach

An approach of warm rolling is used since Hadfield steel is known to deform under many kinds of imposed deformation states to strain induced combined slip-twinned microstructures [4,10-13], and it has been widely known or suggested that fcc deformation twinning can influence deformation substructure [4,9-20,28,29] and therefore plastic flow behavior [4,9,11,12,14-17,19,20,28,29].

Other than TMT, there may not be any practical alternative strengthening mechanism or approach that can simultaneously greatly increase strength yet retain the original deformation mechanisms and excellent plastic flow behavior and properties of low strength, solution treated Hadfield steel. Strength and hardness are known to be developed in Hadfield steel during strain, but the deformation mechanisms and structures of Hadfield steel responsible for strain hardening remain uncertain [4,21]. If alternative approaches to strengthening from alloying or precipitation mechanisms are introduced, the deformation mechanisms responsible for Hadfield steel behavior are likely to be affected. Toughness, uniform strain and strain hardening may be reduced with an equivalent decrease in tensile strength and hardness [2,3].

Solid solution hardening and precipitation hardening using alloy additions such as molybdenum or strong carbide formers may be used but this approach only results in modest increase in strength in some instances, and ductility levels usually decrease [2,5]. This approach also may easily change the deformation mechanisms in Hadfield steel.

Since carbon content has the greatest influence on strength of steels for the least amount of alloying [2,7,34], at first it seems logical that increasing carbon content is the easiest approach for strengthening Hadfield steel. The approach of increased carbon content in Hadfield steel has the disadvantage that the standard grade of Fe-12.5Mn-1.2C is near the practical limit of carbon solubility and that further increases in carbon content tend to degrade mechanical properties of strain and strength [2]. Further increases in manganese do not provide increased benefits of greater cabon solubility, strength, or ductility above 12-14% Mn [1,2].

An alternative approach could be similar to that of Zuidema, Subramanyam, and Leslie [22] who used aluminum in 1.75% C - 2.75% Al modified Hadfield steel to decrease activity of carbon in austenite for greater carbon solubility limits. Zuidema's

approach has the disadvantage that deformation mechanisms and mechanical behavior may be influenced by the greatly different alloy content within Hadfield steel as observed by the reported absence of twinning in the 1.75C-2.75Al alloy and by lower values of toughness and wear resistance in comparison to an unmodified grades of Hadfield steel at optimal carbon contents.

Thermomechanical treatment [35], ausforming, or warm rolling has been used previously with metastable Fe-Mn-C system alloys [9,20,32,33] and, as shown in Figure 2, with other Fe-Cr-Ni-C metastable austenitic steels [24-27] that undergo strain induced and temperature dependent transformations. These metastable alloys that have temperature dependent strain induced transformations can be greatly improved by thermomechanical treatment for both increased strength and ductility in comparison to the solution treated condition and in comparison to high strength conditions obtained by precipitation hardening or cold working.

At high TMT temperatures, martensitic strain induced transformation may be eliminated or decreased and strengthening can occur by increased dislocation density or twinning and solute-dislocation strain induced interaction [24,27]. Subsequently after TMT and during deformation at lower temperatures, the strain induced transformation is again favored and now this transformation during strain at high strength levels may be either suppressed [20,33] or enhanced [24-27] from prior deformation as shown in Figure 2.

The rate of transformation may be increased or decreased, so that the plastic flow behavior is influenced both by rate and the extent of transformation. Ductility levels at high strength levels can be enhanced over particular temperature ranges by Fe-Mn-C [20,33] alloys that have suppressed transformation and by Fe-Cr-Ni-C [24-27] alloys that have enhanced transformation. Generally, in Fe-Mn-C system alloys ductility is decreased with increasing strength from TMT.

Deformation twinning in Hadfield steel [4], in Fe-Mn-C system alloys [4,9,20] and in other fcc metals [9,15,19,20] is known to be influenced by both imposed temperature and strain. During warm rolling, deformation twinning could be reduced or prevented and greater plastic flow and hardening contributions may be contributed by slip. After warm rolling to high strength levels and during subsequent deformation in service at lower room temperatures, deformation twinning in warm rolled Hadfield steel could possibly be again favored as a deformation mechanism by a strain induced transformation and by kinetics [9,15,20] so that the strain induced Hadfield steel

combined slip-twinning transformation could provide and influence plastic flow behavior from high rather than low strength levels.

Hadfield steel deformation twins, like other fcc deformation twins [9,14,17-20,28,29] and in particular like the solution treated Fe-20Mn-4.2Cr-0.5C alloy of Sipos, Remy, and Pineau [20], can influence plastic flow. At high warm rolled strength levels, twins may provide contributions to strain by the twin shear itself and by accommodation dislocations [34] that could be biased by resolved stresses and by active twin systems as in other strain induced transformations [27,35]. Further strain hardening from high warm rolled strength levels could be provided by twin substructure refinement that promotes dislocation pile-up in a manner analogous to Hall-Petch grain refinement [9,11,14-17] (see Appendix). Adler, Olson, and Owen [4] (see Appendix) have proposed that Hadfield twins themselves have high hardness from a lattice distortion caused during the twin shear. Adler et. al. also suggest that twinning can provide a softening contribution with strain as an alternative or parallel deformation mechanism to dislocation slip.

Softening contributions during imposed strain and during the accompanying strain induced deformation transformation are known in strain induced martensites [25-27,35] and it is possible that fcc deformation twins may provide contributions of softening during strain. Michels and Jones [19] have reported that fcc deformation twins may form as an accommodation mechanism to relieve stress concentrations caused by linear dislocation arrays. Since the stress to propagate twins is known to be less than that stress required for twin nucleation [14,17,18,34], localized stresses from dislocation defects may be relaxed by twinning and the ensuing dislocation slip twin accommodation.

Some earlier efforts of Hadfield steel thermomechanical treatments are shown in Table 3 (TMT) These efforts have been used to increase strength by warm swaging [36] or by warm rolling [37,38]. These efforts have not been entirely successful for developmental applications, demonstrating either high strength and low ductility [36] or lower strength with good ductility [37]. The preliminary results suggest that the optimal warm rolling thermomechanical treatment may not have been achieved during previous developmental efforts [36-38].

Unlike the previous studies [36-38] that used low rates of reduction by many low increments of strain interspersed with air reheats during thermomechanical treatment, the present study has used high increments of roll reduction. The selection of a TMT procedure for high rates of reduction was based on examination of previous warm rolling

results [38] that suggested operation of a softening mechanism caused by carbide precipitation and an associated void coalescence fracture during tension tests. Optical metallography and scanning electron microscopy (SEM) results also suggested a void nucleation and coalescence fracture mechanism occurred in material from this previous warm roll study [38] (refer to Section 5.1, 5.7).

The objective of determining effects of warm rolling on plastic flow behavior and microstructure of Hadfield steel is made by the approach of an evaluation of a warm roll material test matrix shown in Figure 3. This test matrix is determined by effective warm roll strain (ε_e) or reduction of thickness (RT) and by warm roll temperature. The test matrix specifies what conditions of warm rolled material were to receive hardness tests, tension tests, optical metallography, and SEM fractography. Hardness (H) values were taken of all warm rolled material. Plastic flow behavior in tension and microstructure after TMT was determined with material rolled from low to high effective strains at a constant 454 °C roll temperature so that the effect of increasing effective warm roll strain could be observed on trends of plastic flow behavior and microstructure. Plastic flow behavior in tension and microstructure was also determined by material rolled at a near constant 50% RT or 0.70-0.75 ε_e at 343 °C, 399 °C, and at 454 °C so that resultant trends dependent upon deformation temperature could be observed. Uniaxial true stress-strain plastic flow curves in tension are plotted to maximum load only, where values of true stress-strain are called *true uniform stress* and *true uniform strain* [39]. These true stress-strain curves evaluate strength and high strain hardening behavior without necking or plastic flow instability.

Electropolishing and electroetching techniques used in the experimental approach are generally those which have previously been used to identify grain boundaries, annealing twins and deformation twins in Hadfield steel by a Na_2CrO_4 glacial acetic acid etch [4,21,22,40]. A limited number of specimens were electrolytically etched experimentally at low temperatures using HCl in methanol.

Optical microscopy of warm rolled material from the test matrix before and after straining in tension revealed details of microstructure that suggest deformation mechanisms present. Optical microscopy of the solution treated and deformed condition provides deformed and twinned structures for comparison to warm rolled microstructures. Optical microscopy of 454 °C - 23% reduction of thickness condition material provides a distinguishable low strain deformed and twinned microstructure in comparison to greater warm roll strains where grain structure is highly deformed from slip and twinning.

Fracture surfaces were investigated by SEM and by optical microscopy and were compared to tension test ductility trends resulting from rolling at a near constant 50% reduction of thickness versus temperature.

3.2 Materials And Procedure

Material used for the study was prepared from argon oxygen decarburized (AOD), continuous cast 3.0 inch diameter ingot, with a composition of Fe-12.5Mn-2.01Mo-1.15C as described by ASTM A128-E2 grade Hadfield steel [2].

Initial processing included machining to remove pipe shrinkage defects and included processing into bars ready for warm rolling. After removal of shrinkage defects from ingot by cutting and grinding, ingot sections were soaked at 1040 °C for one hour, followed by rough forging to rectangular bar shape and water quenching. The bars were painted with ceramic paint for protection against decarburization, and were homogenized at 1120 °C for 20 to 24 hours followed by a water quench. After homogenization the bars were finish forged at 1040 °C to cross sections of 1.4 inch width and 0.88 inch thickness, and were water quenched. The finish forged bars were solution treated at 1030 °C to 1040 °C for one hour and water quenched to obtain an austenitic structure.

The final solution treatment temperature of 1030 °C to 1040 °C was selected from results of a previous recrystallization and grain growth study [38] that determined Hadfield steel mean grain diameter versus solution treatment temperature at one hour. The Hadfield Fe-12.5Mn-2.01Mo-1.15C steel used in this solution treatment study had been initially solution treated and warm rolled at a rate of reduction of 0.010 inch reduction per pass to a 50% reduction of thickness at 427 °C.

After solution treatment, all bars were conditioned by mechanical grinding to 3.2-3.5 x 1.38 x 0.77 inch. Dye penetrant and ultrasonic non-destuctive testing was then used, and despite some small surface flaws, the bars were found to be free of defects.

After conditioning to size, the bars were warm rolled on a 12.5 inch diameter roll at a 12 revolution per minute roll speed. To decrease time at temperature and to inhibit carbide precipitation, 0.050 to 0.070 inch reductions per roll pass were used.

These high roll reductions are assumed to quickly introduce kinds of strain induced, dislocation boundary structures and twin boundary structures with accompanied high localized pile-up or accommodation stresses. The high reductions can thus favor strain induced defect carbon clustering or segregation rather than time-temperature dependent and strain enhanced kinds of carbon-solute segregation and precipitation.

Warm rolling approaches included constant reduction of thickness (RT = $(t_o-t_f)/t_o$) at temperatures of 343 °C, 399 °C, and 454 °C and included constant temperature and varied effective strains at 23%, 35%, 50%, and 61% RT. Bar dimensions were recorded before and after warm rolling in order to calculate true effective strains (ε_e) that could be related to true uniaxial strains in tension testing.

An electric furnace with natural air convection and radiation heat transfer was used to reheat bars 5 to 15 minutes between reductions. Rolling temperatures were verified by a fine gage thermocouple held between pairs of bars being heated and rolled.

One bar rolled to 40% reduction of thickness was again solution treated for the purpose of obtaining as-solution treated material for tension test and microstructural comparisons.

Warm rolled bar specimen preparation included longitudinal transverse section hardness readings, longitudinal transverse section metallography specimens and longitudinal section tension specimens. Two tensile specimens per bar were prepared from center sections of bars warm rolled approximately 50% reduction of thickness (RT) at 343 °C, 399°C, and 454 °C; from bars warm rolled at 454 °C at 35% and 61% RT, and from a bar in the as-solution treated condition. Tension specimens were ground to a size of 0.225 inch gage diameter, 0.90 inch 4 to 1 L/D gage length and reduced section length of 1.25 inch; or to a size of 0.160 inch gage diameter, 0.64 inch 4 to 1 L/D gage length and reduced section length of 1.00 inch.

Tension tests were conducted to fracture at 23 °C and 50% relative humidity, using a screw driven machine with a constant cross head speed of 0.02 inch per minute, equipped with a 20,000 pound load capacity frame and load cell. Engineering strains were recorded by either a 1.00 inch - 50%, or 1/2 inch - 50% extensometer to 0.06 to 0.12 engineering strains, and thereafter engineering strain was determined by chart speed, time and cross head displacement over the specimen reduced section length. More appropriate instrumentation for recording instantaneous minimum diameter was not available. Engineering stress vs engineering strain curves were converted to true stress vs true strain using reduced section engineering strains to maximum load. The true stress-strain values at maximum load are called true uniform stress and true uniform strain [39].

Tension specimens strained to fracture were studied by low power macroscopy, scanning electron microscopy (SEM), chemical analysis, and optical microscopy. Low power macrographs of broken tension specimens were taken in order to illustrate the general extent of plastic flow without necking. Scanning electron microscopy and optical

microscopy of fracture surfaces were completed so that fracture mechanisms could be determined, and chemical analysis of tested tension specimen sections was completed in order to determine whether any decarburization had occurred during processing.

Metallography specimens of long transverse sections were cut by a low speed metallographic sectioning saw from warm rolled bar, tension specimen threaded sections, and tension specimen gage lengths or shoulder sections. Mechanical grinding and polishing of all specimens included grinding by SiC papers to 600 grit, 5-1 diamond autolap rough polishing, 1 micron alumina or 1.0-0.25 diamond fine polishing, and final 0.05 micron alumina fine polishing. Electropolished specimens were prepared with a solution of 80 grams Na_2CrO_4 in 420 ml of glacial acetic acid, at 30-36 V for about 2 to 3 minutes at room temperature. Specimens were electrolytically etched in the sodium chromate-glacial acetic acid solution at 23 °C, or in 10% HCl in methanol at 4 to 6 V at -78.3 °C for 10 to 20 seconds.

4.0 Results

4.1 Solution Treatment Study

Results of the solution treatment study are shown in Figure 4 by a plot of mean grain size diameter (calculated by 1.6 times the mean intercept length) versus solution treatment temperature, for one hour solution treatment of the argon oxygen decarburized (AOD), Fe-12.5Mn-2.01Mo-1.15C composition, Hadfield steel used in the present study. These results are plotted along with high purity, lower carbon content, argon arc melt Fe-14Mn-2.01Mo-0.97C.

Microstructures of AOD Hadfield steel solution treated conditions are shown in Figure 5 for solution treatments at 975 °C, 990 °C, 1020 °C and 1050 °C. Grain shapes were characteristic of annealing twin structures at all temperatures above 975 °C.

Grain size in the AOD Hadfield steel was observed to increase within two regions of temperature, with the largest increase in grain size occurring above 990 °C, at a temperature just above the A_{cm} line that separates the austenite and austenite plus carbide regions of the Fe-12Mn-1.15C phase diagram. Another region of grain size growth was observed just above 1020 °C. In comparison to the high purity, low carbon, argon arc melt, AOD grain growth was retarded, possibly by aluminum oxide precipitates, carbide precipitates, or lower cleanliness, so that the AOD solution treated steel had smaller grain size.

Optical metallography indicated that large grain boundary precipitates were not visible above 1020 °C.

4.2 Warm Roll Strengthening

A summary of warm rolling results that includes roll temperature, reduction of thickness (RT) effective plastic strain (ε_e), and Rockwell Rc hardness is shown in Table 4. Deviation from non-plane strain rolling conditions increased as temperature and reduction of thickness increased, so that reduction of area or cold work (r) was not appropriate for calculation of effective strains by the relation $\varepsilon = \ln(1/(1-r))$.

Hardness values were near equal for approximate 50% RT or 0.75 ε_e at 343 °C, 399 °C and 454 °C, with a slight decrease in hardness with increased rolling temperature. Plots of resulting Rc hardness, versus warm rolled reduction of thickness, and versus effective warm roll strain are plotted in Figure 6. Two regions of hardening behavior

were observed by high rates of hardening at low effective strains and by low rates of hardening at high effective warm rolling strains.

4.3 Metallography: Solution Treated And Warm Rolled Conditions

Metallography results of as-solution treated and deformed in tension 0.64 ε, gage length sections of Fe-12.5Mn-2.01Mo-1.15C Hadfield steel are shown in Figure 7 with the Na_2CrO_4 and glacial acetic acid electrolytic etch. Identical material electrolytically etched with HCl and methanol at -78 °C shown in Figure 8, include tension specimen shoulder sections with strains of less than 0.64 ε_u. Superior results of high resolution were obtained with the HCl-methanol electrolytic etch. Figure 7 indicates a high density of structures previously identified by TEM and by optical microscopy as Hadfield steel fcc deformation twins [4,10,11,21,22,40].

Micrographs of low strain near shoulder sections, before concurrent slip causes twins to developed a slip shear-band like appearance, indicate that the fcc combined slip deformation twins are more clearly recognizable as twin structures rather than as slip structures. The structures developed at low strains in Figure 8 (b) have developed at least three deformation systems, and fine twins within some grains are observed at a stage of incipient growth and at grain boundary intersections where high incompatibility stresses are known to occur. These boundary intersection twin structures are quite different from slip shear bands, since slip bands will extend from grain boundary to grain boundary. The extent of twin structures observed within different grains may correlate to Schmid factors for fcc slip-twinning that are dependent on crystallographic orientation under conditions of axisymmetric deformation [28,29].

Grain boundary precipitates observed in solution treated material shown in Figures 7 and 8 may possibly be $(FeMn)_3C$ carbides resulting from inadequate solution treatment practice of temperature, time, or quench rate.

Metallography results in Figure 9 of the 454 °C warm rolled material with 23%, 35% and 50% RT or equivalent 0.29, 0.46, and 0.75 ε_e, indicate structures suggested to be Hadfield steel deformation twins. The twin markings were more distinguishable at low effective strains of 0.29 and 0.46 than at 0.75 strain where the marking more closely resemble slip bands. The amount of deformation twinning was observed to increase with increased strain among the 454 °C warm rolled bars. For the 0.75 ε_e, 454 °C warm rolled microstructure, a large amount of deformation twins were observed. The amount of deformation twinning or slip undergone by each grain varied

significantly, depending upon each grain orientation. Grain rotation, anisotropic twinning for grains dependent upon orientation and a sliplike appearance of the twins could suggest a high contribution of deformation from concurrent slip.

A small difference in the amount of deformation twinning may have occurred between the low and high warm rolling deformation temperatures as shown in Figure 10 for warm rolling temperatures of 343 °C, 399 °C, and 454 °C at a near constant reduction of thickness of 50% or effective strain of 0.75. More extensive microstructural study would be required in order to detect increased twinning and more active twin systems in the lower roll temperatures. A slightly higher volume fraction of twins at lower rolling temperatures may correlate to the slightly higher observed hardness values shown Figure 6.

4.4 Tension Test Behavior And Specimen Macroscopy

Specimens shown left to right in Figure 11 (a) illustrate the tension tested appearance of material in the solution treated condition, and the tension tested appearance of material in the 454 °C, warm rolled 0.46, 0.75, and 1.00 ε_e conditions. Specimens shown left to right in Figure 11 (b) illustrate the tension tested appearance of material warm rolled to about 0.75 ε_e or 50 RT at 343 °C, 399 °C, and 454 °C. All of the strained to fracture tension specimens clearly showed that strain occurred predominantly in a uniform manner along the length of the specimen without large contributions from localized necking or plastic instability strains. Fracture surfaces shown in Figure 11 indicate fracture contributions of tension-cup and shear-cone fractures for all specimens. The kind of plastic flow leading to fracture may not be fully described as a kind of brittle, propagation limited fracture, or as a kind of ductile flow and fracture, since the plastic strains to maximum load of all specimens were large, but after maximum load, fracture was brittle with little or no engineering necking strain (e_n). The final fracture beyond maximum load occurred with a rapid unloading rate and over a small range of necking strain, catastrophically, without significant previous geometric softening.

4.5 Tension Test Stress-Strain Curves

Curves of engineering stress (s), engineering strain (e) and true stress (σ), true strain (ε) for as solution treated condition material are shown in Figure 12. The engineering curve indicates increasing load to fracture, and the corresponding true stress-true strain curve indicates upward curvature strain hardening [27,28] to high uniform strains with near linear plastic flow to high stress-strain values before fracture. The curve shapes are similar to those of Fe-12Mn-1.15C Hadfield steel by Hadfield LTD [1] for s versus e, and to those of Doepkin [3], and Adler [4] for σ versus ε.

Stress-strain curves in tension for material warm rolled at 454 °C with 0.46, 0.75 and 1.00 ε_e or 35%, 50% and 61% RT, are shown in Figures 13-15 for engineering stress-strain and true stress-strain. Both the curve shapes and stress-strain values are closely similar for each specimen in each identical condition. The engineering curves all indicate increasing load to fracture, with corresponding near linear, true stress-strain plastic flow to high values of stress and strain.

Figure 16 plots one specimen each of the 454 °C warm rolled condition with effective strains of 0.46, 0.75 and 1.00 (35%, 50%, 61% RT). Observed trends of Figure 16 are increased strength and decreased strain for increased warm rolled effective strain.

Plots of stress and strain in tension for material warm rolled with 0.73 ε_e, or 49% RT at 343°C and with 0.70 ε_e or 48% RT at 399 °C are respectively shown in Figure 17 and 18. The plots of each specimen per condition are closely similar except for the 0.73 ε_e-343 °C material plot where the cross head speed was intermittently interrupted. All curve shapes of stress and strain were generally similar to curve shapes of specimens of the 454 °C warm rolled bars, with engineering stress increasing to near fracture and near linear plastic, true stress-strain curves.

A comparative grouping of stress-strain plots of material rolled at 343 °C, 399 °C and 454 °C with near 0.75 effective roll strain or 50% RT roll reductions shown in Figure 19, indicates that a slight decrease in strength for increased warm rolling temperature occurred, consistent with results of decreased hardness with increased warm rolling temperature shown in Figure 6.

During tension testing, work hardening continued to, or near, fracture so that little or no warning of imminent catastrophic fracture was observed by necking strain (e_n). For a near constant 0.75 effective warm roll strain, the observed engineering necking

strains increased along with increased warm roll temperature and were maximum in material warm rolled 454 °C.

4.6 Tension Test Values

A large increase of strength occurred for solution treated material rolled with a near constant effective warm roll strain of 0.75 or 50% RT. Engineering tension test data listed in Table 5 indicates that 0.2% offset yield stress increased from the solution treated condition of 64.0 ksi (441 MPa) to the warm rolled condition of 201.6-213.8 ksi (1390-1474 MPa). Ultimate tensile strength (U.T.S.) increased from the 161.9 ksi (1,116 MPa) solution treated condition to the warm rolled 259.4-267.6 ksi (1,789-1,845 MPa). Material rolled near 50% RT, at the low 343 °C roll temperature had the greatest yield strength values with 0.2% yield stress of 213.8 ksi (1,474 MPa), and the greatest ultimate tensile strength of 267.6 ksi (1,845 MPa).

Ductility was greatest for material rolled at high temperatures, and lowest for material rolled at low temperatures for near constant effective warm rolling strains of 0.75 or 50% RT. Engineering ductility was greatest among the 454 °C rolled material that showed a maximum fracture strain (e_f) of 0.23. This maximum ductility in material rolled at 454 °C with 50% RT was observed in values of 23% 4 to 1 L/D gage length percent elongation (El.%) and 22% reduction of area (RA%). Ductility was lower in material rolled at 343 °C and 49% RT with a minimum observed fracture strain of 0.17.

For material warm rolled 454 °C with effective warm rolled strains of 0.46, 0.75, and 1.00 or equivalent reductions of thickness of 35%, 50%, and 61%, minimum limits of yield strength and minimum ultimate tensile strength were observed from effective roll strains of 0.46, and maximum limits of yield strength and maximum ultimate tensile strength were observed from roll strains of 1.00. The values of these minimum and maximum yield strengths (0.2%Y.S.) were 166.5 and 233.7 ksi (1,148 and 1,611 MPa). Minimum and maximum limits of ultimate tensile strength (UTS) were 238.5 and 276.0 ksi (1645 and 1903 MPa).

Engineering ductility for the 454 °C, 35%, 50%, and 61% RT warm rolled bars ranged between 27% and 14% elongation, and 27% and 16% reduction of area.

True uniform stress (σ_u) listed in Table 6 for the near constant 0.75 effective strain or approximate 50% RT warm rolled bar material increased to within a range of 307.0 to 320.6 ksi (2,108 to 2,210 MPa) from the 305.8 ksi (2,109 MPa) solution

treated condition. Maximum values of true uniform stress (σ_u) and true uniform strain (ε_u) of the approximate 50% RT warm rolled bars were observed at 399 °C, with values of 320.6 ksi (2211 MPa) and 0.19 strain.

Material warm rolled at 454°C with 1.00 ε_e, had maximum results of true strength and minimum results of ductility in comparison to all warm rolled bar. This maximum observed true uniform stress was 324.7 ksi (2,239 MPa) and the minimum true uniform strain was 0.14. Specimens obtained from bar rolled 35 % reduction of thickness at 454 °C, showed maximum true strain of 0.27, in comparison to all warm rolled bar.

4.7 Chemical Analysis Results

After completion of tensile tests, threaded sections of tension specimens prepared from the 454 °C, 0.75 ε_e rolled material were cut into chips, and then analyzed for determination of carbon content. Results indicated a carbon content of 1.15% C, so that no decarburization from processing had occurred in material used for specimen preparation.

4.8 Optical Metallography of Tension Tested Material

Metallography results shown in Figure 20 for the near constant 0.070-0.75 ε_e warm rolled and tension tested to fracture material showed only a slight difference in microstructure from the warm rolled microstructures of Figure 10. True uniform strains in tension were near identical at 0.16 to 0.18 and were low in magnitude relative to the high warm roll effective strains. Since this 0.75 ε_e warm rolled material was greatly deformed before and after tension testing, tension tested warm rolled microstructures were usually only distinguished from warm rolled microstructures by darker etches along grain boundaries and along twin structures, that could suggest that greater amounts of localized twinning and slip had occurred in tension tests.

For the 454 °C, 0.46 ε_e warm rolled material deformed an additional 0.27 true strain in uniaxial tension, a distinct difference of microstructure was observed from the warm rolled condition shown in Figure 9, by both the Na_2CrO_4 electrolytic etch in Figure 21, and by the HCl electrolytic etch shown in Figure 22. Whereas the 0.46 effective strain warm rolled microstructure had near equiaxed grain boundaries and a

small amount of deformation twins widely spaced within and among the grains, the 0.46 ε_e + 0.27 ε_u specimen shown in Figure 21 and in Figure 22 shows greater grain flow, and a greater density of structures suggested to be fcc deformation twins.

Figure 22 showed clear and distinct differences of structures observed as grain boundaries, annealing twins, deformation twins and shear bands. The warm rolled and tension deformed structure of Figure 22 includes indications of localized deformation in the form of slip shear bands that were the less common structure observed, but appear to have contributed more to deformation than the normal twinned microstructure usually observed. The light structures that suggest shear bands extend in a planar manner across grains, and have sheared deformation twins, grain boundaries and other shear bands.

Some large, dark structures in Figure 22 that may have been formed during rolling have a distinct lamellar twin band appearance upon close examination. In general appearance, these structures suggest deformation twin bands. The twin structures and shear bands observed in Figure 22 have a wide variety of structural differences in thickness, shape, and size possibly dependent on deformation temperature, crystallographic orientation, and imposed stress and strain from rolling compression and uniaxial tension. Grains clearly indicate an orientation dependence since grains are dominated by favored structures of slip shear bands, or by deformation twins of different orientations.

The microstructures of Figure 22 suggest anisotropic hardening and deformation possibly contributed from compatibility requirements of highly deformed grains or from some load axis relation between slip and twin systems. Greatly deformed, shear banded grains have influenced deformation structures in neighbor grains as shown by shear bands that extend across the greatly deformed grains into and through neighbor grains. These shear bands are more often localized at grain boundaries where incompatibility stresses are high. Grains that have few twins appear to have the greatest localized deformation as suggested by larger numbers of shear bands with high localized shears. Grains that have some twins generally have less shear bands, and some grains where twins and slip systems may be closely oriented have no distinguishable shear bands.

4.9 Fractography Results by Optical and Scanning Electron Microscopy

Fracture surfaces of specimens warm rolled approximately 50% RT and tension tested are shown by scanning electron microscopy (SEM) in Figures 23-25.

Initial onset of fracture in all specimens was initiated in tension by grain boundary decohesion through ductile void nucleation-growth and through brittle cleavage at annealing twin boundaries. Micrographs of fracture profiles shown in Figure 26 revealed that ductile fractures of grain boundaries by decohesion were associated with void formation and grain boundary precipitates, possibly $(FeMn)_3C$. Cracking was observed with grain boundary decohesion and cleavage as shown in Figure 26 (a).

After necking and flow localization had initiated by grain boundary decohesion fracture in tension, all specimens failed catastrophically in shear as shown in Figures 23, 24 and 26. Shear fracture surfaces had mainly a ductile appearance characteristic of void nucleation and growth, but shear cleavage fractures on twin surfaces were also observed, as shown in Figure 24.

The extent of initial fracture by grain boundary decohesion that occurred in tension, relative to catastrophic fracture that occurred in shear, increased with increased warm roll temperature for the material rolled approximately 0.75 ε_e. The fracture surfaces with large areas of grain boundary decohesion in tension correlated to high values of engineering fracture strains e_f , and correlated to high values of necking strains e_n, given in Table 5.

5.0 Discussion

5.1 Solution Treatment Study

High toughness, and optimal work hardening to high levels of strength and ductility in Hadfield Mn steel are known to be dependent upon an initial solution treated, austenitic microstructure of fine grain size and upon the absence of grain boundary carbide precipitates [2,5]. Too low of a solution treatment temperature, or low cooling rates during quenching can often result in $(FeMn)_3C$ carbide microstructures and inferior mechanical properties of work hardening [1,2,5].

Solution treatment temperature can determine grain size by the dependency of grain growth on carbide or other precipitates [34]. A fine dispersion of particles can stabilize grain size at high temperatures by particle drag force against the surface free energy driving force for grain growth. When particles dissolve at high temperatures, or coalesce to form fewer and larger particles, the retarding effect of the inclusions on grain growth is removed or decreased, and an accompanying increase of grain size also occurs. The retarding influence of precipitates may be observed from the results of this study since the low carbon and high purity Fe-14Mn-2.0Mo-0.97C had larger grain size compared to the high carbon and aluminum killed AOD Fe-12.5Mn-2.01Mo-1.15C ingot material.

The solution treatment temperature of 1030 °C to 1040 °C used for Hadfield steel bars in this study was selected for the purpose of ensuring complete dissolution of primary carbides and to allow a relatively small grain size. Complete carbide dissolution in steels during heat treatment is important to avoid the introduction of primary carbides or precipitates of low interfacial strengths that can initiate softening, plastic instabilities, and ductile fracture by the void coalescence and growth mechanism [8].

Unlike the stress and strain induced martensitic transformation, combined slip and deformation twinning in Hadfield steel does not have a transformation toughening volume change, so the strain induced combined slip-twinning transformation responsible for high strain hardening in Hadfield steel could be susceptible to an initial high volume fraction of void nucleating carbides, particularly if plastic flow is localized as observed in Figure 22. This behavior was suggested by an earlier investigation [38] of warm rolled Hadfield steel that included low rates of reduction and hence a long period of time where time-temperature strain enhanced precipitation could occur. The previous study

[38] included behavior in tension, SEM fractography, and optical microscopy, and the results were consistent with a void nucleation-coalescence plastic flow localization softening and fracture mechanism. This behavior is also suggested by the poor low ductility and low strength properties of high carbon content Hadfield steel alloys of greater than 1.4% C [2] when are carbides result from inadequate solution treatment practice and the linear increase in A_{cm} [2] with increasing carbon content of Hadfield steel.

If many carbides are present and void nucleation softening occurs at low strains, deformation twinning may not have a opportunity to influence plastic flow later during deformation.

Grain size determined by heat treatment temperatures can significantly affect polycrystalline deformation behavior [5,35]. Yield stress and hardness are increased in many alloys with decreased grain size by the Hall-Petch relation. Fine grain size can also lower elastic incompatibility stresses, reduce localized plastic deformation before macro-yielding occurs, and increase Charpy blunt notch impact energy at low temperatures. Fine grain size may also be important for achieving high strength during warm rolling by a dislocation hardening contribution, since a fine grain size can provide a greater area of potential dislocation sources, and favor deformation by slip over deformation twinning.

5.2 Chemical Analysis

For a constant carbon content near 1.15%, solution treated, Fe-12.5Mn-1.15C, Hadfield steel has been related to minimal stacking fault energy, a high rate of deformation twinning, and optimal properties of strain hardening [4,6]. Hadfield steel alloys of Fe-12.5Mn-1.15C have also been shown empirically [2,5] to result in combined optimal properties of strain hardening, strength and ductility. Decarburized or low carbon content Hadfield steel with a minimum carbon content of 0.80% C, has resistance to reheat carbide precipitation, and the effect of the low carbon may not be entirely harmful [5], although strength levels are reduced. Fe-Mn-C steels of less than 0.80% C [6], should not be considered true Hadfield steel since a martensitic strain induced transformation is possible at low temperatures. The low carbon Fe-Mn-C steels that undergo strain induced martensitic transformation have high strain hardening rates and high strengths but also have lower levels of ductility and toughness.

Experimental results that indicated carbon content had remained constant at 1.15% C before and after processing heat treatments implied that combined slip and deformation twinning may be expected in the solution treated condition as a deformation mechanism [6,10,11].

It is known that both dislocation and twin structures can act as obstacles to inhibit twin growth [9,11,16,28], so that for highly strained warm rolled Hadfield steel containing a high population of deformation twins and dislocations as shown in Figure 10 and in Figure 22, the possible further extent of strain induced, fcc deformation twinning possible is not known.

5.3 Hardness

Warm roll results indicated that achievement of high hardness levels in Hadfield steel is possible by warm rolling. Rapid rates of hardening to high strengths were obtained with low strains, but low rates of hardening were obtained at the highest strength levels as shown in Figure 6. A slight decrease in hardness was observed with increased rolling temperature of Figure 6, that together with results of fcc combined slip-deformation twinning shown by optical microscopy in Figure 10, could suggest that a corresponding decrease in the amount of deformation twinning may be occurring at higher warm roll temperatures.

5.4 Metallography: Solution Treated And Warm Rolled Conditions

Metallography results in Figure 9 of bar material and tension specimen threaded sections of material warm rolled at 454 °C with 23%, 35%, and 50% RT or equivalent 0.29, 0.46, and 0.75 ε_e, indicated structures previously identified as fcc deformation twins, that were most recognizable as twins at low strains where accompanied slip strain was low.

With material warm rolled 49%, 48%, and 50% RT with respective roll temperatures of 343 °C, 399 °C and 454 °C, microstructures shown in Figure 10 indicate that only small differences in the amount of density of twin structures may be present between 343 °C and 454 °C such that for lower temperatures, more active twin systems may have contributed to deformation.

For 454 °C warm rolled material, an increased amount of structures suggested to be Hadfield steel deformation twins were observed versus increased strain. Increased

indications of concurrent slip was suggested by the curvilinear appearance of twins at high strains in comparison to the low strained formed, near linear twin bands.

More extensive optical and electron microscopy not within the scope of this study is required to conclusively determine combined slip-twinning deformation behavior in Hadfield steel in relation to temperature, strain rate, and state of stress.

The observation of Hadfield steel deformation twins at these compressive deformation roll temperatures as shown in Figure 9 suggests that Hadfield steel twin formation is relatively insensitive to temperature in comparison to the strain induced martensitic transformation and that it may be possible for fcc combined slip and deformation twinning to act as a strain hardening mechanism under optimal conditions of stress state at high temperatures and strain rates.

5.5 Tension Tests: Plots, Strain Hardening Fits, and Value Trends

Tension tested specimens shown in Figure 11 demonstrate that the solution treated condition and the warm rolled conditions, deformed similarly with high true uniform strains to fracture, and with small necking strains. The similar uniform elongation could suggest that similar deformation and hardening mechanisms were operating in all specimens, namely fcc combined slip and deformation twinning.

Tension tests of all test specimens indicated that loads increased to near fracture at high engineering stresses and strains, but the engineering stress-strains curves in the plastic region had low rates of hardening below 0.04 strains in comparison to engineering curves of low alloy, ultra-high strength steels [24,27,38].

In comparison to the TRIP steel true stress-strain curves of 25 °C and 60 °C shown in Figure 2 [25], the warm rolled Hadfield steel true stress-strain curves demonstrated higher flow stresses and higher flow strains to necking. In comparison to engineering stress-strain curves of Zackay, Parker, Fahr and Busch [24] that demonstrated martensitic TRIP steel characteristics of constant load Luder strain, the warm rolled Hadfield steel (454 °C - 61%RT) demonstrated only increasing load engineering stress-strain curves. The 454 °C - 61% RT warm rolled Hadfield curve engineering strains and stresses were comparable in magnitude to the hardening portions of engineering strain in TRIP steel (test No. 8, [24]).

Engineering strains to fracture e_f were high, but necking strains e_n after peak load were usually quite low as shown in Table 5, implying that strain hardening occurred to plastic instability and close to fracture. With the low necking strains, fractures were of

a catastrophic nature, with little warning of imminent fracture, unlike alloys that undergo large localized necking strains and softening. In comparison to the as-solution treated condition, the warm rolled material specimens all showed decreased engineering strains to fracture, but in comparison to the solution treated condition, material of optimal ductility rolled at 399 °C and 454 °C, showed equal or greater necking strains.

True stress, true strain plots in all conditions showed near linear plastic strain hardening rates ($d\sigma/d\varepsilon$) to high levels of true uniform stress and true uniform strain, that correlated to engineering curves of increasing load to near fracture. The near linear strain hardening flow in all specimens could suggest similar deformation mechanisms of fcc combined slip and deformation twinning. In comparison to the solution treated condition, warm rolled material showed increased values of true uniform stress.

In order to demonstrate the near linear manner of the experimental true stress-strain hardening observed during deformation in tension, the true stress-strain curves were plotted on log-log axis in order to attempt a power law $\sigma = K\varepsilon^n$ fit, by $\log(\sigma) = \log(K) + n\log(\varepsilon)$ as attempted by Doepkin [3] and as shown in Figure 27.

An extrapolated log σ versus log ε elastic slope intercept at $\varepsilon = 1.00$ in Figure 27 (a) indicates an elastic modulus of approximately 28 $(10)^6$ psi, consistent with high strength austenitic steel. In the plastic region, similar results of plastic flow behavior were obtained as found by Doepkin for the solution treated condition. At low plastic strains shown clearly in Figure 27 (b), the log σ versus log ε plot correlated with linear behavior and power law hardening to strains of 0.02 to 0.04 corresponding to dislocation slip dominated flow [28]. For strains greater than 0.04, increasing deviation from linear behavior occurred, so that hardening behavior must have been influenced by some other mechanism than by power law hardening attributed to dislocation avalanche and dislocation dynamic recovery.

Exponential type hardening $\sigma = \sigma_o \exp^{k\varepsilon}$, has described a growing population of strain induced martensite and effects of transformation plasticity static hardening and dynamic softening during the strain induced transformation in metastable austenitic stainless steels [26-28].

An attempt was made to determine whether exponential hardening could describe plastic flow of any of the experimental tensile curves based upon a growing population of deformation twins-dislocations, and based upon contributions of strain softening and strain hardening. Plots of log σ versus ε indicated close fits in some cases, but the best

kind of correlation to the experimental true stress-true strain plastic flow curves above 0.04 strain was by simple linear $\sigma = k\varepsilon + \sigma_o$ plastic flow.

A higher correlation to exponential hardening plastic flow may have been obtained by recording instantaneous minimum diameter versus load [3], rather than an averaged reduced section engineering strain versus load. Exponential hardening plastic flow in Hadfield steel was not observed with the warm rolled material and procedure used in this study, but may be better obtained by strain hardening at deformation temperatures near -100 °C, as shown in Figure 1 [3].

Fits of true stress-strain plastic flow between approximately 0.04 strain to maximum true uniform strain, were made for linear plastic hardening as shown in Figure 28 for the as solution treated and for 454 °C warm rolled material. The maximum average strain hardening rate $d\sigma/d\varepsilon$ was 457 ksi for material rolled 454 °C with 0.46 ε_θ. Material rolled at 454 °C with 1.00 ε_θ and 0.75 ε_θ, had respective strain hardening rates of 442 and 440 ksi. High ductility solution treated material had an average strain hardening rate of 388 ksi. All linear fits indicated a close correlation to simple linear plastic strain hardening with the average strain hardening rates and the correlation coefficients listed in Table 7.

The values listed by engineering yield strength, engineering tensile strength, engineering strains and engineering ductility in Table 5 are trend plotted versus rolling temperatures for an effective near constant 0.75 effective warm roll strain in Figure 29, and are trend plotted versus effective warm roll strain for a constant roll temperature of 454 °C in Figure 30.

Figure 29 shows that for a near constant effective warm roll strain of 0.70 to 0.75, there was slight reduction of 0.2% yield strength and ultimate tensile strength with increased rolling temperature. Fracture strain, necking strain, per cent elongation, and reduction of area, all indicated a trend of approaching near optimal values of ductility for roll temperatures between 399 °C and 454 °C.

For the near optimal ductility, 454 °C warm rolled temperature condition, Figure 30 illustrates that a near linear increase of 0.2% yield stress and ultimate tensile strength occurred with increased effective warm roll strains of 0.46, 0.75, and 1.00. Ductility in fracture strain, per cent elongation, and reduction of area, all decreased near linearly with increased effective warm roll strain, but necking strain ductility reached a maximum value at 0.75 effective warm roll strain. These necking strains from the 0.75 ε_θ, 454 °C rolled material were equal or greater than the necking strain values from the as-solution treated condition material.

True uniform stress and strain shown Table 6 are plotted in Figure 31 for material rolled a constant reduction at 0.70-0.75 ε_e versus roll temperatures of 343 °C, 399 °C, and 454 °C. Figure 31 illustrates that both true uniform stress and true uniform strain reach near maximum average experimental values at, or slightly above 399 C.

True uniform stress-strain average and peak values are shown in Figure 32 for a constant roll temperature of 454 °C versus warm roll effective strains of 0.46, 0.75, and 1.00. The trends of Figure 32 (a) indicate that warm roll strains beyond 0.75 sharply increased average and peak values of true stress. True uniform strain average, and peak values shown in Figure 32 (b), for a roll temperature of 454 °C, showed a near linear decrease of uniform strain versus effective warm roll strain.

It is known that in order to process materials to high strength levels, yet obtain satisfactory and consistent values of ductility and fracture toughness, high purity and optimal ingot solidification grain structures that reduce segregation are required. High strength materials not of high purity, such as air melted steels are known to result in high strength materials with low ductility and toughness.

Since the present study used continuous cast ingot material not of the highest cleanliness, that also included shrinkage and solidification segregation defects, further improvements in mechanical properties of warm rolled Hadfield steel could be achieved by using advanced processing techniques of electroslag refining or vacuum/argon induction melting and casting, followed by vacuum arc refining.

Along with requirements of high purity and optimal ingot structure for optimal mechanical properties, select forging, solution treatment, and warm rolling techniques must be used. Hadfield steel forge temperatures near 980 °C may result in hot shortness [5] and improper solution treatment or warm rolling may introduce carbides. Carbide precipitates of low interfacial strength may have caused low uniform strain and low strain hardening shown in Table 3 from an earlier study [38] by introduction of a void nucleation softening and fracture mechanism.

5.6 Metallography of Warm Rolled and Tension Tested Material

Microstructures of 0.75 ε_e warm rolled material tested in tension 0.16 to 0.18 ε_u shown in Figure 20, are similar to 0.75 ε_e warm rolled microstructures shown in Figure 10, because any microstructural changes acquired during low strains in tension after the high rolling strains were not greatly distinguishable.

Material warm rolled at 454 °C to $0.46\varepsilon_e$, then tested in tension at 23 °C to $0.27e_u$ had more equal distribution of strains and clearly showed recognizable differences in structure as demonstrated in Figure 9(b) for warm roll strains of 0.46, and as demonstrated in Figure 21 for warm roll strain of 0.46 plus uniaxial 0.27 strain in tension. The most recognizable difference is apparent from increased grain elongation and by increased density of structures previously identified as Hadfield steel deformation twins [4,10,11,21,22]. This 0.46 ε_e + 0.27 ε_u condition shown in Figure 22 indicates that a complex microstructure of twins and shear bands has developed after both warm rolling and after tension testing, and that the extent of twinning and dislocation slip among the grains is dependent on crystallographic orientation.

The crystallographic orientation of microstructures in Figure 22 may be basically understood by orientation dependence of Schmid factors for fcc slip and twinning [28,29] during axisymmetric deformation, as shown in Figure 33. For the particular {111} plane shown in Figure 33, the most favorable Schmid factor in compression is shown to be along the [001] load axis for deformation by twinning and the least favorable Schmid factor in compression is along the [111] load axis by twinning. For deformation in tension, the most favorable Schmid factor is along the [001] load axis for slip, and the least favorable Schmid factor is along the [001] load axis for twinning. Thus grains may have high values of Schmid factors for slip, for mixed slip and twinning, or for twinning, and a particular grain orientation may favor one or a more of these deformation mechanisms as shown by the observed results of Figure 22.

It is known that twinning, in comparison to slip, cannot alone provide strains of the large magnitudes observed in solution treated Hadfield steel. A single fcc crystal originally oriented so as to have the maximum resolved shear stress applied to it, may have a first order twinning contribution of strain in tension of approximately 0.40 [14]. Thus, crystals that undergo high strains by twinning and slip must undergo a large strain contribution by slip deformation. The slip contribution may be provided by slip bands, twin accommodation dislocations, and shear bands made up of highly active and localized slip bands.

Although the slip shear bands shown in Figure 22 are the less common structure than structures suggested to be deformation twins, the contribution of strain contributed by the shear bands is large and localized, and suggests that slip has contributed significantly to deformation. The observed shear bands of Figure 22 have usually localized within one or two grains and are most common within grains of low twin density. The shear bands appear to be present in all grains, but are hardly

distinguishable in some grains where twins and slip bands are oriented in particular orientations.

5.7 Fractography

Material that was warm rolled to 0.70 to 0.75 effective warm roll strains at 343 °C, 399 °C, and 454 °C, and that was strained in tension to fracture, showed a trend of increased ductility versus increased warm roll temperature. This increased ductility by material rolled at 454 °C shown in Figure 29, correlated to a trend of increased strain to necking as determined by strain to fracture less necking strain ($e_f - e_n$). Increased ductility also correlated to greater necking strain and to greater grain boundary decohesion in tension as shown in Figure 26, rather than catastrophic final fracture by shear as observed in specimens rolled at lower temperatures. The roll temperature of 454 °C resulted in higher values of engineering fracture strains, and of engineering necking strains, with engineering necking strains that equalled or exceeded the necking strains of lower strength solution treated condition material.

Grain boundary decohesion fracture that correlated to results of optimal ductility may have been initiated by grain boundary precipitates as shown in Figure 26. These precipitates may have been the result of warm rolling reheating, or improper solution treatment practice. The solution treatment temperature chosen was within the standard range used in commercial practice and was from within a solution treatment temperature range that resulted in an austenitic structure in an earlier study [38].

It is possible that the specimens that failed predominantly in shear after only small decohesion fractures in tension had become sensitive to embrittlement during processing at the lower rolling temperatures. Although grain boundary precipitates are known to cause embrittlement in Hadfield steel, steel embrittlement mechanisms may be dependent upon processing temperature and may be the result of carbide structure or of impurities that segregate to grain or boundary structures [34,35]. Grain boundary or structure impurity segregation in low cleanliness steels at high strength levels may also enhance sensitivity to stress corrosion cracking.

A preliminary warm rolling strengthening and tension test study of Fe-12.5Mn-2.01Mo-1.15C Hadfield steel [38] resulted in inferior mechanical properties and in flow behavior that inferred that a dominant softening mechanism occurred. The softening mechanism is suggested to have resulted from carbide precipitates, that were observed by optical microscopy to have formed after warm rolling. This occurrence of

carbide precipitation in the preliminary study is suggested by known precipitation and phase transformation behavior in Hadfield steel that is enhanced by prior strain [5,41].

The Hadfield steel used in the preliminary study [38] was solution treated at 1030 ° C for one hour and water quenched, then rolled to 50% reduction of thickness by a reduction rate of 0.010 inch reduction per pass with air furnace reheats between passes. The long periods of time at temperature during this warm rolling may easily have promoted carbide precipitation not closely associated with strain defect structure.

The preliminary warm rolling study of Hadfield steel had low values of true uniform strain and true uniform stress, but high values of yield stress. Fracture surfaces of the preliminary tension specimens showed a high population density of ductile dimples on fracture surfaces associated with void nucleation and growth. This fracture microstructure provided evidence of a deformation mechanism that could influence plastic flow and dislocation slip through void nucleation and growth softening, and that could influence fracture by a void coalescence fracture mechanism.

The preliminary results shown in Table 3 that included large reductions of area, low per cent elongation, and low true uniform strain, also suggested void nucleation softening may have prevented hardening by influencing plastic flow and dislocation slip through a strain softening mechanism rather than a twinning influenced strain softening-hardening mechanism.

5.8 Potential Armor Applications

Since this study was initially motivated by the potential application of high strength warm rolled Hadfield steel to armor structures, several subjects of interest should be discussed. Although some results suggest that this material may provide resistance to adiabatic shear instability at high strength levels, high strain rate adiabatic deformation and shock resistance of this experimental warm rolled Hadfield steel has not been studied under ballistic conditions and thus the potential for severe or armor service is unknown.

Armor service primarily requires high hardness for resistance against plastic flow or ductile penetration [42],but as strength levels increase in armor other problems such as adiabatic shear instability [43] or spalling can occur. Cold rolled high hardness Hadfield steels have shown comparable resistance to ballistic penetration as that of quenched and tempered steels of lower hardness [43], and the hardness levels between Rc 52-53 of warm rolled Hadfield steel in the present study could be competitive with quenched and tempered steel in some armor applications.

Adler [4] has shown that Hadfield steel shows weak hardening in tension compared to hardening in compression during mixed slip-twinning deformation, and it is known that stress of high intensity in tension, in combination with intrinsic material flaws, can lead to fracture.

Roberts [10], Champion [12] and Dorph [13] have investigated the shock hardening response of solution treated Hadfield steel by TEM, and it is known that this steel is hardened to high strengths above 600 DPH by compressive shock through structural refinement. Structural refined shock hardened microstructures of Hadfield steel are known to contain a large volume fraction of fine deformation twins accompanied by a large population of dislocations.

Ballistic impact or explosive loading may introduce high shock pressures in tension from interface shock wave reflection so that it is conceivable that high pressures sustained earlier in compression by structural refinement hardening would not be sustained in tension. This high anisotropic hardening in compression compared to low hardening and high stress intensity in tension from a rapid reversal of stress state is predicted to cause catastrophic failure of warm rolled Hadfield steel under shock loading through spall fracture or shattering.

Hadfield steel sustainable loads and hardening in compression could be greater than those sustainable in shear. If initial ballistic pressures are compressive, high strength Hadfield steel would again sustain damage by structural refinement and hardening. If the compressive state of stress transitions to shear, it may infer that high pressures would not be further sustained by lower structural refinement hardening and by the high levels of stress intensity combined with material flaws.

Some approaches of modeling the behavior of ballistic failures from adiabatic shear have come to the conclusion that high rates of strain hardening at high strength levels are especially important for resistance to adiabatic shear instabilities at high strain rates [43]. Results of the present study have demonstrated high strength and resistance to plastic flow instability by strain hardening and by increased load carrying capacity to high engineering strains to fracture. Since the linear plastic strain hardening rate, of warm rolled Hadfield steel was increased by warm rolling from 388 ksi to the 440-457 ksi range and since plastic flow was described by high engineering strains and increasing loads, warm rolled Hadfield steel could provide improved resistance to adiabatic shear.

One uncertainty or disadvantage of warm rolled Hadfield steel strain hardening rate is the relatively low rate of strain hardening at low strains of less than 0.04 strain in comparison to quenched and tempered steels.

6.0 Conclusions and Recommendations

6.1 Conclusions

The purpose of the study was successfully met in that warm rolled material plastic flow behavior at high levels of strength was observed to be similar to solution treated Fe-12.5Mn-1.15C and Fe-12.5Mn-2.0Mo-1.15C Hadfield steel. Increasing load was carried to high levels of uniform strain with accompanied moderate rates of linear plastic strain hardening to high values of stress.

In comparison to previous results [36,38] shown in Table 3, the present study and investigator has obtained significant improvements of strength, ductility, and strain hardening rate ($d\sigma/d\varepsilon$) for TMT processed Fe-12.5Mn-2.0Mo-1.2C Hadfield steel.

Thermomechanical treatment by warm rolling provided improvement of yield stress, ultimate tensile strength, true uniform stress at initiation of necking instability, and slight but detectable necking strain improvements in one material condition. Strain hardening rates in linear plastic flow were significantly increased over the solution treated condition.

Plastic flow of solution treated and of warm rolled material at low levels of plastic strain from 0.01 to 0.04 was consistent with power law hardening by a linear relation of log stress vs log strain. In comparison to quenched and tempered steel hardening at low strains, the Hadfield steel work hardening rates are low.

At increasing plastic strains above 0.04 strain to fracture, the strain hardening exponent of power law hardening continuously increased so that power law hardening did not correlate with experimental strain hardening behavior. Plastic flow above 0.04 strains in all conditions instead correlated to linear plastic strain hardening and in this range of plastic flow the work hardening rates of Hadfield steel are high in comparison to quenched and tempered steel. These high strain linear plastic strain hardening rates were increased from the solution treated condition of 388 ksi to 440-457 ksi.

Optical metallography results of material warm rolled at 454 °C with increasing effective strains of 0.29, 0.46, and 0.75 demonstrated increasing density of Hadfield steel deformation twins. Material warm rolled at a near constant strain 0.70 to 0.75 effective strain with increasing temperatures of 343 °C, 399 °C and 454 °C resulted in deformation twins at all temperatures and a slight trend of decreasing twin density with increasing roll temperature.

Warm rolled hardness results demonstrated that hardness was strongly dependent on warm roll strain and only weakly dependent on roll temperature, so that a slight decrease of hardness occurred with increased warm roll temperature. Rapid hardening increments were obtained for warm roll effective strains less than 0.60 and a lesser rate of hardening with further strains. Maximum hardness of Rc 53.2 was obtained at 343 °C by an effective warm roll strain of 0.93 while hardness of Rc 52.2 was obtained for 1.00 effective strain at 454 °C.

Material warm rolled at a near constant 0.70 to 0.75 effective strain demonstrated a weak dependence of yield and ultimate tensile strength upon warm roll temperature, but engineering strain to fracture, elongation, and reduction of area increased with increased warm roll temperature. True uniform strength and true uniform strain increased to a maximum value between 399 °C and 454 °C. Yield strengths of this 0.70-0.75 effective strain material ranged between 203-214 ksi, and ultimate tensile strength ranged between 259-268 ksi with 0.17 to 0.23 engineering strains to fracture

Material warm rolled at 454 °C demonstrated that yield and ultimate tensile strength increased in a near linear manner with increased effective warm roll strain. Engineering strain to fracture and ductility as measured by elongation and reduction of area decreased at a decreasing rate with increased warm roll effective strains. True uniform stress at initiation of fracture increased with increased warm roll strain and true uniform strain decreased with true uniform stress such that an inverse relation was observed with between true uniform strength and true uniform strain. This material that was rolled at 454 °C with 0.46, 0.75 and 1.00 effective strain resulted in yield strength of 167 ksi to 233 ksi, ultimate tensile strength of 239 ksi to 276 ksi, and engineering strain to fracture of 0.32 to 0.17. True uniform stress and strain ranged from 313 ksi and 0.27 ε_u to 323 ksi and 0.16 for this material rolled between effective strains of 0.46 to 1.00.

Fracture of warm rolled material with the greatest engineering strains to fracture and the greatest necking strains demonstrated fracture initiation by a mixed mode fracture that included grain boundary decohesion by void nucleation-coalescence ductile dimple fracture and cleavage fractures at annealing twin boundaries. The decohesion fractures were associated with necking strain of near constant or decreasing loads in tension. Final fracture occurred catastrophically with little warning and without significant necking or geometric softening as observed in maraging steels and low alloy

quenched and tempered steels. Cracking was observed but could not be directly associated to early or final fracture.

The results suggest that warm rolled Hadfield steel deformation twins may be utilized for the purpose of influencing plastic flow behavior. Some evidence of this is provided by deformation twin structures of near equal twin density observed for equivalent roll reductions over the range of roll temperatures and by deformation twins that appear to increase in density as warm roll strain is increased. Optical microscopy of warm rolled and tension tested material provides evidence of a anisotropic twin structure that is dependent upon grain orientation.

Other circumstantial evidence is consistent with twinning behavior. Hardening in tension at high levels of plastic strain was not described by power law hardening as it was at low strains and the power law strain hardening exponent increased with strain as in previous results [3]. Plastic flow at high strains was described by linear plastic flow. The plastic flow behavior at ultra-high strength levels in comparison to low alloy steel at the same yield stress was described by fairly low rates of hardening at low strains of less than 0.04 and by high rates of hardening at high strains during uniform elongation and increasing loads to near fracture. Finally the uniform ductility and increasing loads in tension to near fracture suggested the operation of a strong hardening mechanism and the relatively low rate of hardening at low strain suggested a softening mechanism, consistent with twinning influenced plastic flow.

6.2 Recommendations

The experiment resulted in material with excellent qualities of high strength, ductility, and high strain hardening, so further work is recommended to demonstrate the potential for service applications. The results strongly suggest, but do not conclusively prove, the occurrence of deformation twinning during warm rolling and in service. The high strain hardening rates, high strength, increasing load to fracture, and high ductility suggest that ductile penetration and adiabatic shear instability resistance may be provided by this material in armor service, but again, conclusive proof is required.

Transmission electron microscopy may easily determine twinning structure. High strain rate torsional shear tests can evaluate adiabatic shear resistance, and ballistic impact testing can evaluate resistance to penetration, adiabatic shear, shock, and spall. Fracture toughness testing by the J- integral method is recommended to determine the toughness, plastic flow and fracture behavior in the presence of a sharp crack defect.

Table 1:
Standard ASTM Specification Grades of Hadfield Steel
Composition Ranges ASTM A128

Grade	C	Mn	Mo	Fe	Si(max)	P(max)
A	1.05-1.35	11.0 (min)	0.0	Bal	11.00	0.07
E2	1.05-1.45	11.0-14.0	1.8-2.1	Bal	1.00	0.07

Table 2 :
Typical Engineering Properties of ASTM Grade Hadfield Steel

Following Standard Processing Method of Solution Treatment and Water Quenching

Cast (C) or Cast-Forge (F),
Solution Treated (ST): Austenitize > 1000°C, Water Quench

Mechanical Properties (typical)

Grade	Condition	Y.S. (ksi)	U.T.S. (ksi)	El.(%)	R.A.(%)
A	C,ST	44-54	80-130	5-40	15-40
A	F,ST	44-56	110-130	40-60	35-50
E2	C,ST	64	130	43	15-40

Table 3 Preliminary Results: Warm Rolled Strengthened Hadfield Steel, Engineering and True Stress-Strain Properties in Tension [36-38]

(a) Engineering Stress-Strain Property Results
High Purity Argon Arc Material Fe-14Mn-2.01Mo-0.97C
Process: 50%ROA @ 427°C
(material provided by Staker [36], tested by Chinella [38])

Tested in Air

0.2% YS	UTS	El	RA	True Uniform Stress	True Uniform Strain	Strain Harden Rate ($d\sigma/d\varepsilon$)
(ksi)	(ksi)	(%)	(%)	(ksi)		(ksi)
180	241	-	-	277	0.15	-
184	241	17	16.4	280	0.15	454

Tested in Vacuum

0.2% YS (ksi)	UTS (ksi)
189	252
-	251

(b) Fe-12.5Mn-2.01Mo-1.15C [37]
AOD/ ESR, Warm Swaged: 50% ROA @ 427°C

0.2% YS (ksi)	UTS (ksi)	El (%)	RA (%)
215	264	13.8	19.8

(c) Engineering Stress-Strain Property Results [38]

Process	Hardness (HRc)	Bar #	0.2% YS (ksi)	UTS (ksi)	El (%)	RA (%)
50% ROA @ 700 F						
	48.3	3	212	254	15.9	47.7
	48.3	4	215	252	-	-
50% ROA @ 800 F						
	48.9	5	207	243	15.3	42.1
	48.9	6	205	248	-	-

True Stress-Strain Tensile Property Results [38]
(Uniform Stress and Uniform Strain At Plastic Instability)

Process	Hardness (HRc)	Bar #	True Stress (ksi)	True Strain (in./in.)	Strain Harden Rate ($d\sigma/d\varepsilon$) (ksi)
50% ROA @ 700 F					
	48.3	3	285.7	0.12	383
	48.3	4	266.4	0.06	572
50% ROA @ 800 F					
	48.9	5	273.7	0.12	329
	48.9	6	279.6	0.12	397

Table 4 Experimental Results of Warm Rolled Reduction of Thickness, Effective Strain, Hardness

Roll Temperature T(°C)	Reduction of Thickness RT(%)	Effective Strain ε_e	Hardness Rc
343	41	0.57	48.7
343	*49	0.73	51.0
343	58	0.93	53.2
399	38	0.52	47.2
399	*48	0.70	49.5
399	54	0.85	51.0
399	59	0.96	52.0
454	23	0.29	39.1
454	*35	0.46	45.3
454	*50	0.75	49.7
454	*61	1.00	52.2

*Tension Specimens Prepared

Table 5 Engineering Stress, Engineering Strain, Tension Test Results

Temp. (°C)	ε_e	0.2% Y.S. (ksi)	U.T.S. (ksi)	e_f	e_n	R.A. (%)	El. (%)
ST	0.0	66.8	162.2	0.87	0.02	51	72
ST	0.0	64.0	161.9	0.90	0.01	50	81
454	0.46	168.3	241.1	0.31	0.01	27	27
454	0.46	166.5	238.5	0.32	0.01	27	30
454	0.75	202.8	259.4	0.22	0.03	22	23
454	0.75	204.4	261.1	0.23	0.01	19	23
454	1.00	233.7	276.1	0.17	0.01	16	14
454	1.00	226.7	274.8	0.18	0.01	18	17
399	0.70	204.3	261.9	0.21	0.02	19	22
399	0.70	201.6	264.1	0.22	0.01	20	23
343	0.73	213.8	260.6	0.19	0.01	17	21
343	0.73	208.7	267.6	0.17	0.01	15	19

ST = solution treated
T = warm roll temperature
ε_e = warm roll effective strain
e_f = engineering strain to fracture
e_n = engineering necking strain

Table 6 True Uniform Stress, True Uniform Strain Tension Test Results

T(°C)	ε_e	σ_u(ksi)	ε_u	σ_f(ksi)	ε_f
ST	0.0	299.6	0.61	306.9	0.70
ST	0.0	305.8	0.64	296.4	0.68
454	0.46	312.3	0.26	315.1	0.30
454	0.46	312.9	0.27	315.9	0.31
454	0.75	310.2	0.18	331.5	0.25
454	0.75	316.6	0.19	311.7	0.21
454	1.00	320.1	0.15	319.3	0.17
454	1.00	322.8	0.16	329.5	0.20
399	0.70	309.3	0.17	322.0	0.21
399	0.70	320.6	0.19	322.4	0.22
343	0.73	307.0	0.16	309.0	0.18
343	0.73	310.2	0.15	312.6	0.15

ST = solution treated

T = warm roll temperature

ε_e = warm roll effective strain

σ_u = true uniform stress = $P/A_o(1+e)$, where P = load

ε_u = true uniform strain = $\ln(1+e)$, where e = eng. strain to max load

σ_f = true fracture stress.= P/A_i, where A_i = instantaneous area

ε_f = true fracture strain = $2\ln(do/di)$, where

d = initial and instantaneous diameters

Table 7 Average Linear Plastic Strain Hardening Rate
($d\sigma/d\varepsilon$, $0.04 < \varepsilon < \varepsilon_u$)

Roll Temperature	Reduction of Thickness	Effective Strain	Strain Hardening Rate	Correlation Coefficient
T (°C)	RT (%)	ε_e	$d\sigma/d\varepsilon$ (ksi)	R
ST	0.0	0.00	388	0.998
454	35	0.46	457	0.999
454	50	0.75	440	0.998
454	61	1.00	442	0.999

ST = solution treated

(a) [3]

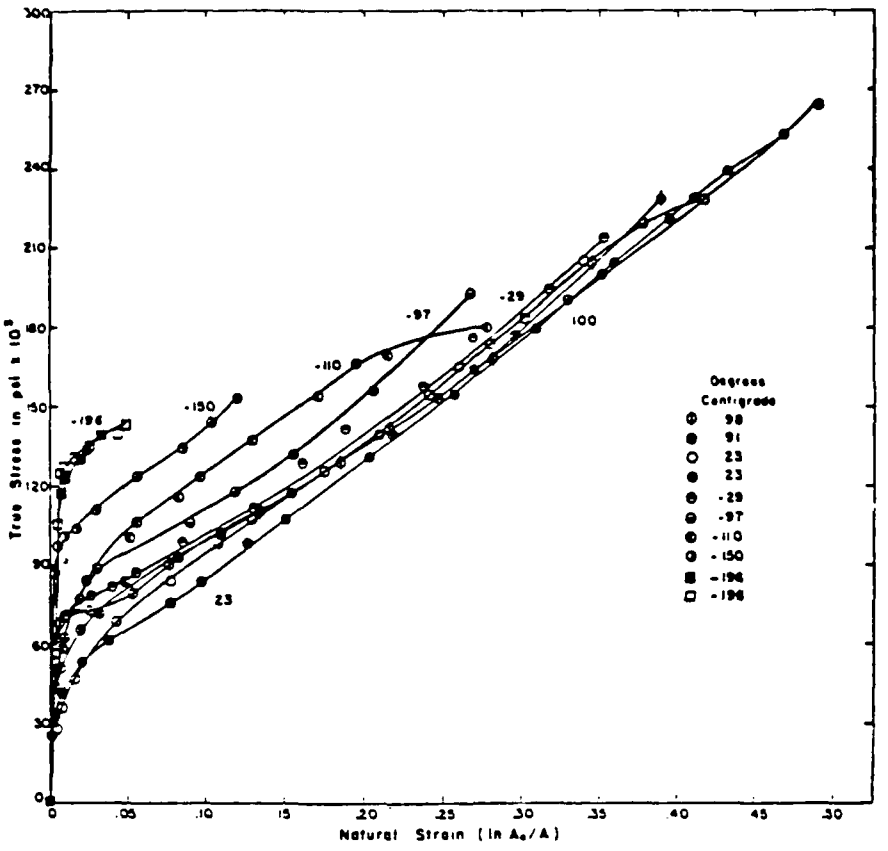

(b) [1]

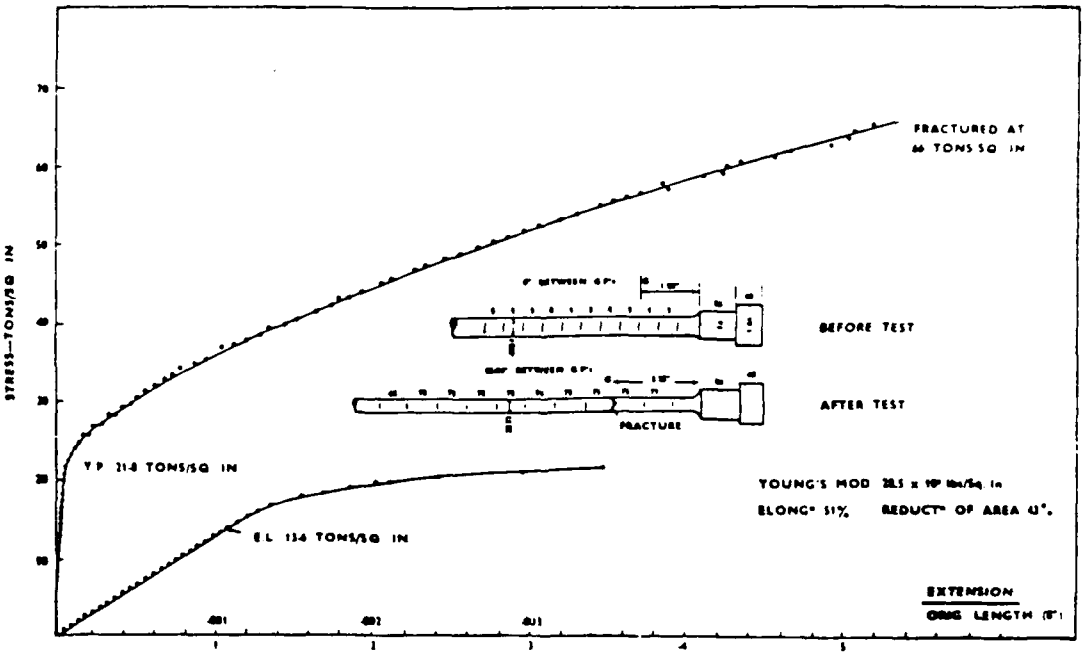

Fig. 1 Hadfield Steel Temperature Dependent True Stress-Strain (a,b) Curves [3], and Engineering Stress-Strain Curves [1]

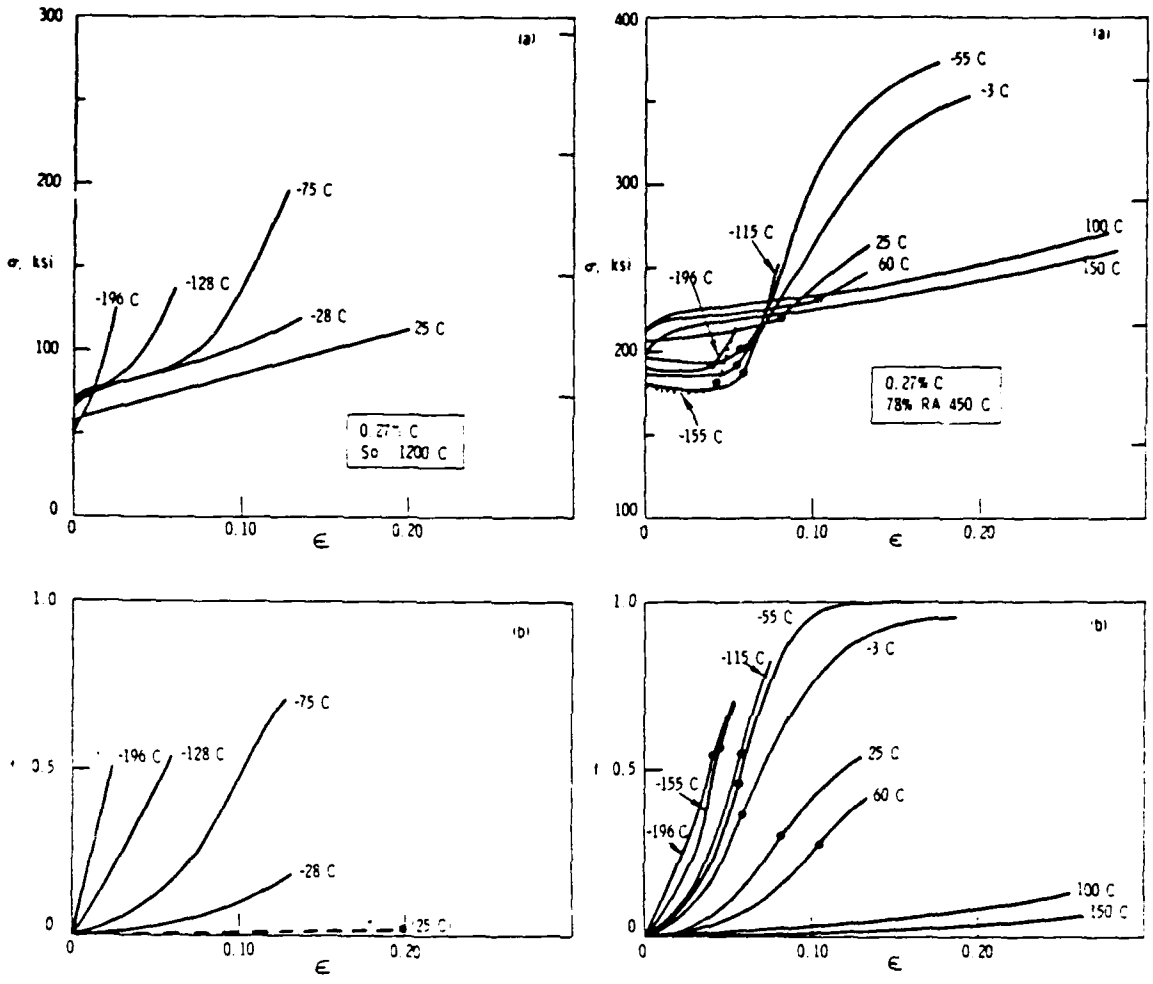

(a) Solution treated condition

(b) Solution treated and warm rolled condition

Fig. 2
(a, b) Temperature Dependent Stress-Strain Curves and Transformation Curves in Tension of 0.27 % C TRIP Steel [12]

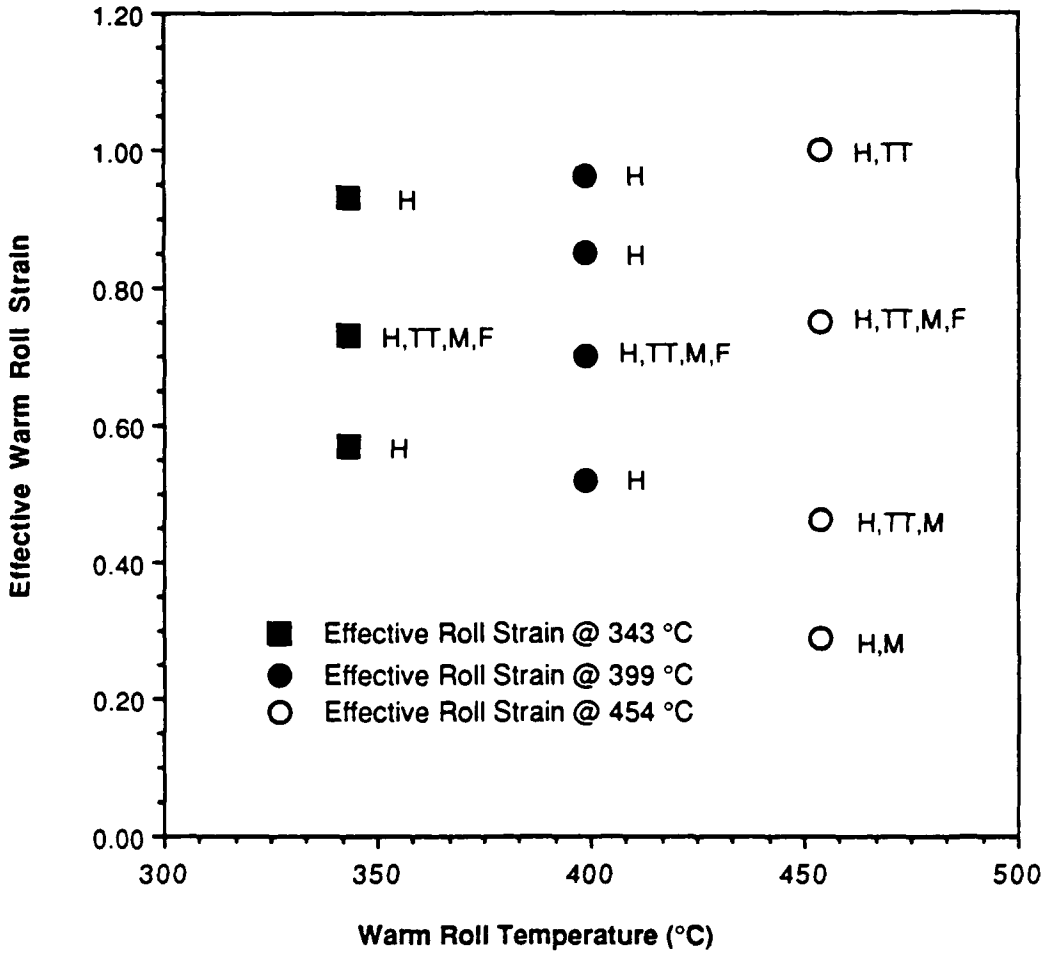

Fig. 3

Experimental Test and Study Matrix of Warm Rolled Fe-12.5Mn-2.01Mo-1.15C Hadfield Steel
Matrix Legend: H = Rockwell Rc Hardness, TT = Tension Test, M = Optical Microscopy, F = SEM Fractography

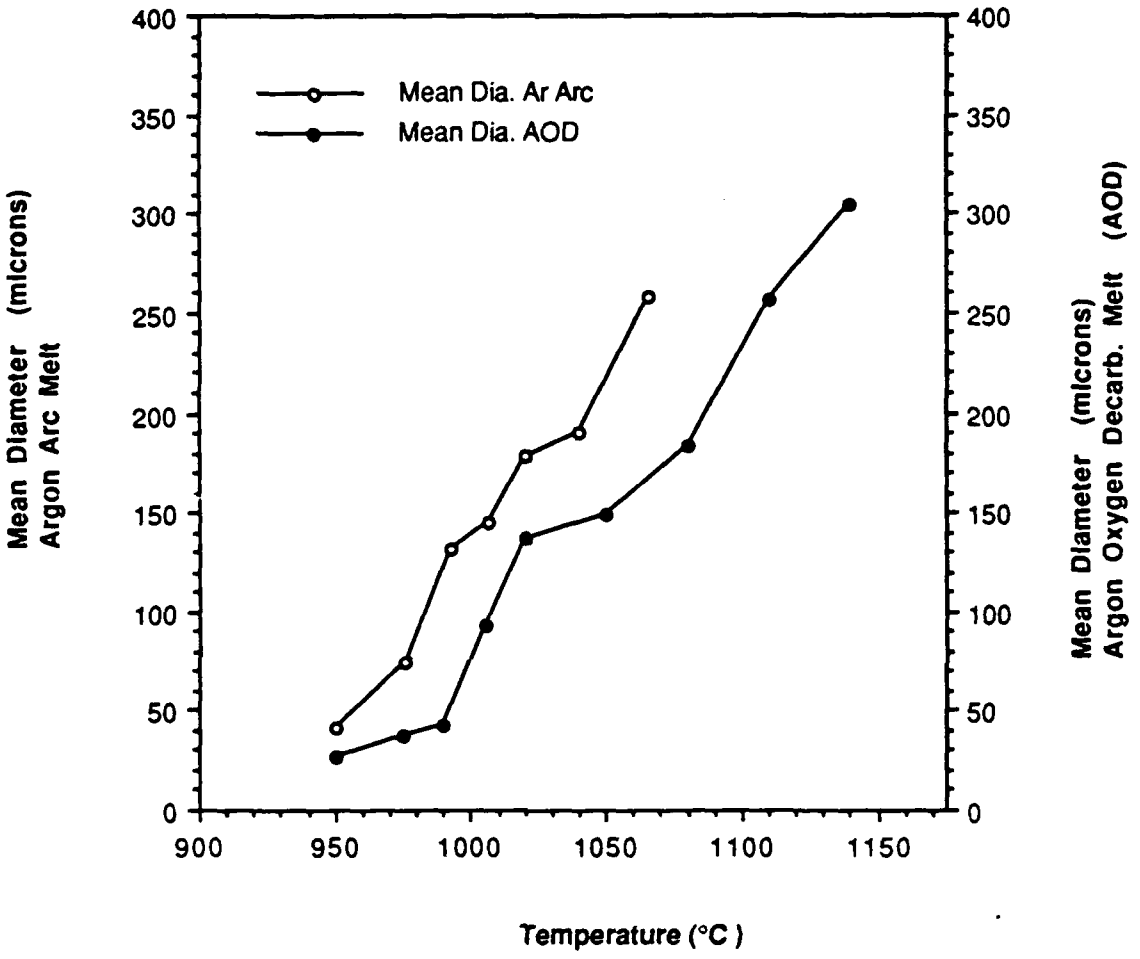

Fig. 4 Mean Grain Size Vs Solution Treatment Temperature, One Hour at Temperature and Water Quench

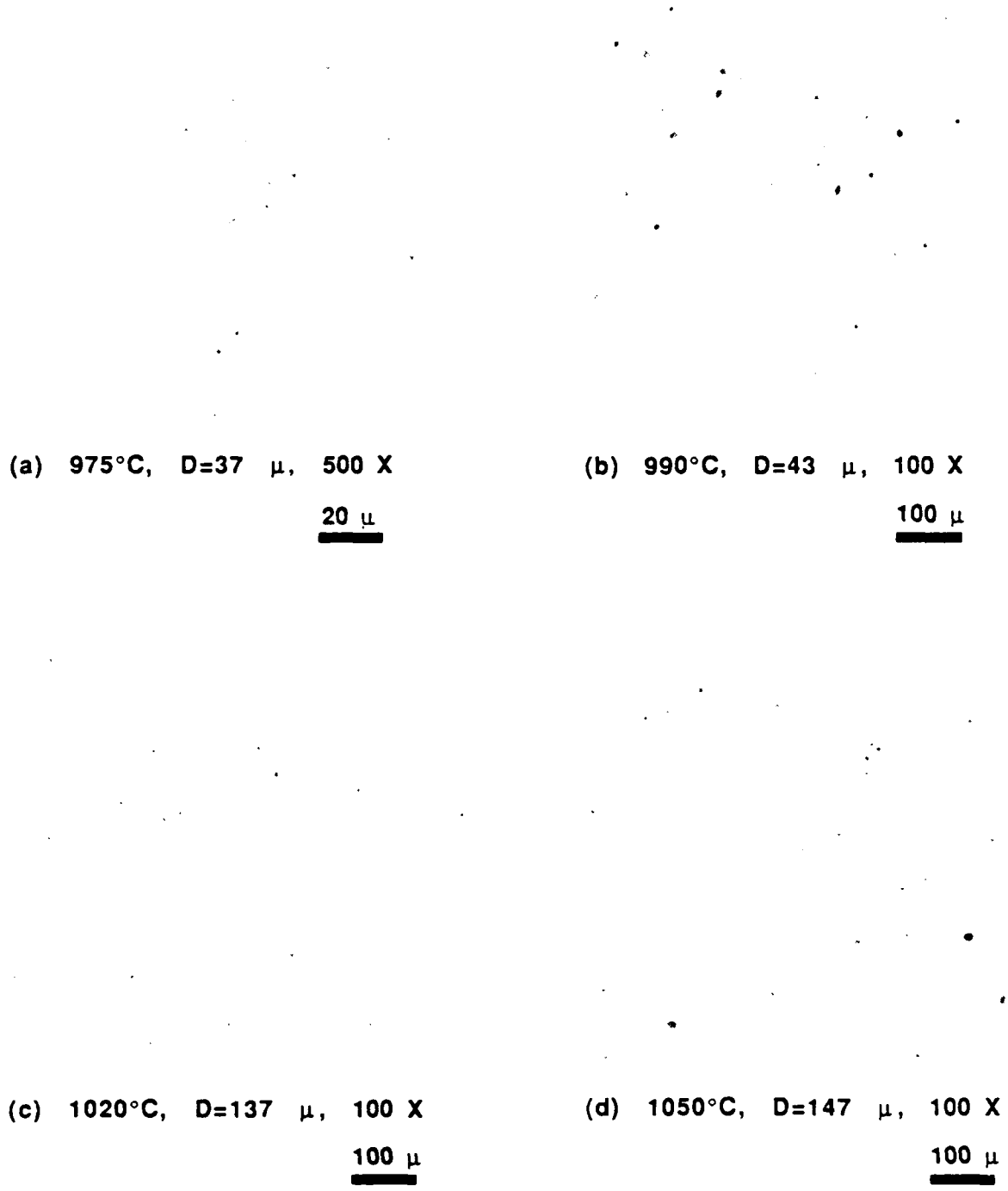

(a) 975°C, D=37 μ, 500 X

20 μ

(b) 990°C, D=43 μ, 100 X

100 μ

(c) 1020°C, D=137 μ, 100 X

100 μ

(d) 1050°C, D=147 μ, 100 X

100 μ

Fig. 5 Solution Treatment Study, Fe-12.5Mn-2.01Mo-1.15C (a-d) Hadfield Steel, Microstructures, Temperatures, and Mean Grain Size (D), Results after One Hour at Temperature with Water Quench, Initial Condition Solution Treated and Warm Rolled 50% RT at 427 °C, Na_2CrO_4 Etch

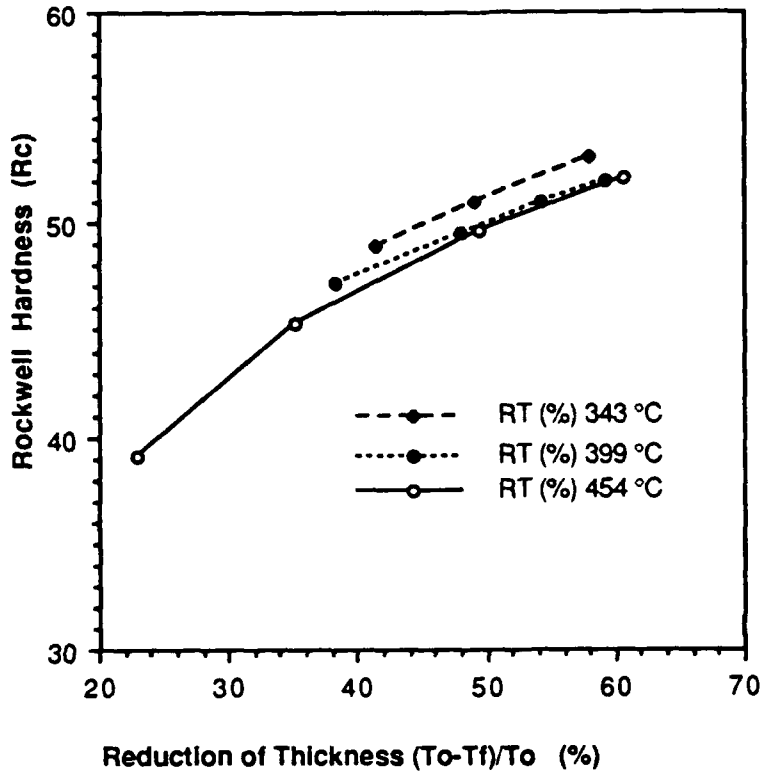

(a)
Rockwell Rc Hardness
Vs Reduction
of Thickness

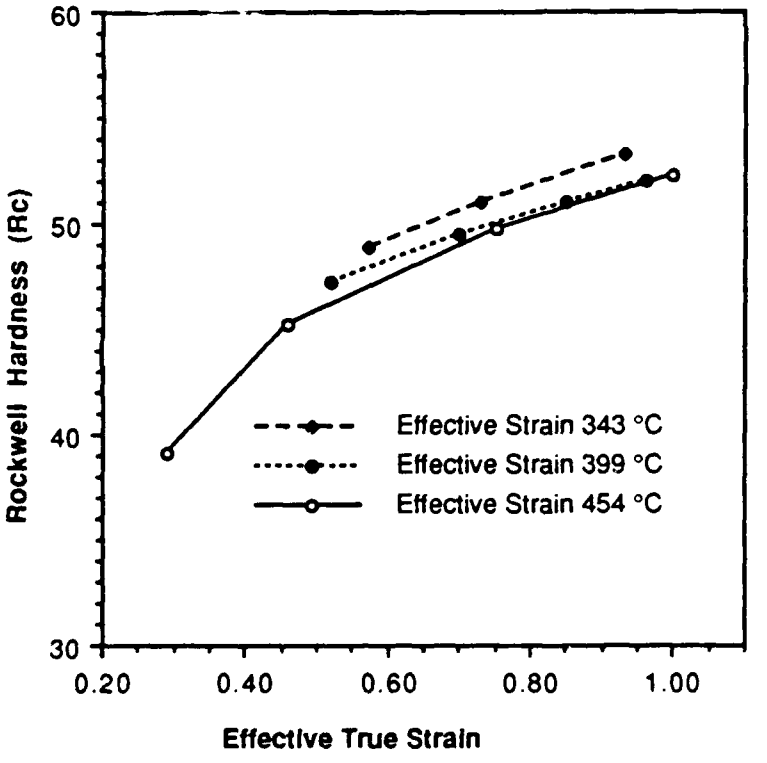

(b)
Rockwell Rc Hardness
Vs Effective Strain

Fig. 6
(a,b) Warm Rolled Fe-12.5Mn-2.01Mo-1.15C Hadfield Steel
Rockwell (Rc) Hardness

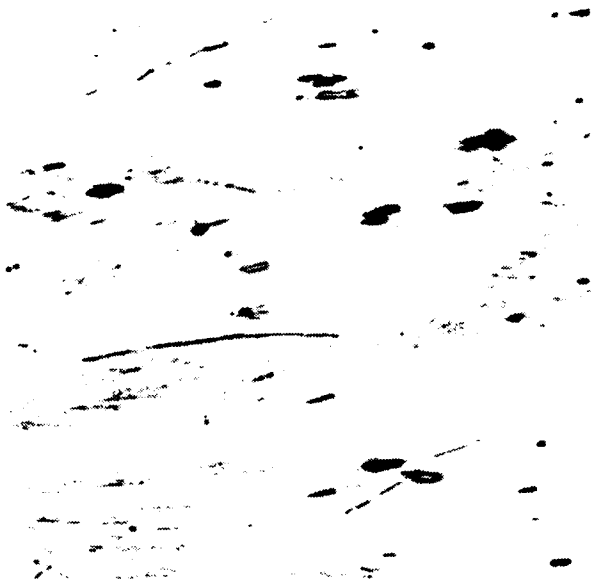

Fig.7

Solution Treated and Tension Tested Microstructure, Fe-12.5Mn-2.01Mo-1.15C Hadfield Steel, Na_2CrO_4 Etch

200 X 50 μ

(a) Less Than 0.64 True Uniform Strain

200 X 50 μ

(b) Less Than 0.64 True Uniform Strain

500 X 20 μ

Fig. 8 Solution Treated and Tension Tested Microstructure, Shoulder (a, b) Section, Fe-12.5Mn-2.01Mo-1.15C Hadfield Steel, HCl Electrolytic Etch

(a) 0.29 Effective Strain

200 X 50 μ

(b) 0.46 Effective Strain

200 X 50 μ

(c) 0.75 Effective Strain

200 X 50 μ

Fig. 9
(a-c)

Warm Rolled Microstructure, Fe-12.5Mn-2.01Mo-1.15C Hadfield Steel, 0.29, 0.46 and 0.75 Effective Strain at 454 °C Na_2CrO_4 Etch

(a) 0.73 Effective Strain at 343 °C

200 X 50 μ

(b) 0.70 Effective Strain at 399 °C

200 X 50 μ

(c) 0.75 Effective Strain at 454 °C

200 X 50 μ

Fig. 10
(a-c)

Warm Rolled Microstructure, Fe-12.5Mn-2.01Mo-1.15C Hadfield Steel, 0.70-0.75 Effective Strain at 343 °C, 399 °C and 454 °C, Na_2CrO_4 Etch

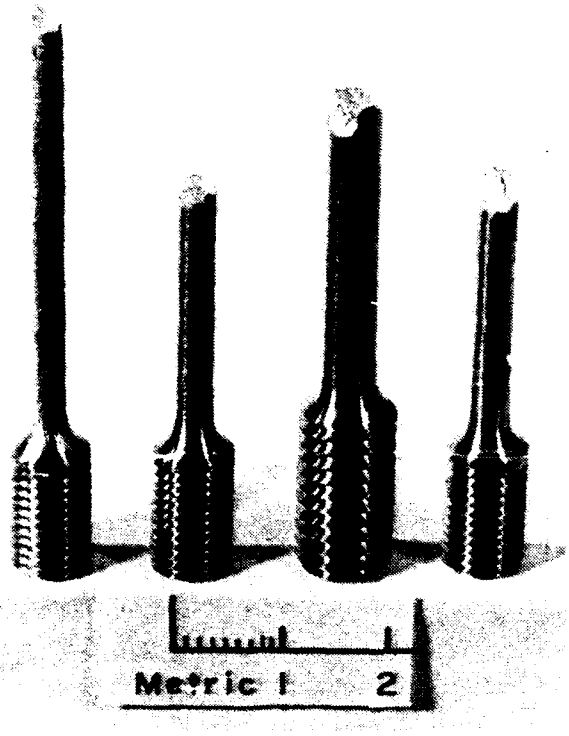

(a) (Left to right)

(1) As solution treated and tested in tension 0.64 ε_u at 23°C, (2) rolled 0.46 ε_e at 454°C and tested in tension 0.27 ε_u at 23°C, (3) rolled 0.75 ε_e at 454 °C and tested in tension 0.19 ε_u at 23°C, (4) rolled 1.00 ε_e at 454 °C and tested in tension 0.17 ε_u at 23°C

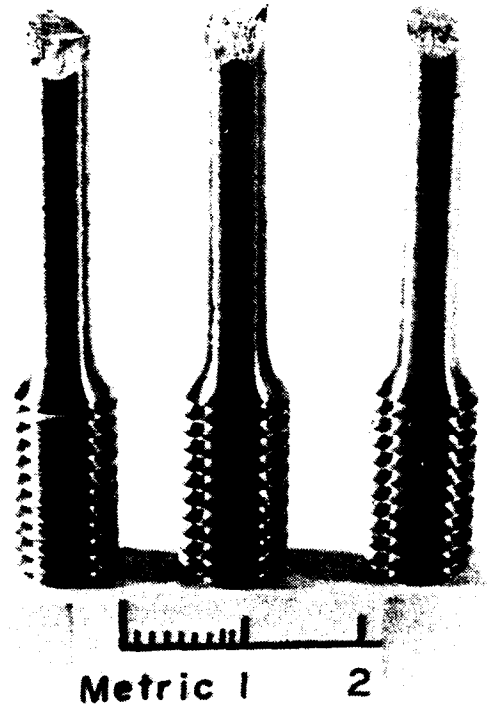

(b) (left to right)

(1) rolled 0.73 ε_e at 343°C and tested in tension 0.15 ε_u at 23 °C (2) rolled 0.70 ε_e at 399 °C and tested in tension 0.19 ε_u at 23 °C, (3) rolled 0.75 ε_e at 454 °C and tested in tension 0.19 ε_u at 23 °C

Fig. 11
(a, b)

Tension Tested Specimen Macrographs
Fe-12.5Mn-2.01Mo-1.15C Hadfield Steel,
Solution Treated Condition,
Warm Rolled Condition

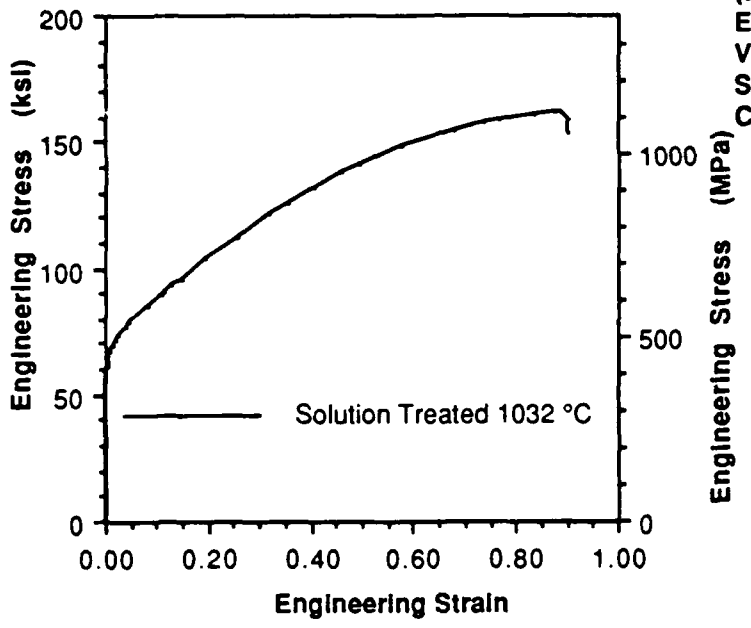

(a)
Engineering Stress
Vs Engineering Strain
Solution Treated
Condition

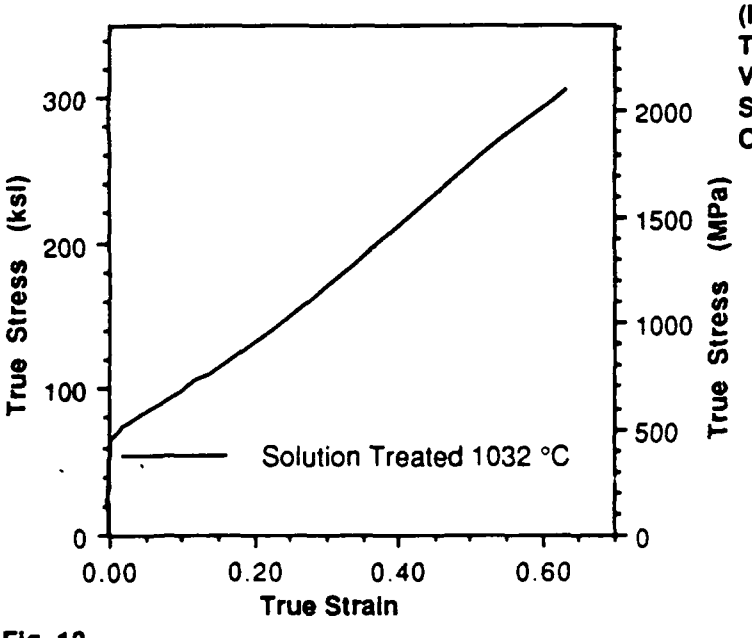

(b)
True Uniform Stress
Vs True Uniform Strain
Solution Treated
Condition

Fig. 12
(a,b) Engineering and True Uniform Stress-Strain Curves Fe-12.5Mn-2.01Mo-1.15C Hadfield Steel

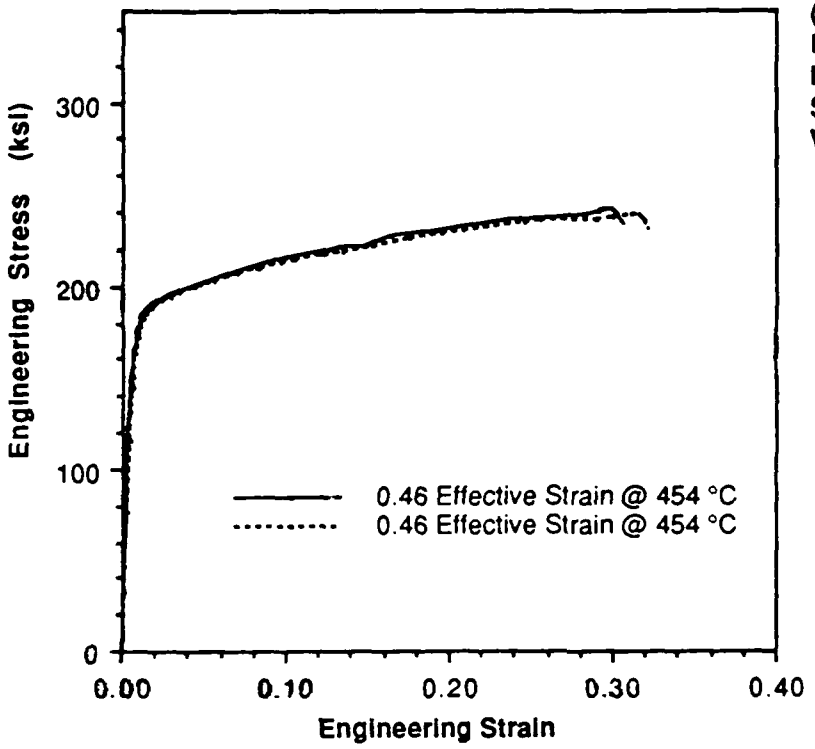

(a)
Engineering Stress Vs
Engineering Strain
Solution Treated And
Warm Rolled

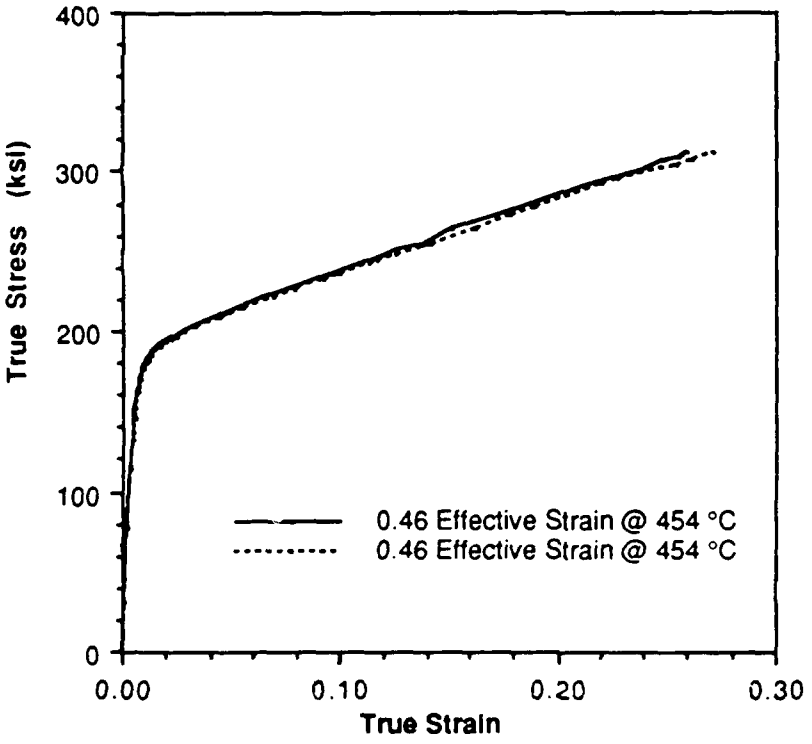

(b)
True Uniform Stress Vs
True Uniform Strain
Solution Treated And
Warm Rolled

Fig. 13
(a,b) Engineering (a) and True Uniform (b) Stress-Strain Curves Fe-12.5Mn-2.01Mo-1.15C Hadfield Steel, Warm Rolled 0.46 Effective Strain at 454 °C

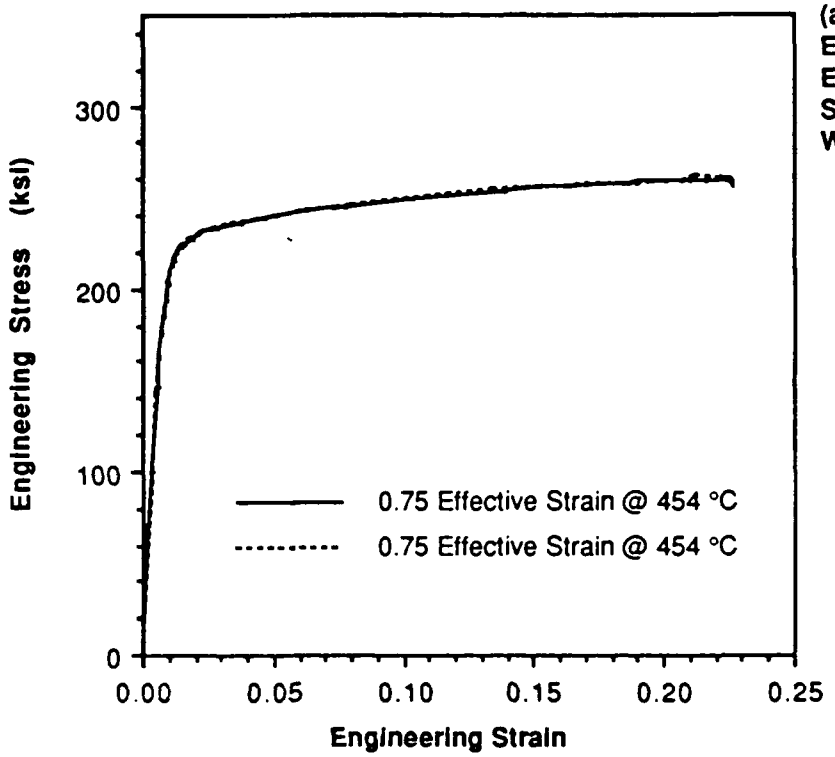

(a)
Engineering Stress Vs
Engineering Strain
Solution Treated And
Warm Rolled

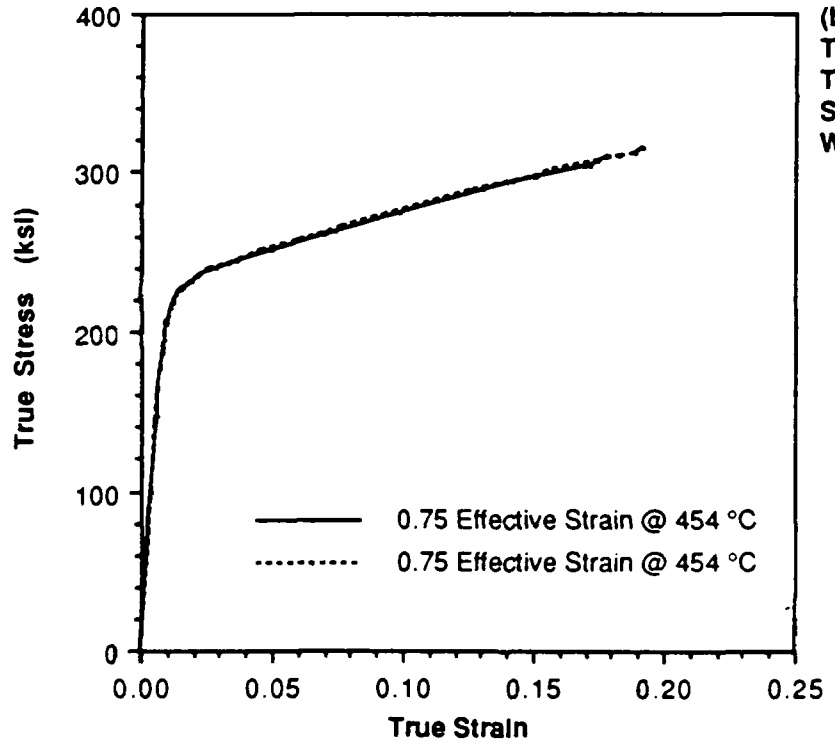

(b)
True Uniform Stress Vs
True Uniform Strain
Solution Treated And
Warm Rolled

Fig. 14
(a,b) Engineering (a) and True Uniform (b) Stress-Strain Curves Fe-12.5Mn-2.01Mo-1.15C Hadfield Steel, Warm Rolled 0.75 Effective Strain at 454 °C

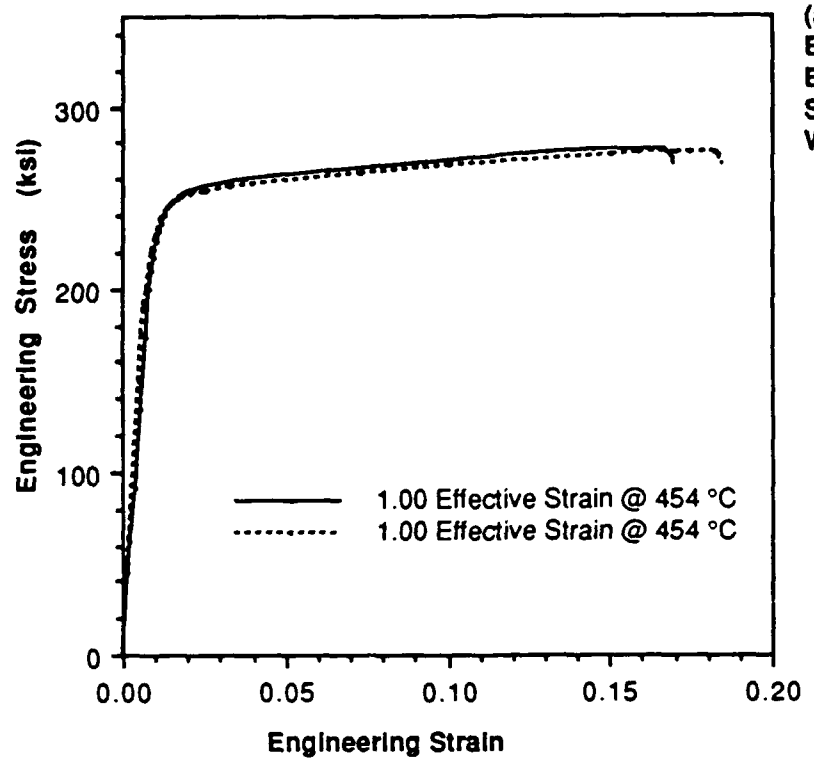

(a)
Engineering Stress Vs
Engineering Strain
Solution Treated And
Warm Rolled

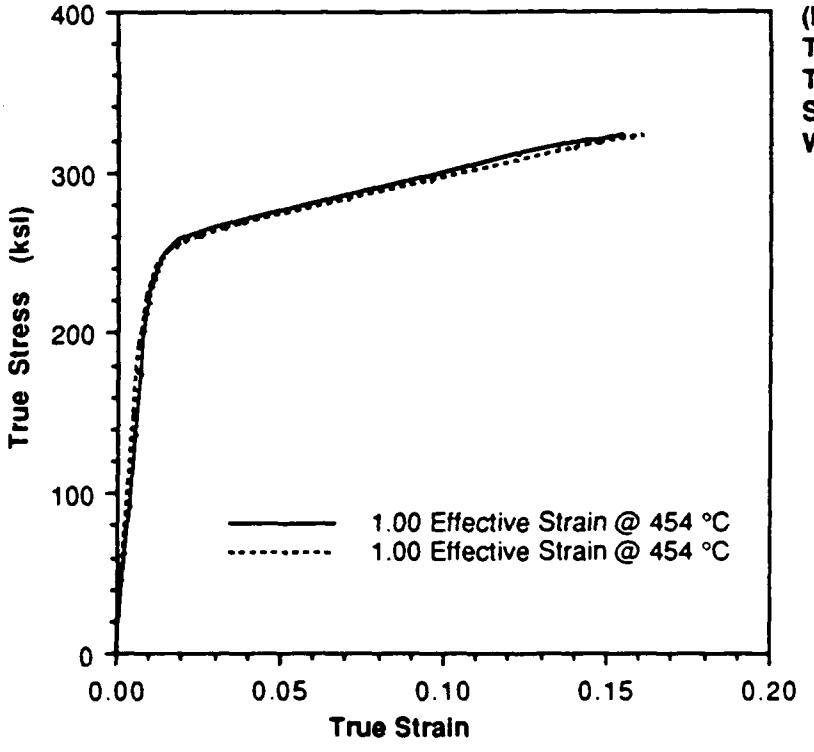

(b)
True Uniform Stress Vs
True Uniform Strain
Solution Treated And
Warm Rolled

Fig. 15
(a,b) Engineering (a) and True Uniform (b) Stress-Strain Curves,
Fe-12.5Mn-2.01Mo-1.15C Hadfield Steel,
Warm Rolled 1.00 Effective Strain at 454 °C

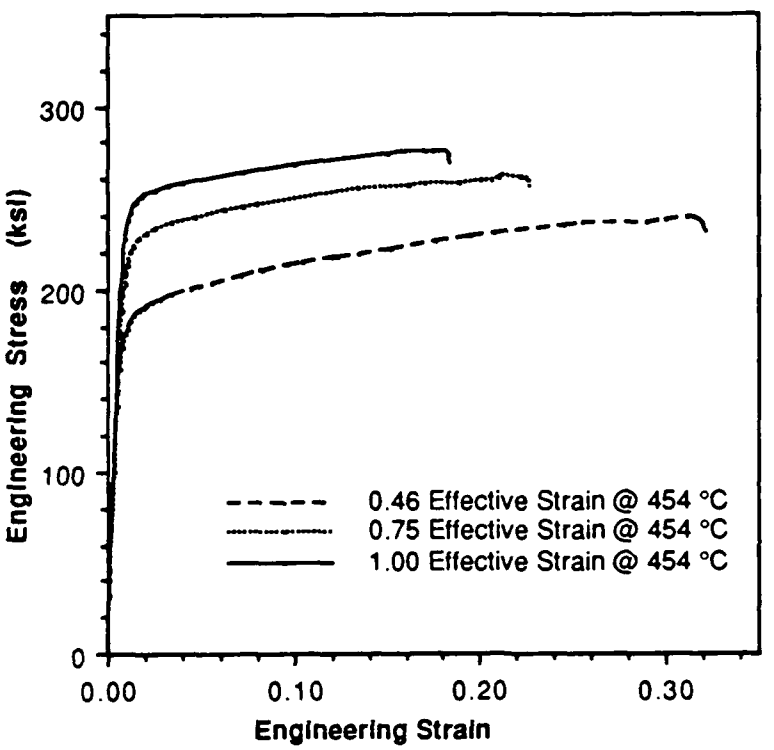

(a)
Engineering Stress Vs
Engineering Strain
Solution Treated And
Warm Rolled

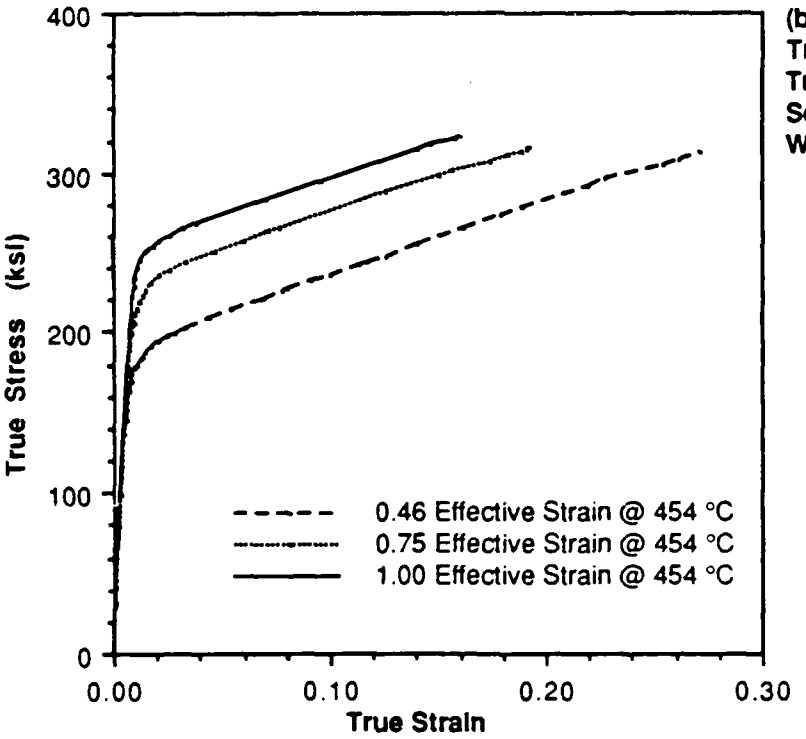

(b)
True Uniform Stress Vs
True Uniform Strain
Solution Treated And
Warm Rolled

Fig. 16
(a,b) Engineering (a) and True Uniform (b) Stress-Strain Curves,
Fe-12.5Mn-2.01Mo-1.15C Hadfield Steel,
Warm Rolled 0.46, 0.75 and 1.00 Effective Strains at 454 °C

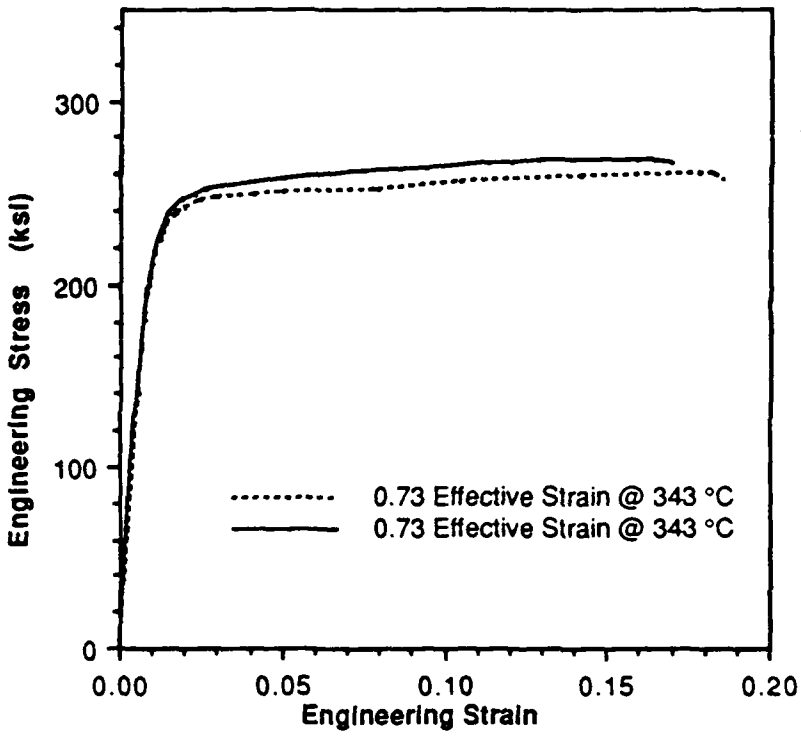

(a)
Engineering Stress Vs
Engineering Strain
Solution Treated And
Warm Rolled

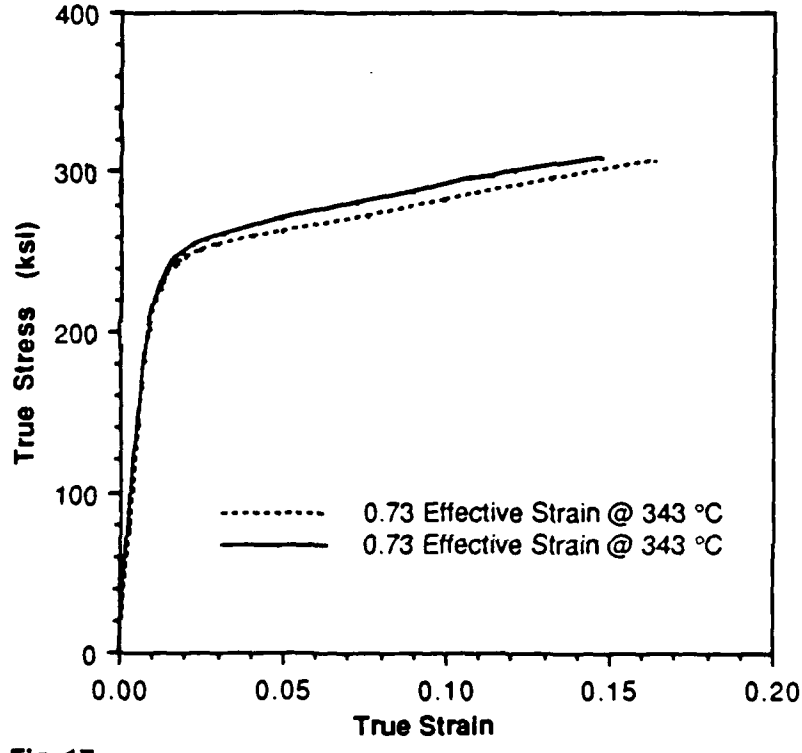

(b)
True Uniform Stress Vs
True Uniform Strain
Solution Treated And
Warm Rolled

Fig. 17
(a,b) Engineering (a) and True Uniform (b) Stress-Strain Curves,
Fe-12.5Mn-2.01Mo-1.15C Hadfield Steel,
Warm Rolled 0.73 Effective Strain at 343 °C

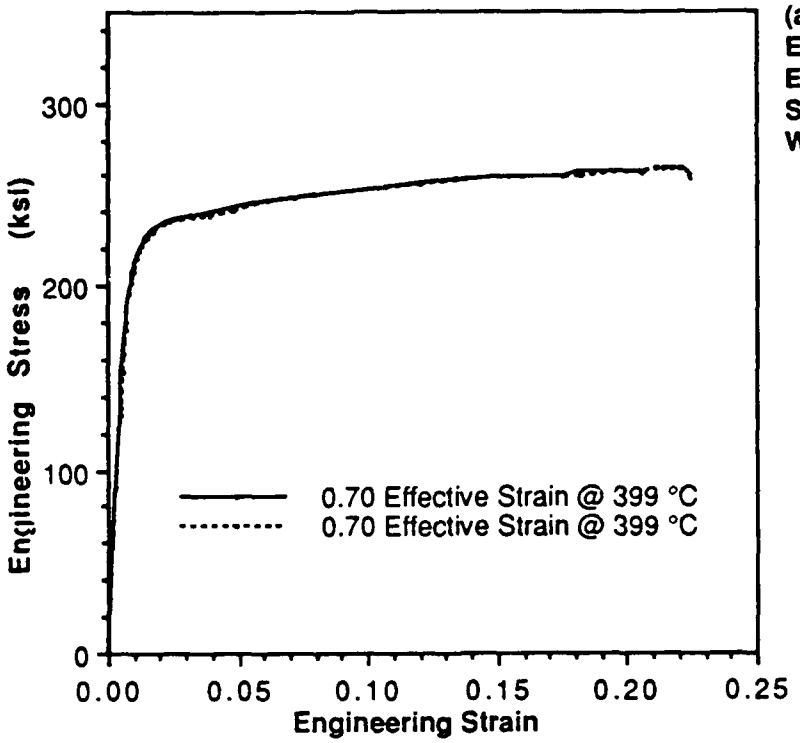

(a)
Engineering Stress Vs Engineering Strain Solution Treated And Warm Rolled

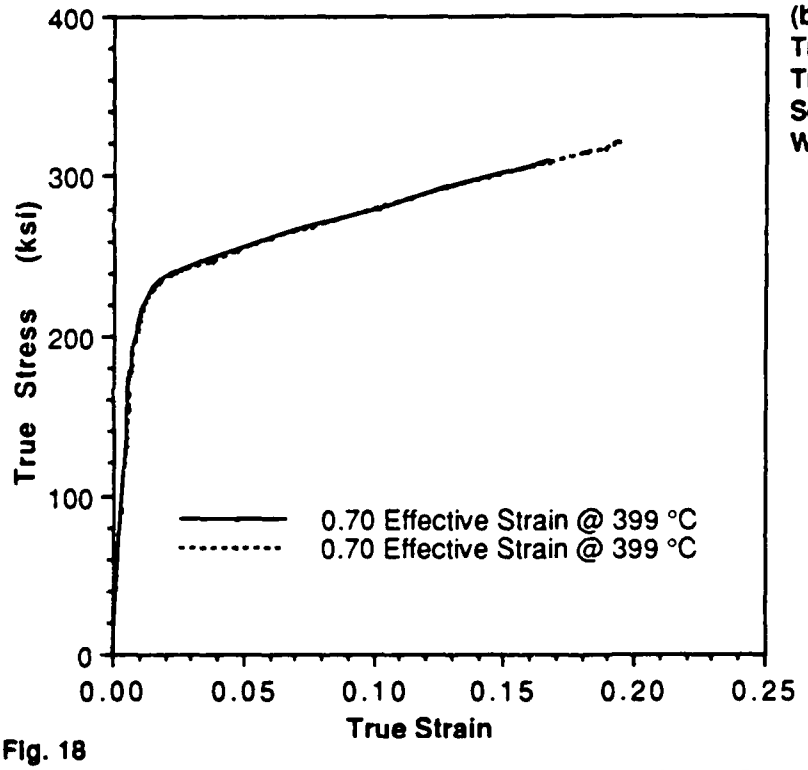

(b)
True Uniform Stress Vs True Uniform Strain Solution Treated And Warm Rolled

Fig. 18
(a,b) Engineering (a) and True Uniform (b) Stress-Strain Curves, Fe-12.5Mn-2.01Mo-1.15C Hadfield Steel, Warm Rolled 0.70 Effective Strain at 399 °C

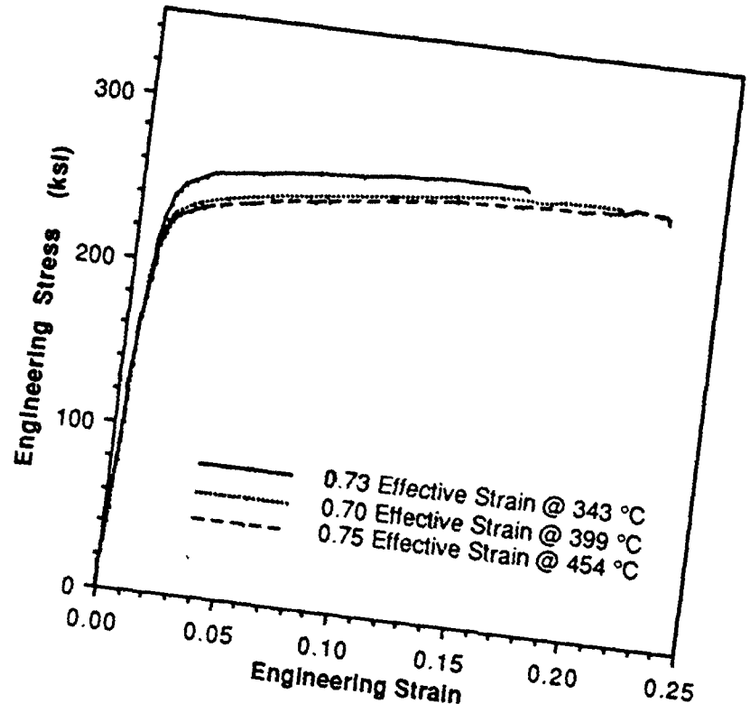

(a)
Engineering Stress Vs
Engineering Strain
Solution Treated And
Warm Rolled

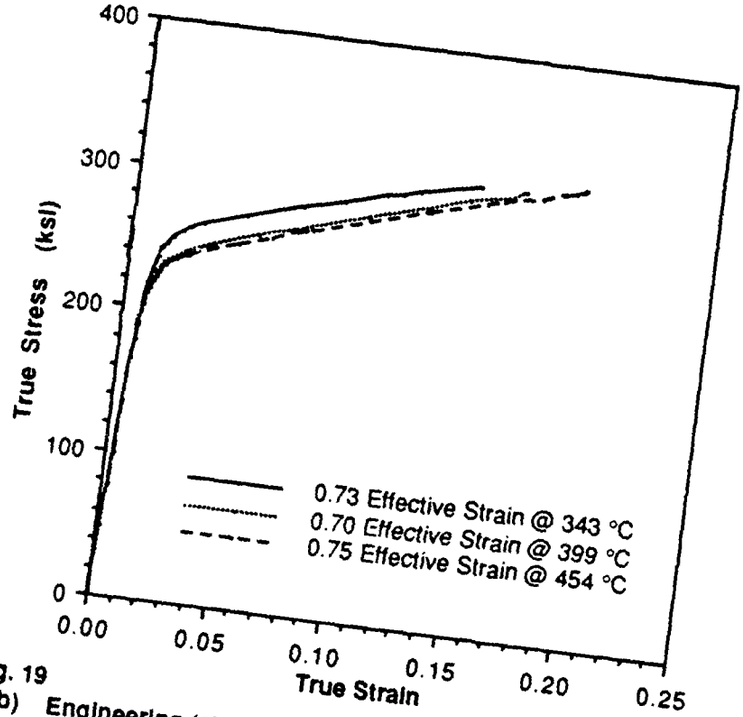

(b)
True Uniform Stress Vs
True Uniform Strain
Solution Treated And
Warm Rolled

Fig. 19
(a,b) Engineering (a) and True Uniform (b) Stress-Strain Curves,
Fe-12.5Mn-2.01Mo-1.15C Hadfield Steel,
Warm Rolled 0.70-0.75 Effective Strain at 343 °C, 399 °C and 454 °C

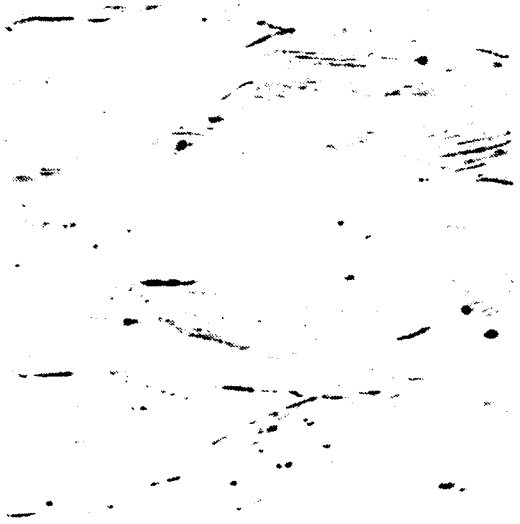

(a)
Rolled 0.73 ε_e at 343 °C and
Tested in Tension 0.16 ε_u at 23 °C

200 X 50 μ

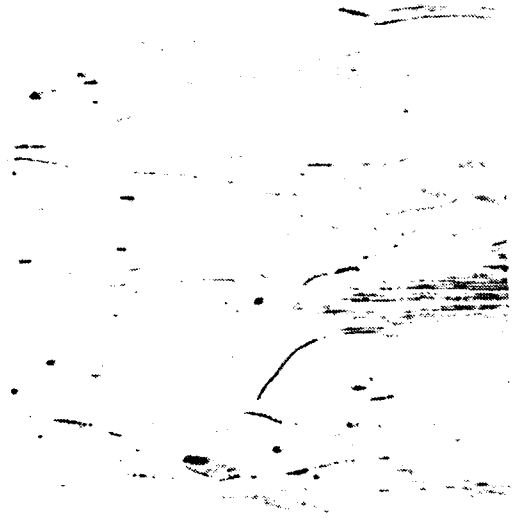

(b)
Rolled 0.70 ε_e at 399 °C and
Tested in Tension 0.17 ε_u at 23 °C

200 X 50 μ

(c)
Rolled 0.75 ε_e at 454 °C and
Tested in Tension 0.18 ε_u at 23 °C,

200 X 50 μ

Fig. 20
(a-c) Warm Rolled and Tested in Tension Microstructures, Warm Rolled 0.70-0.75 Effective Strain and Tested in Tension 0.16-0.18 Uniform Strain, Na_2CrO_4 Electrolytic Etch

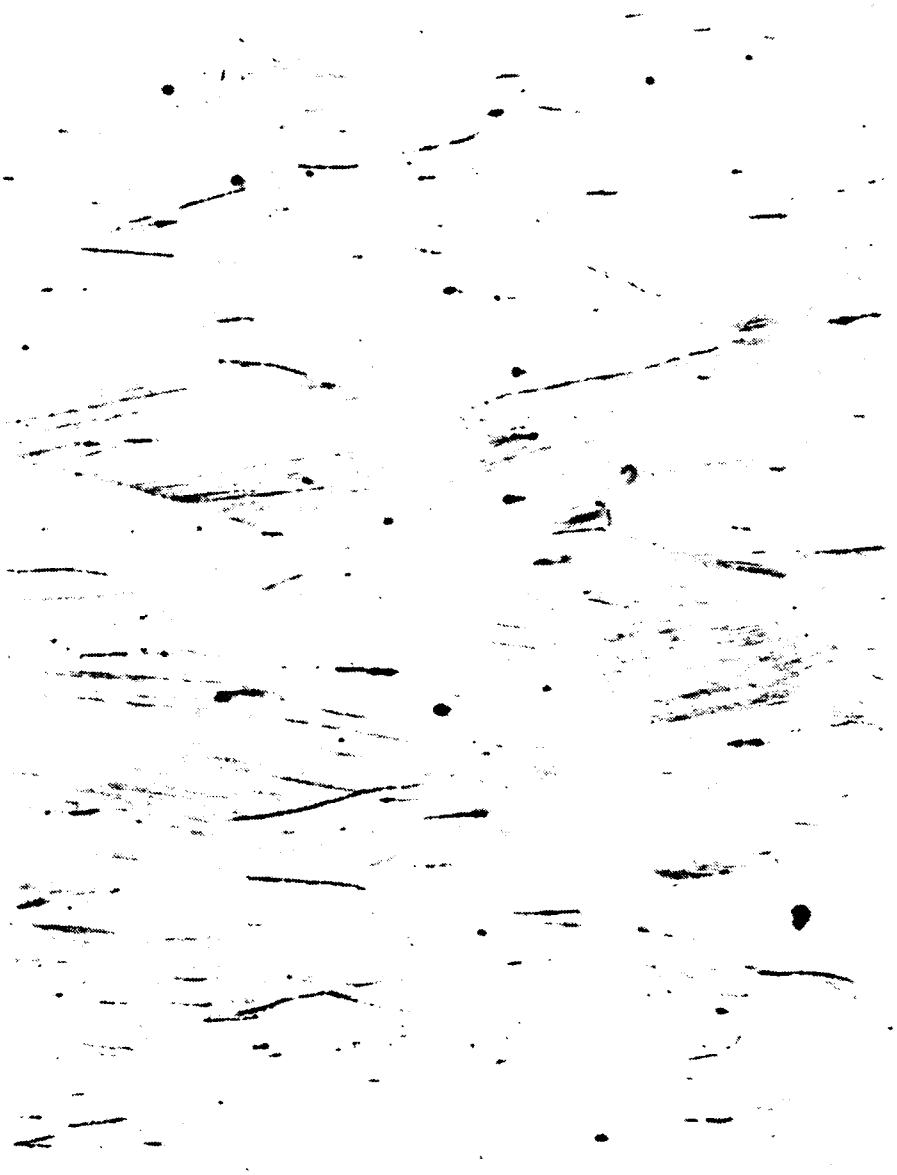

Fig. 21
Warm Rolled and Tension Tested Microstructure,
Warm Rolled 0.46 ε_e at 454 °C and Tested in Tension 0.27 ε_u at 23 °C, Na_2CrO_4 Electrolytic Etch

200 X 50 μ

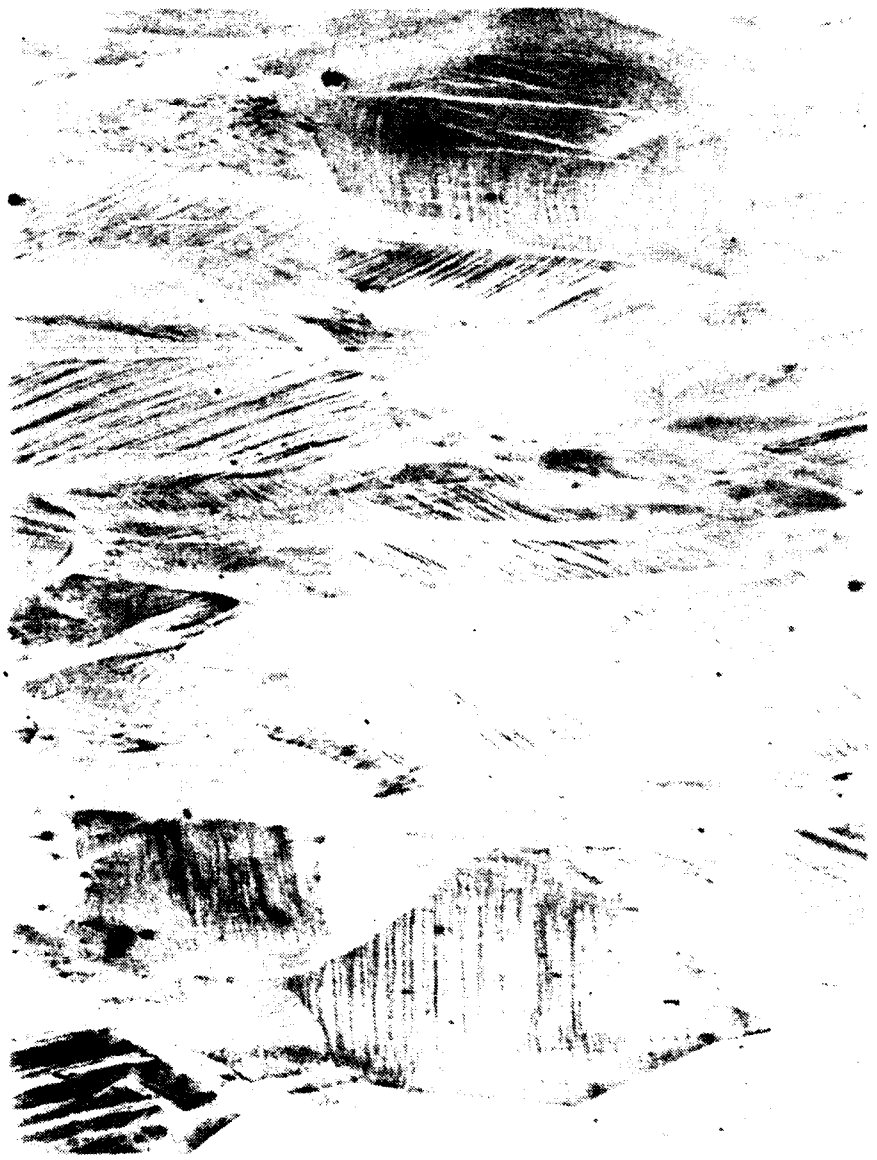

Fig. 22
(a-c) Warm Rolled and Tension Tested Microstructure, Warm Rolled 0.46 ε_e at 454 °C and Tested in Tension 0.27 ε_u at 23 °C, (identical microstructure at 200 X, 500 X and 1000 X), HCl Electrolytic Etch

(b)

500 X 20 μ

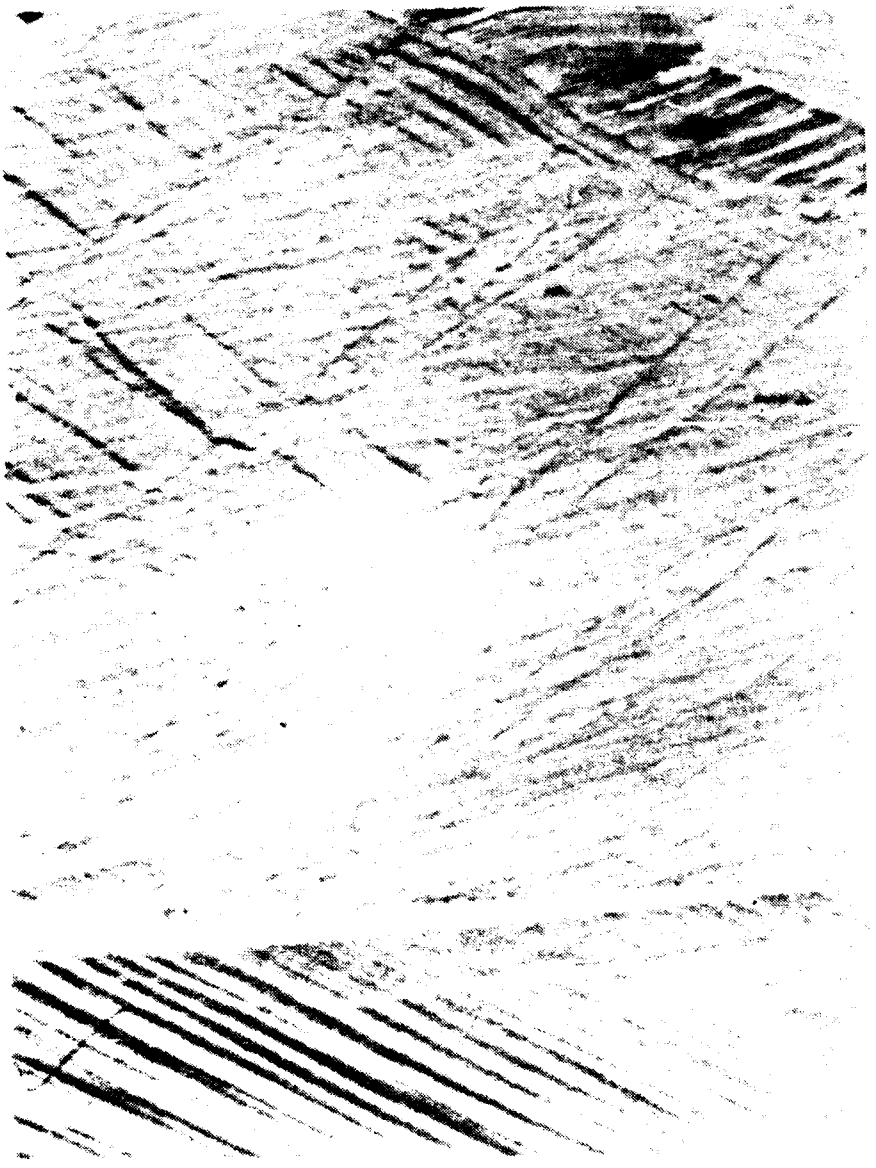

(c)

1000 X 10 μ

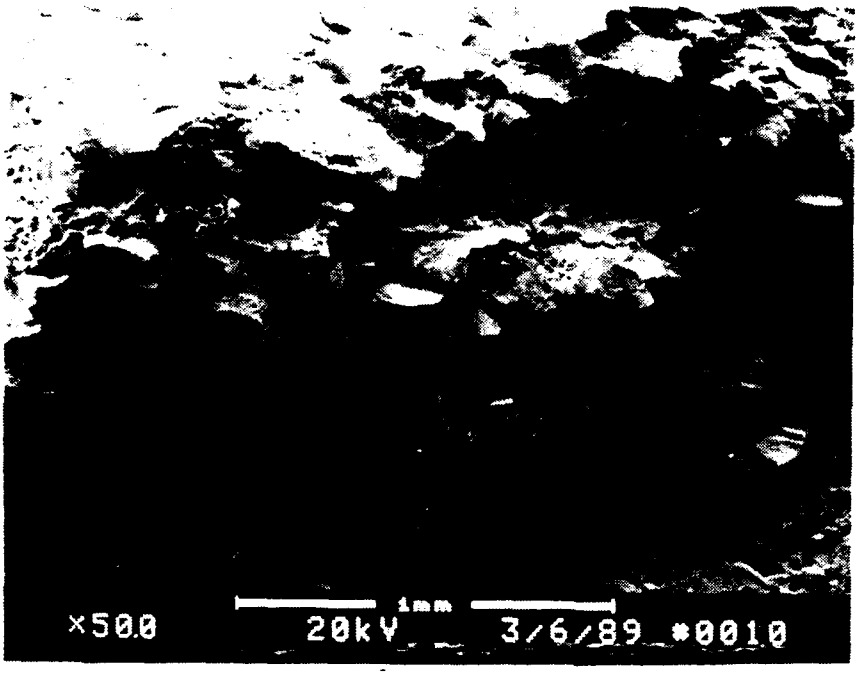

(a) Grain boundary Decohesion Fracture Initiation in Tension

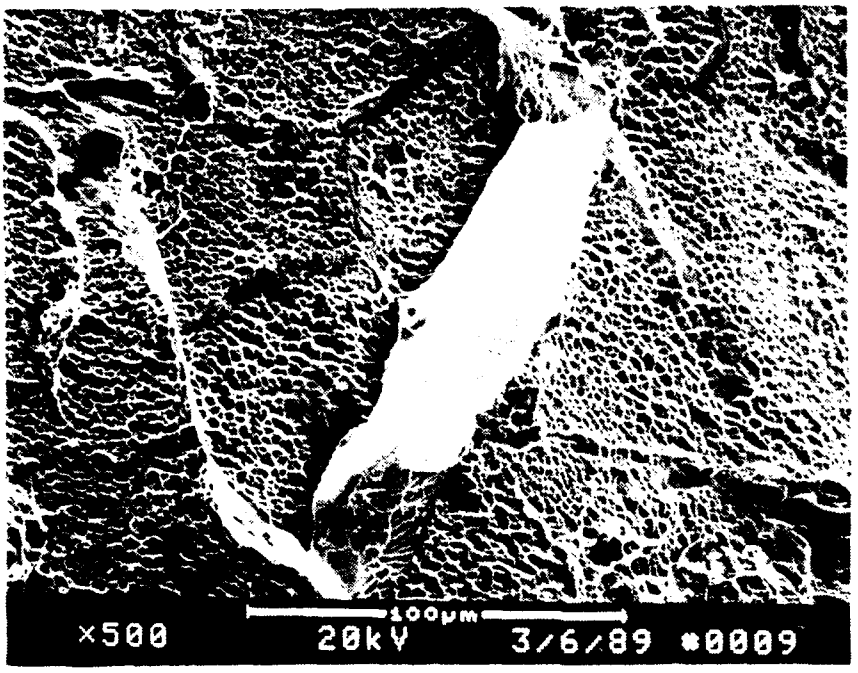

(b) Cleavage Fracture and Ductile Dimple Fracture in Shear
(same specimen as above)

Fig. 23
(a,b) SEM Tension Specimen Fracture Surfaces, Warm Rolled 0.73 ε_e at 343 °C and Tested in Tension 0.15 ε_u at 23 °C Grain Boundary Decohesion, Cleavage, Ductile Dimple Fracture

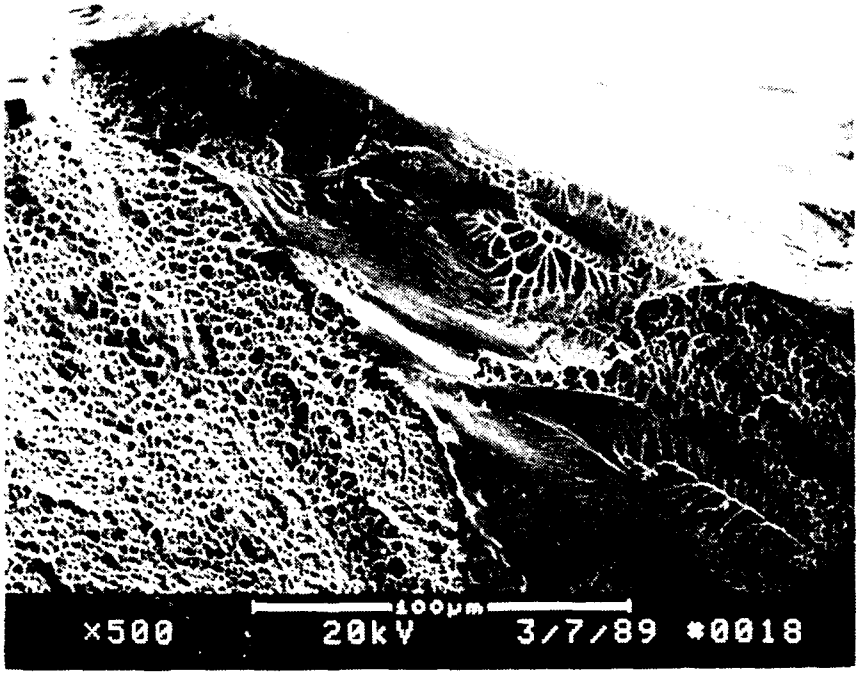

Fig. 24
SEM Tension Specimen Fracture Surface,
Warm Rolled 0.70 ε_e at 399 °C and Tested in Tension 0.19 ε_u at 23 °C, Twin Cleavage Fracture and Ductile Dimple Fracture in Shear

Fig. 25
SEM Tension Specimen Fracture Surface,
Warm Rolled 0.75 ε_e at 454 °C and Tested in Tension 0.19 ε_u at 23 °C, Grain Boundary Decohesion in Tension by Ductile Fracture and by Cleavage Fracture

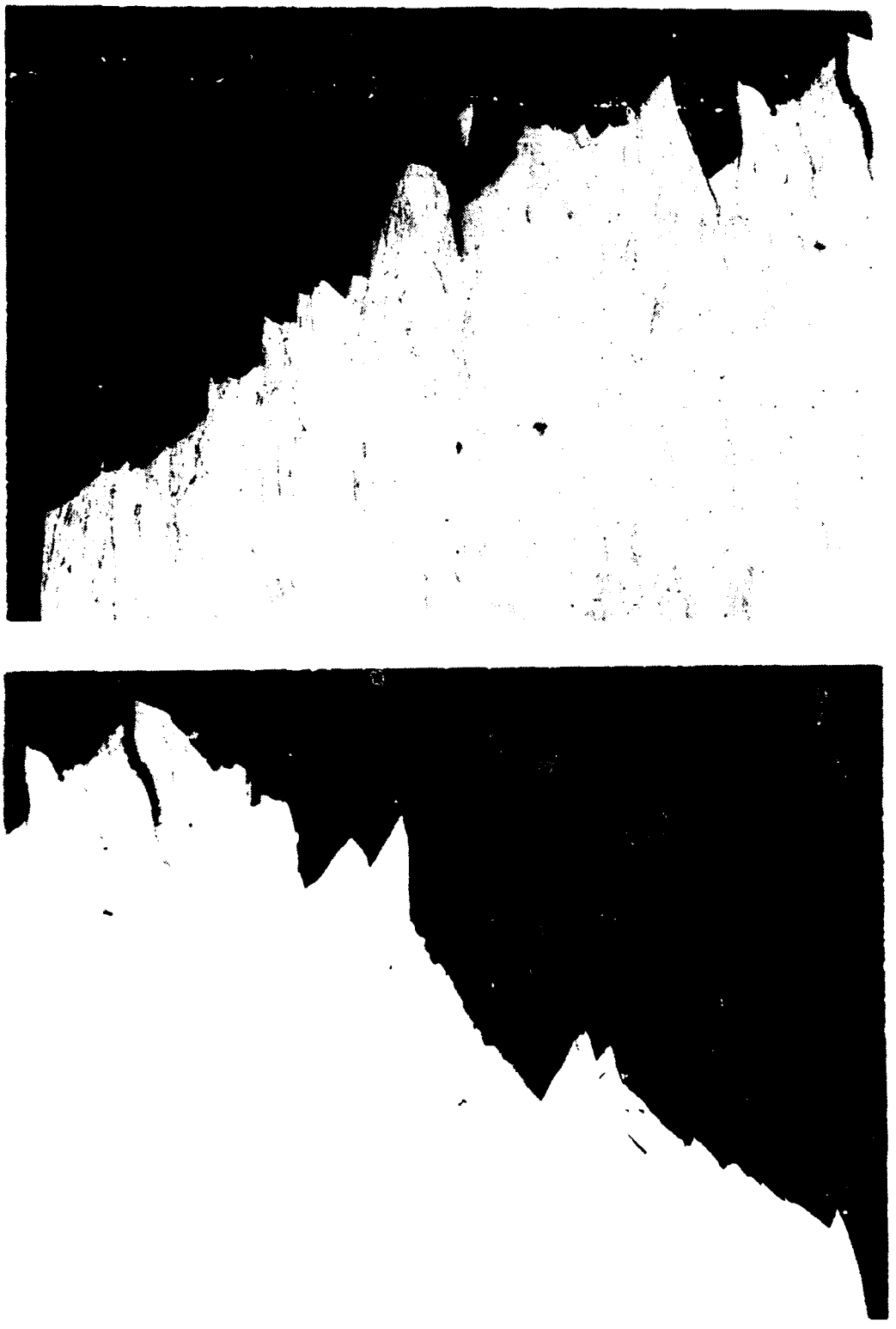

Fig. 26
(a, b) (Left and Right Section) Tension Specimen Fracture Profile Metallographs, Warm Rolled 0.75 ε_e at 454 °C and Tested in Tension 0.18 ε_u at 23 °C, 3% Nital - 10% HCl Alternating Etch

(a) Fracture Profile 50 X 200 μ

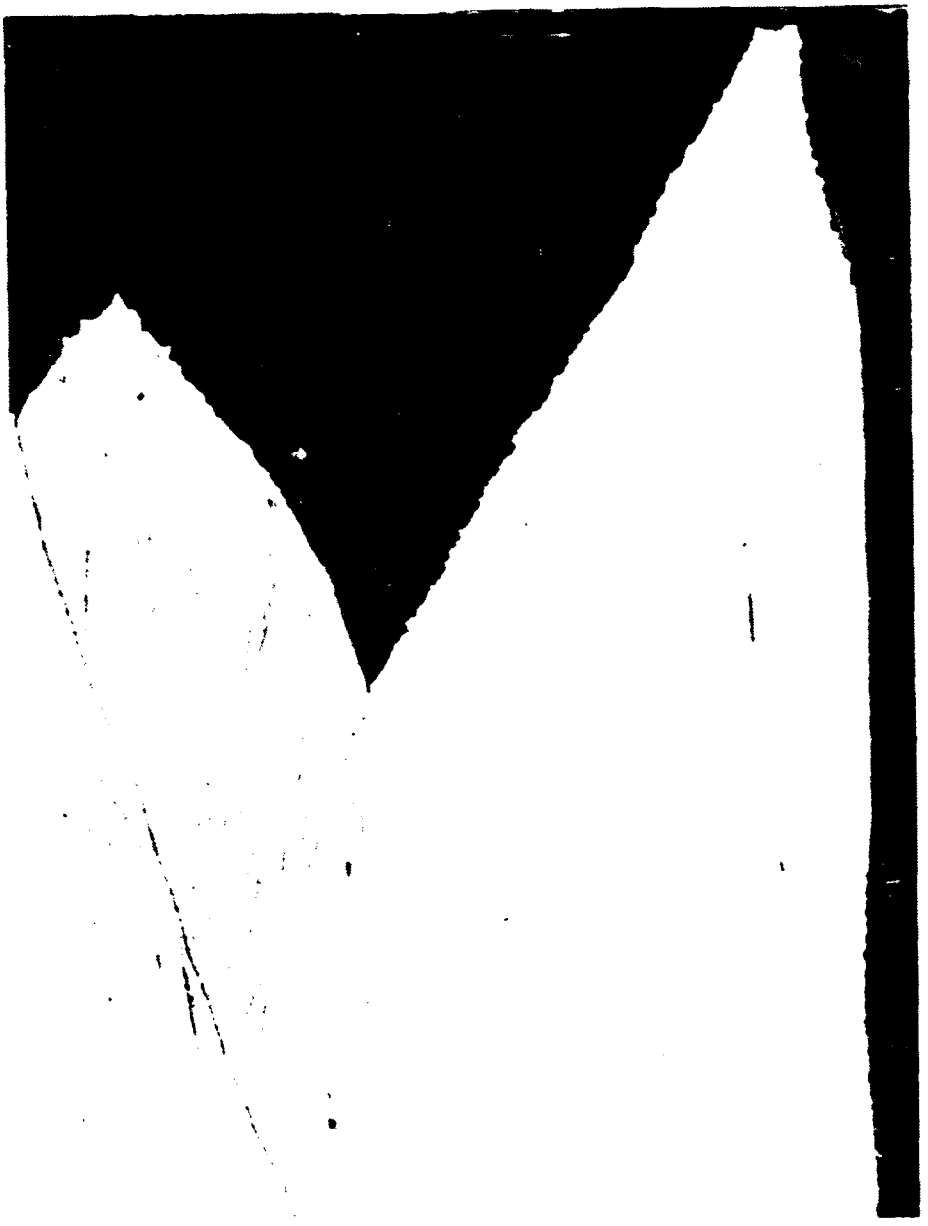

(b) Fracture Profile of Grain Boundary Voids and Precipitates

500 X 20 μ

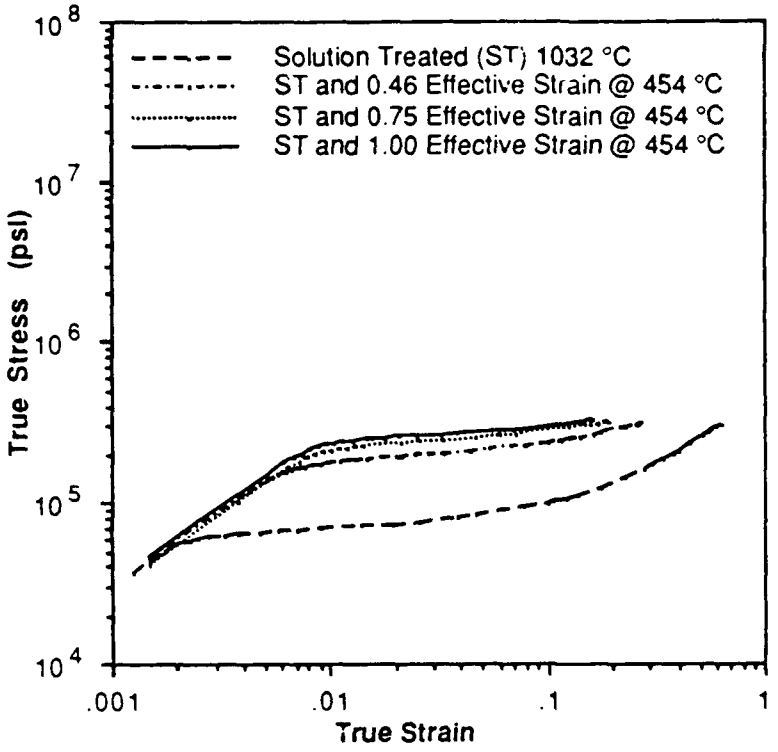

(a)
Elastic and Plastic
True Uniform Stress Vs
True Uniform Strain
Logarithmic Plot

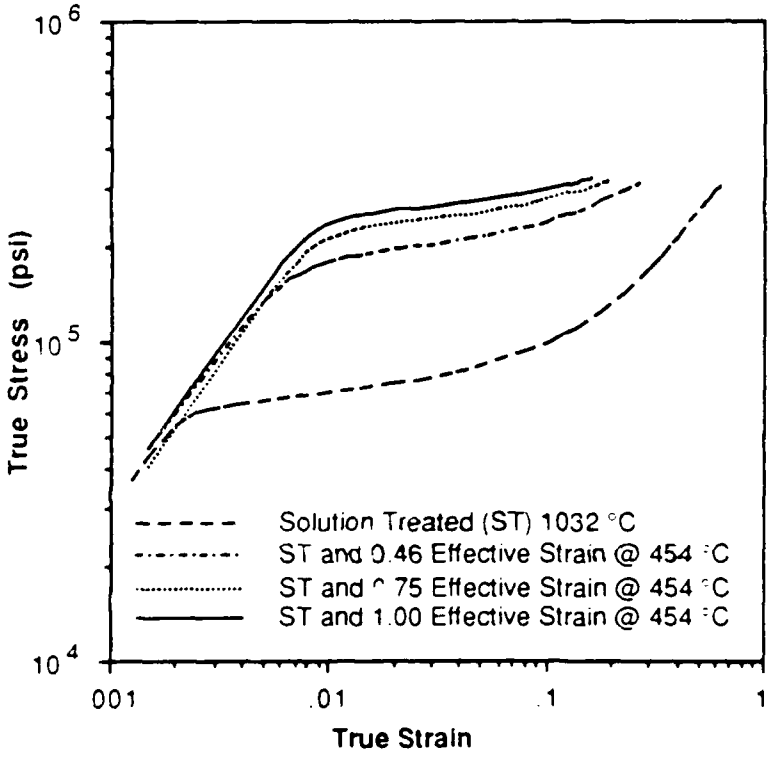

(b)
Plastic
True Uniform Stress Vs
True Uniform Strain
Logarithmic Plot

Fig. 27
(a,b) **Power Law Hardening Curves**
Fe-12.5Mn-2.01Mo-1.15C Hadfield Steel,
As Solution Treated, Warm Rolled at 454 °C

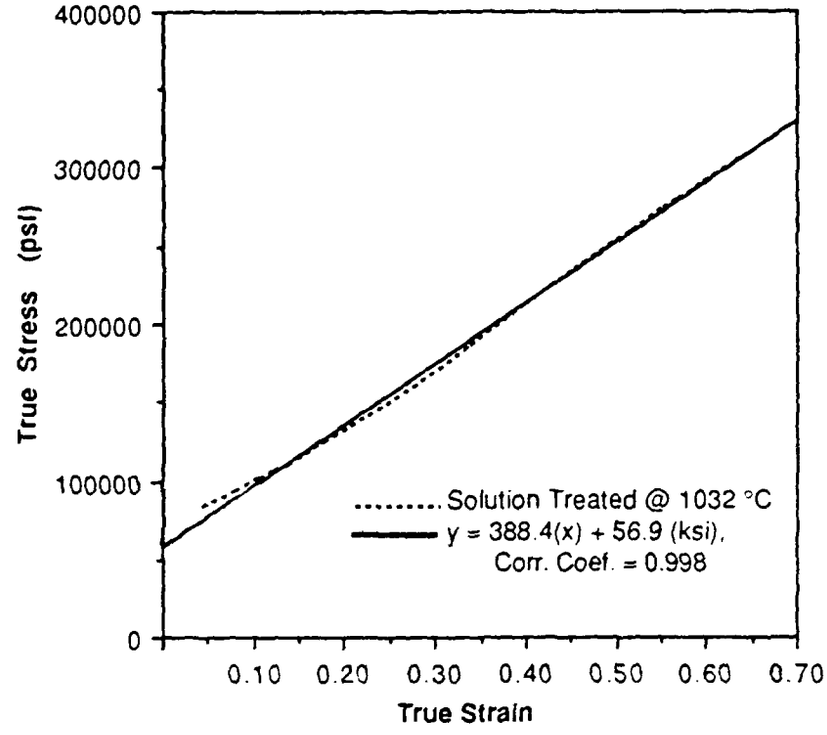

(a)
As Solution Treated

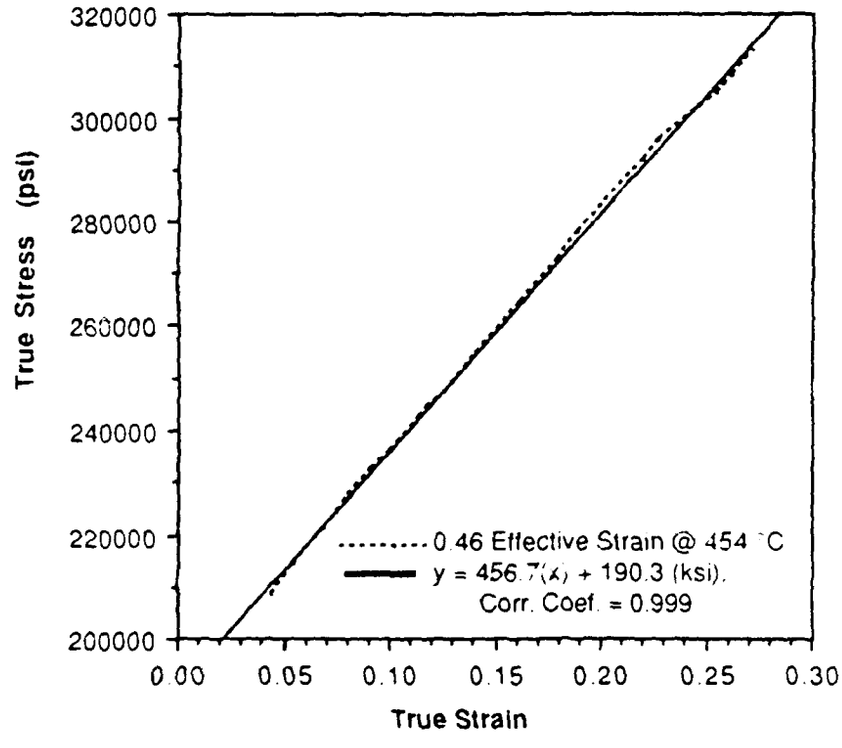

(b)
Solution Treated
And Warm Rolled

Fig. 28
(a-d) Linear Plastic Strain Hardening Curve Fits (y)
(a) As Solution Treated, (b) Warm Rolled 0.46 Effective Strain at 454 °C

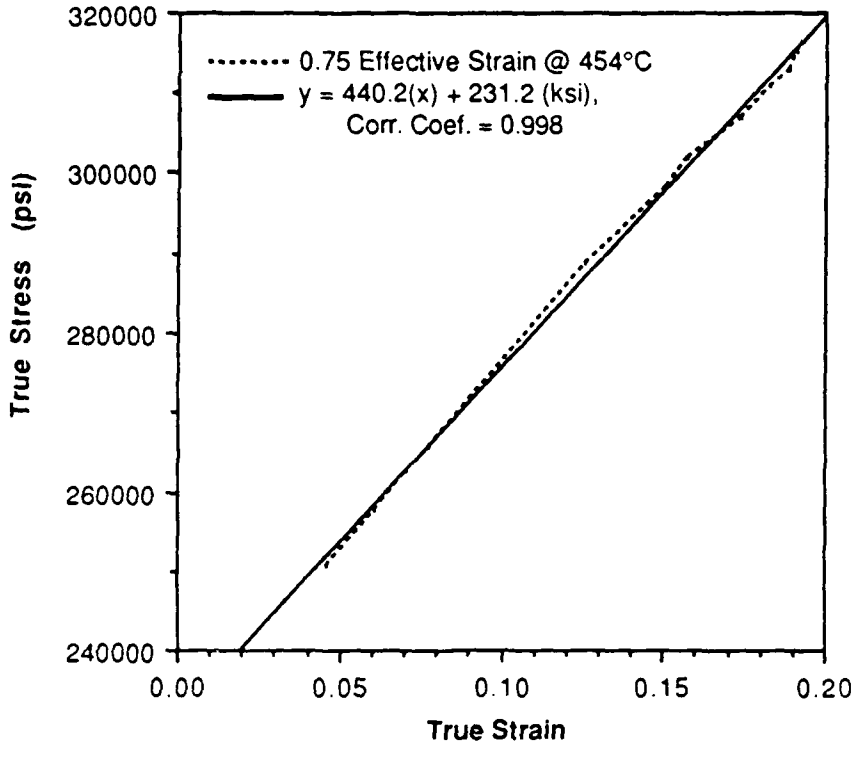

(c)
Solution Treated
And warm Rolled

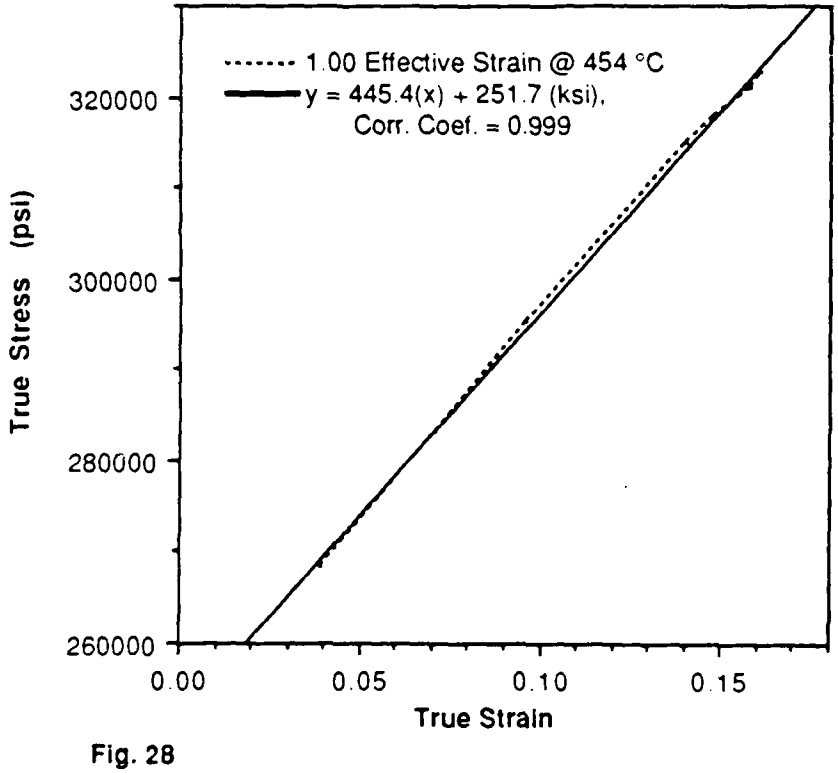

(d)
Solution Treated
And Warm Rolled

Fig. 28
Linear Plastic Strain Hardening Curve Fits (y)
(c) Warm Rolled 0.75 Effective Strain at 454 °C,
(d) Warm Rolled 1.00 Effective Strain at 454 °C

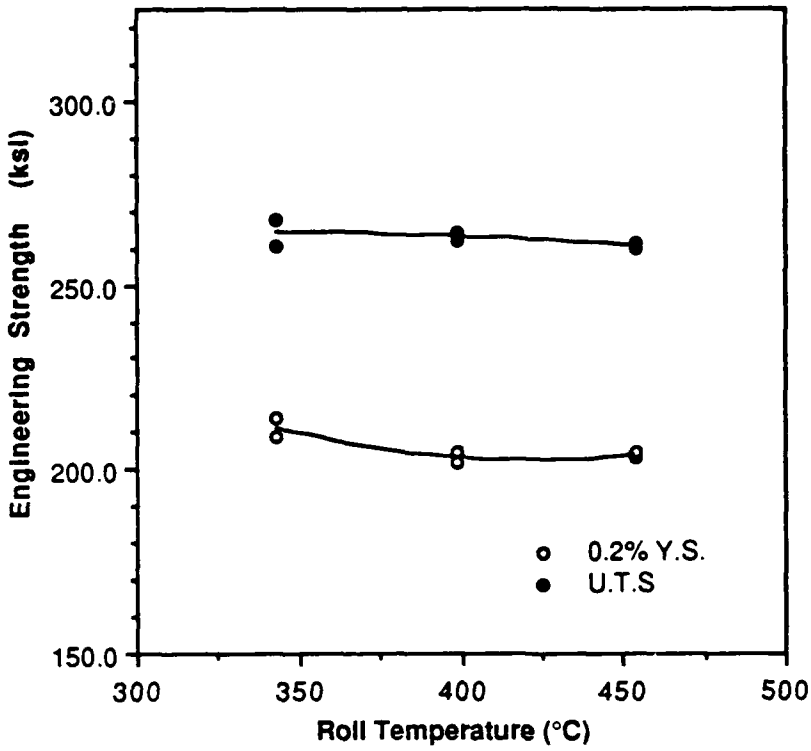

(a)
Engineering Strength Vs
Roll Temperature

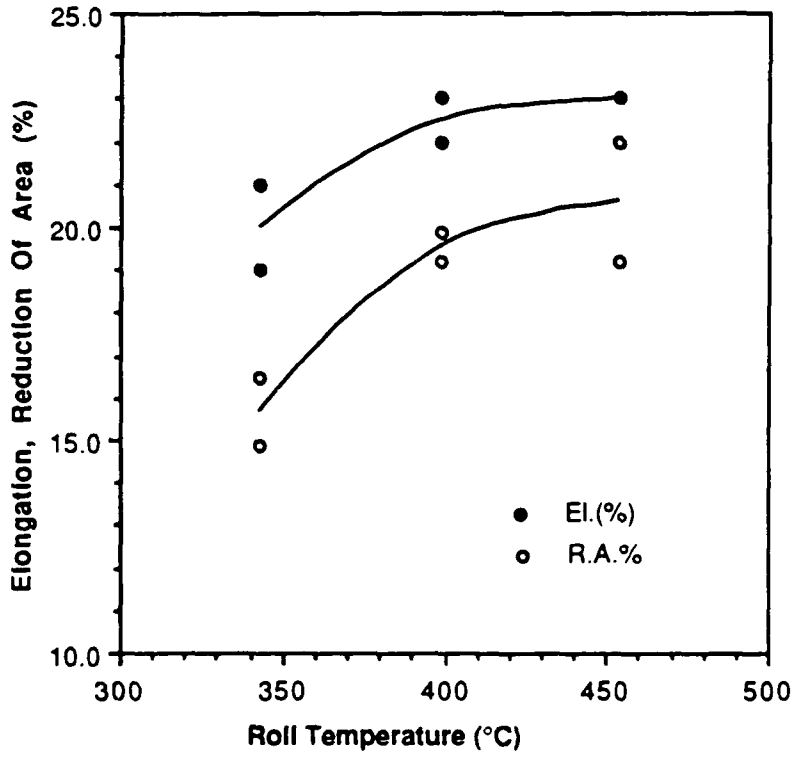

(b)
Engineering Ductility Vs
Roll Temperature

Fig. 29
(a-d) Trend Curves of Engineering Strength and Ductility in Tension Vs Roll Temperature at 0.70-0.75 Warm Roll Effective Strain

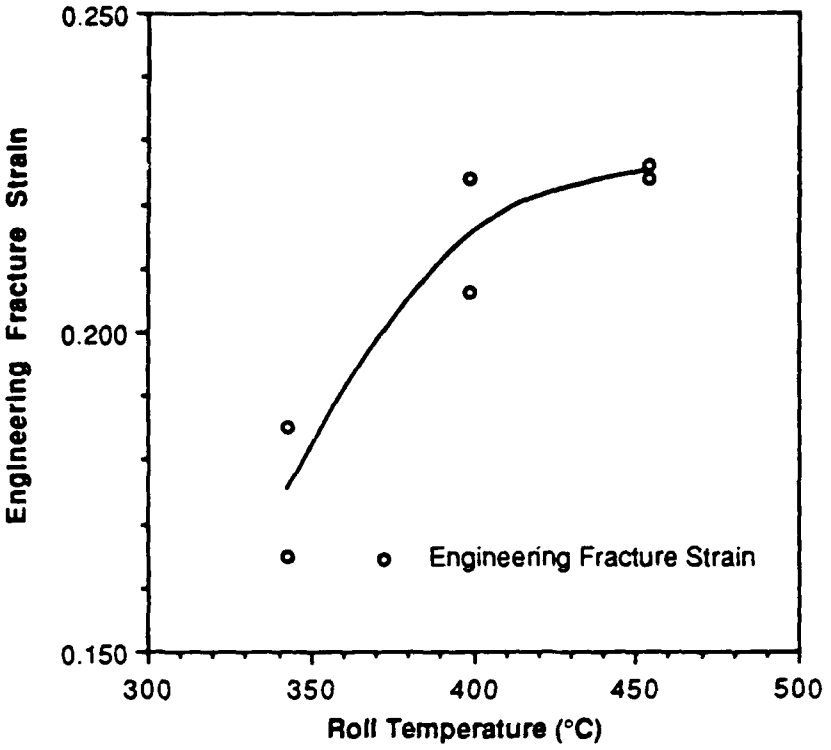

(C)
Engineering Fracture Strain Vs Roll temperature

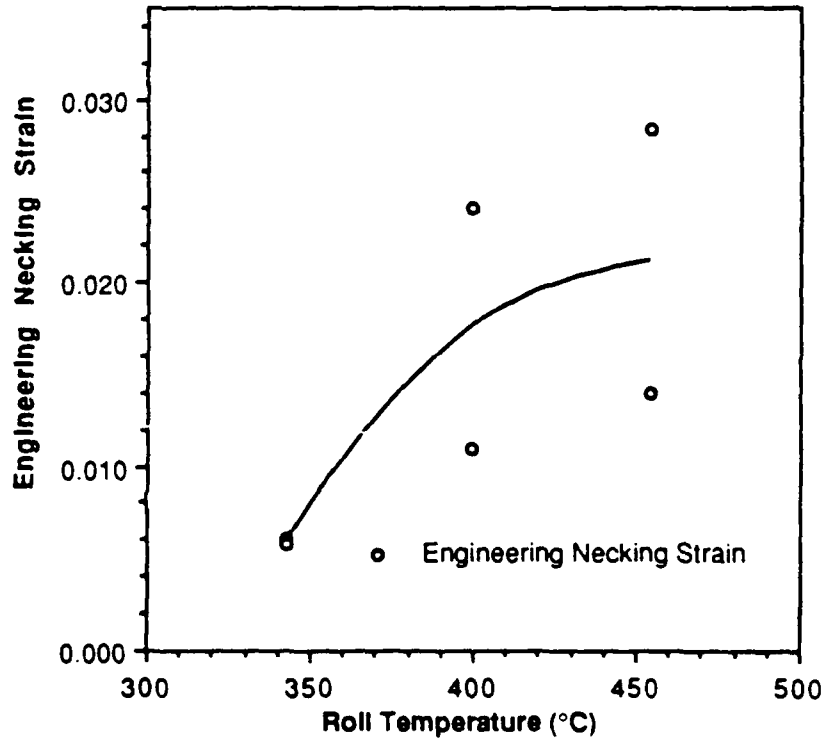

(d)
Engineering Necking Strain Vs Roll Temperature

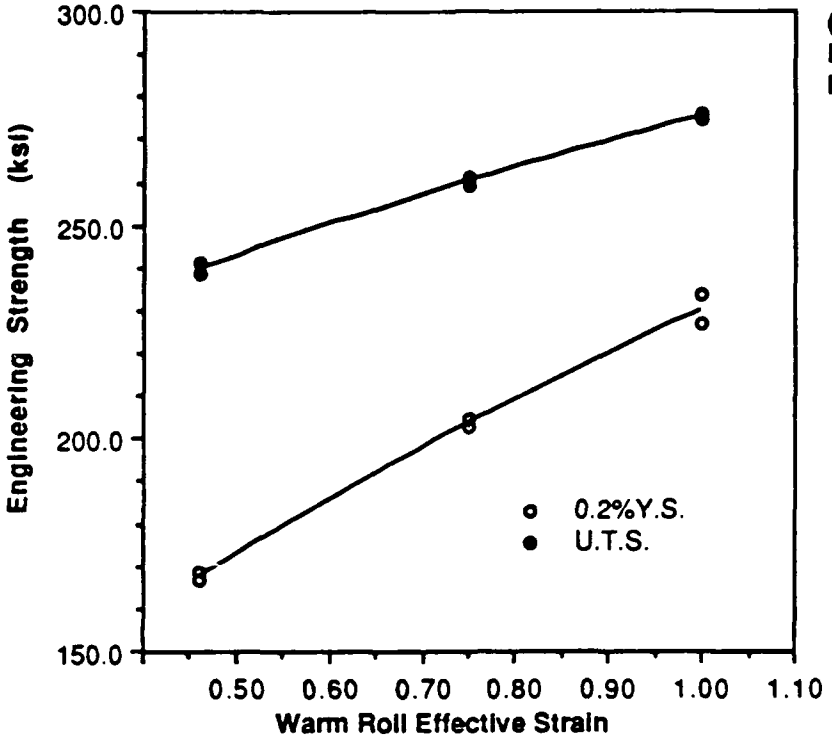

(a)
Engineering Stress Vs
Effective Roll Strain

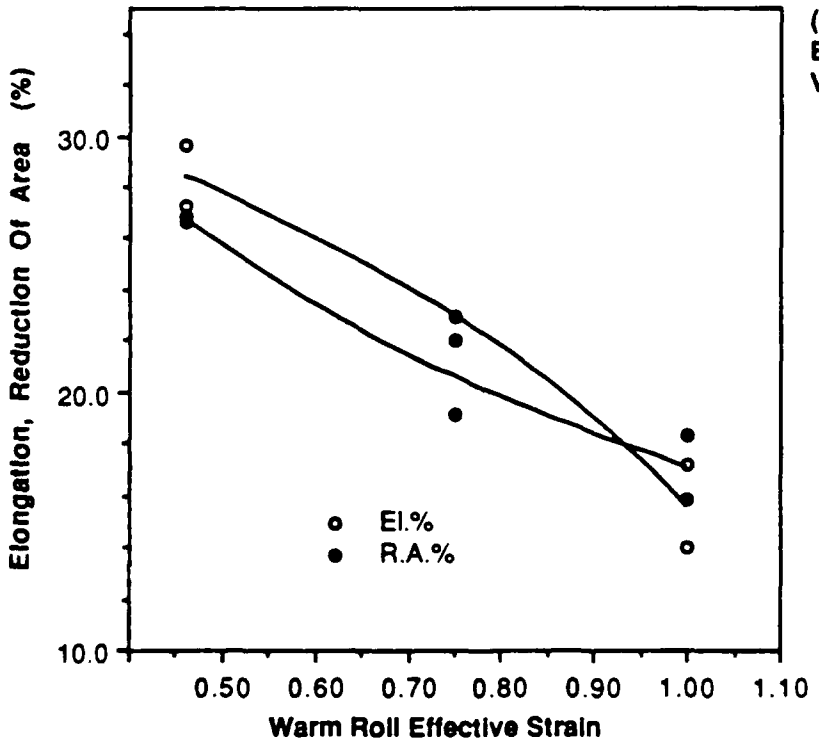

(b)
Engineering Ductility
Vs Effective Roll Strain

Fig. 30
(a-d) Trend Curves of Engineering Strength and Ductility in Tension Vs Warm Roll Effective Strain at 454 °C

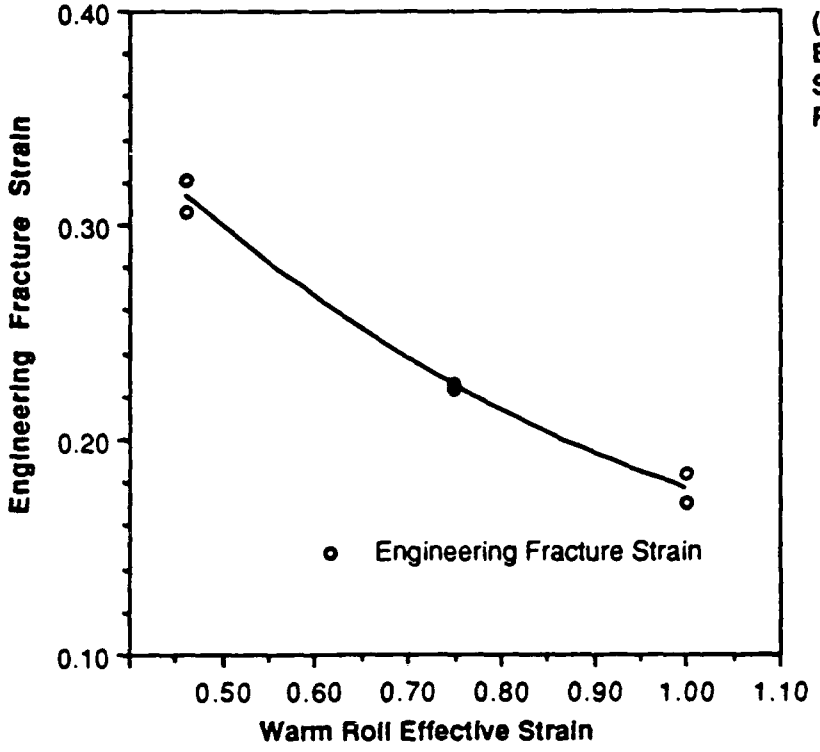

(c)
Engineering Fracture Strain Vs Effective Roll Strain

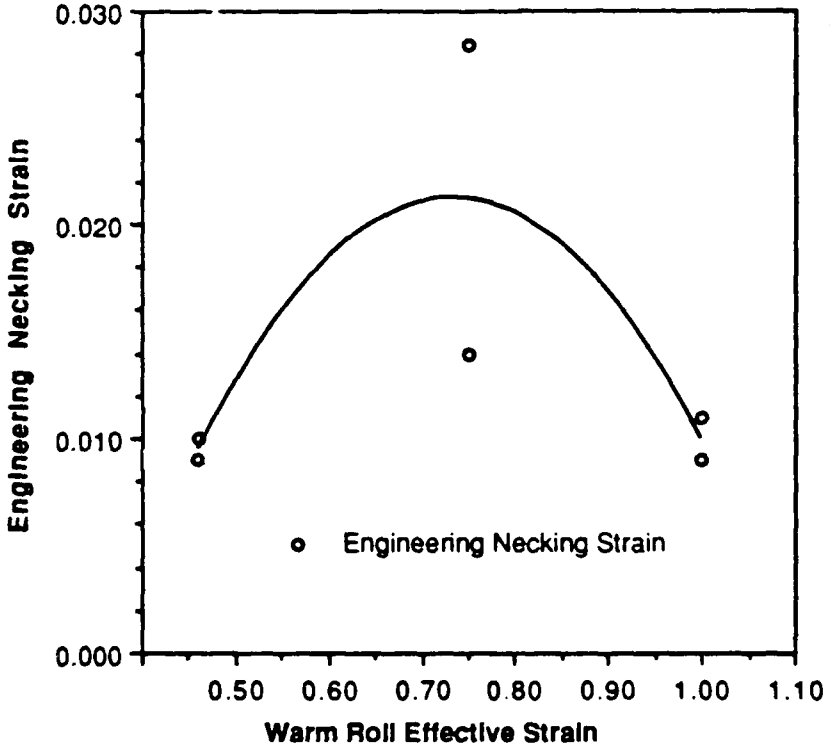

(d)
Engineering Necking Strain Vs Effective Roll Strain

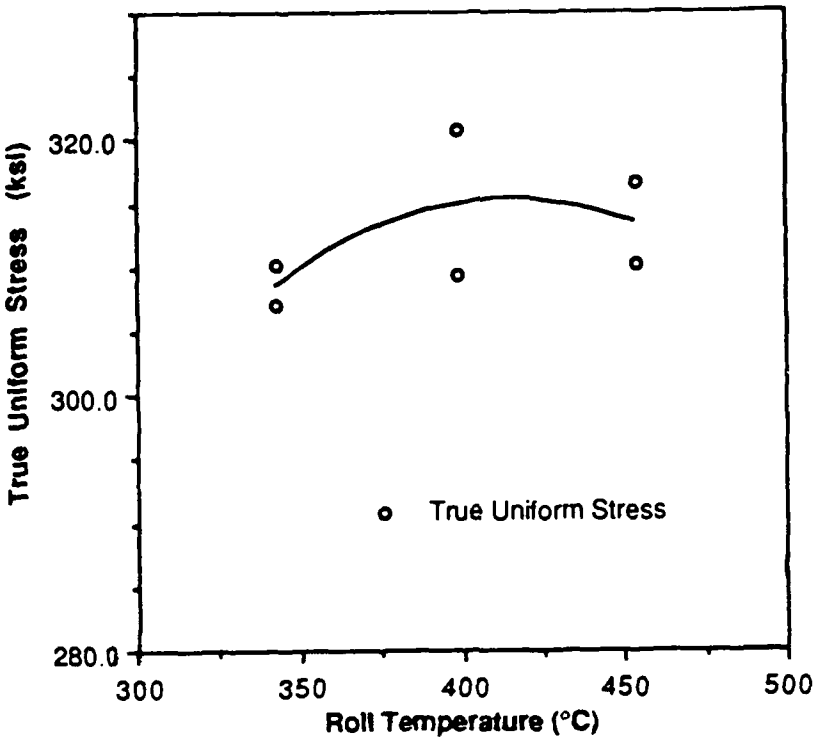

(a)
True Uniform Stress
Vs Roll Temperature

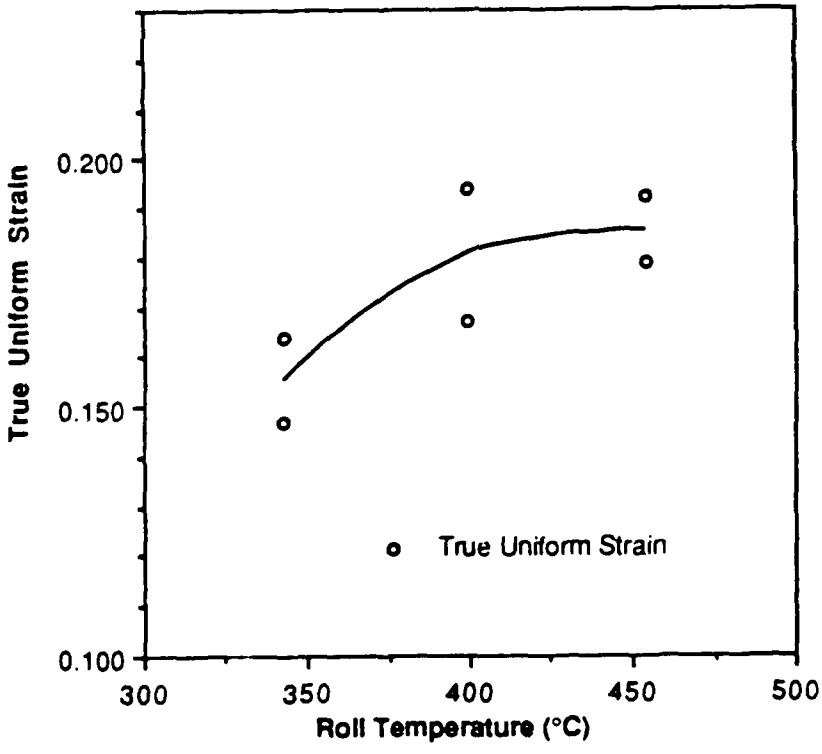

(b)
True Uniform Strain
Vs Roll Temperature

Fig. 31
(a,b) *Trend Curves of True Uniform Stress-Strain in Tension Vs* Roll Temperature at 0.70-0.75 Effective Roll Strain

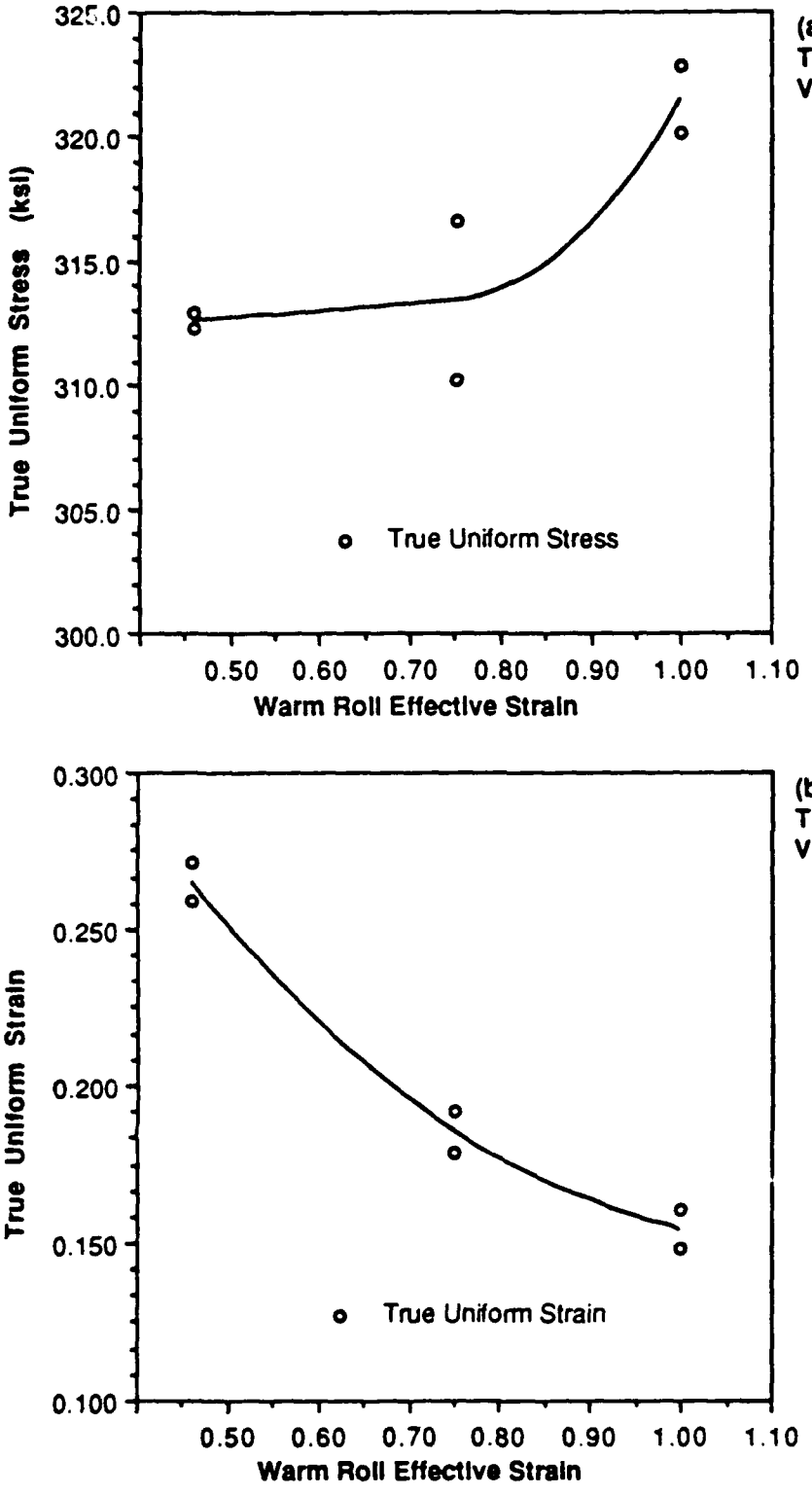

Fig. 32
(a,b) Trend Curves of True Uniform Stress-Strain in Tension Vs Warm Roll Effective Strain at 454 °C

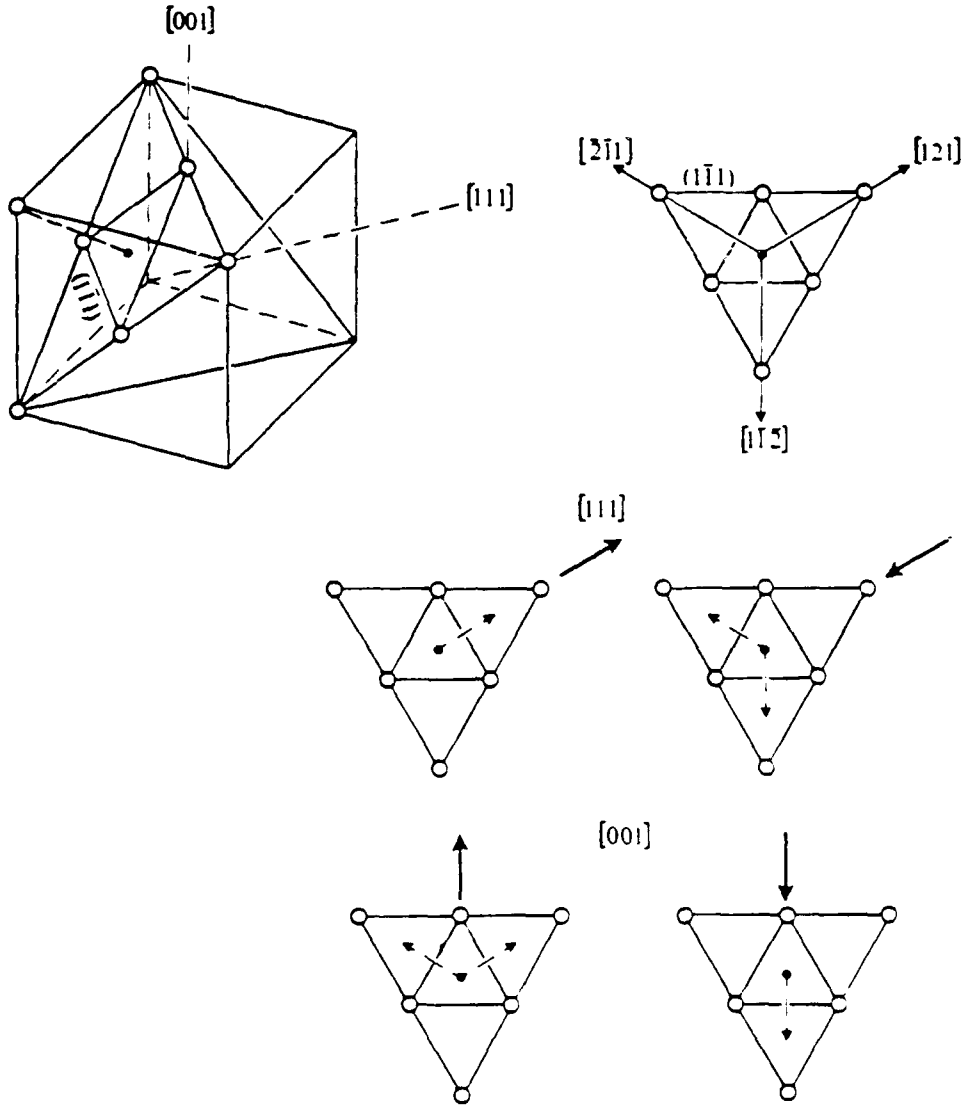

orientation	m	m'	
		tension	compression
[111]	$2.3\sqrt{6}$	$2\sqrt{2}.9$	$\sqrt{2}.9$
[001]	$1.\sqrt{6}$	$1.3\sqrt{2}$	$\sqrt{2}.3$

Fig. 33
Schmid Factors of FCC Slip and Twin Systems [15]. Directionality of mechanical twinning in a FCC crystal stressed along [111] and [001] is shown for components of applied forces acting on the (1$\bar{1}$1) plane.

Bibliography

[1] Anonymous. *Manganese Steel*. London, Oliver and Boyd, 1956.

[2] *Properties and Selection: Stainless Steels,Tool Materials and Special Purpose Metals*. Metals Handbook, Vol. 3. Ninth Ed. Metals Park, Ohio: A.S.M.,1980.

[3] Doepkin, H.C. Tensile properties of wrought austenitic manganese steel in the temperature range from +100°C to -196°C. J. Met., 1952, *Feb.*:166-170.

[4] Adler, P.H., G.B. Olson, and W.S. Owen. Strain hardening of Hadfield manganese steel. Met. Trans. A, 1986, *17A:* 1725-1737.

[5] Avery, H.S. and H.J. Chapin. Austenitic manganese steel welding electrodes. Weld. J., 1954, *May:* 459.

[6] White, C.H. and R.W.K. Honeycombe. Structural changes during the deformation of high purity iron-manganese-carbon alloys. J. Iron Steel Inst., 1962, *200:* 457-466.

[7] Cohen, M. The strengthening of steel. Trans. Met. Soc. AIME, 1962, *224:* 638.

[8] Hayden,H. W. , W. G. Moffatt, and J. Wulff, *The Structure and Properties of Materials*. Mechanical Behavior, vol. III. N. Y. : John Wiley & Sons, 1965.

[9] Remy, L. The interaction between slip and twinning systems and the influence of twinning on the mechanical behavior of fcc metals and alloys. Met.Trans. A, 1981, *12A:* 387-408.

[10] Roberts, W.N. Deformation twinning in Hadfield steel. Trans. Met. Soc. AIME, 1964, *230:* 372-377.

[11] Raghavan, K.S., A.S. Sastri, and M.J Marcinkowski. Nature of work-hardening in Hadfield's manganese steel. Trans. Met. Soc. AIME, 1969, *245:* 1569-1575.

[12] Champion, A. R. and R. W. Rnode. Hugoniot equation of state and the effect of shock stress amplitude and duration on the hardness of Hadfield steel. J. Apl. Phys.,1970, *41*: 2213.

[13] Dorph, K. Strain hardening of Hadfield manganese steel by explosive shock hardening. Scand. J. Met.,1977, *6* : 38-39.

[14] ASM, *The Inhomogenity of Plastic Deformation*, Metals Park, Ohio: ASM, 1973.

[15] Remy, L. Kinetics of f.c.c. deformation twinning and its relationship to stress-strain behavior. Acta Met., 1978, *26:* 443-451.

[16] Mahajan, S. and G.Y. Chin. Twin-slip, twin-twin and slip-twin interactions in Co-8 wt% Fe alloy single crystals. Acta. Met., 1973, *21*: 173.

[17] Mahajan, S. and D.F. Williams. Deformation twinning in metals and alloys. Int. Met. Rev., 1973, *18* : 43-61.

[18] Mahajan, S. and G.Y.Chin. Formation of deformation twins in fcc crystals. Acta. Met. 1973, *21*: 1353.

[19] Michels, H. T. and R. M. Forbes Jones. Work strengthening in a Fe-Ni-Co-Cr-Mo alloy. Met. Trans. 1974, *5:* 847-851

[20] Sipos, K., L. Remy, and A. Pineau. Influence of austenite predeformation on mechanical properties and strain induced transformations of a high manganese steel. Met. Trans. A 1976, *7A:* 857-864.

[21] Dastur, Y.N. and W.C. Leslie. Mechanism of work hardening in Hadfield manganese steel. Met. Trans. A, 1981, *12A:* 749-759.

[22] Zuidema, B. K., D. K. Subramanyam, and W.C. Leslie. The effect of aluminum on the work hardening and wear resistance of Hadfield Manganese steel. Met. Trans. A 1987, *18A* : 1629-1639.

[23] Collette, G., C. Crussard, A. Kohn, L. Plateau, G. Pomey, and M. Weisz. Rev Metall., 1957, 54: 433.

[24] Zackey, V. F. , E. R. Parker, D. Fahr and R. Busch. The enhancement of ductility in high-strength steels. Tran. ASM, 1967, *60* : 252.

[25] Olson, G. B. and M. Azrin. Transformation behavior of TRIP steels. Met Trans. A, 1978, *9A:* 713-721.

[26] Narutani, T., G. B. Olson and M. Cohen. Constitutive flow relations for austenitic steels during strain-induced martensitic transformation. J. De Phy. 1982, *43:* C4-429.

[27] Olson,G.B. Transformation plasticity and the stability of plastic flow, ASM Metals/Materials Technology Series, SAN-7586, 1983.

[28] Backofen, W. A. *Deformation Processing.* Reading, MA.: Addison - Wesley,1972.

[29] Chin, G.Y., W. L. Mammel and M. T. Dolan. Taylor analysis for {111}<112>twinning and {111}<110> slip under conditions of axisymmetric flow. Trans. Met. Soc. AIME, 1969, *245:* 383.

[30] Cahn, W. J. Thermodynamic and structural changes in deformation twinning of alloys. Acta Met. 1977, *25:* 1021-1026.

[31] Suzuki,T., H. Kojima, K. Suzuki, T. Hashimoto and M. Ichihara. An experimental study of the martensite nucleation and growth in 18/8 stainless steel. Acta. Met., 1977, *25:* 1151-1162.

[32] Drobnjak, D. J. and J. Gordon Parr. Deformation substructure and strain hardening characteristics of metastable Fe-Mn austenites. Met. Trans. 1970, *1*:759-765.

[33] Drobnjak, D. J. and J. Gordon Parr. Thermomechanical treatment and t ransformation characteristics of Fe-Mn Austenites. Met Trans. 1970, *1*:1521-1526.

[34] Reed-Hill,R. E. *Physical Metallurgy Principles*. 2nd ed. Monterey, Calif.:Brooks/Cole, 1973.

[35] Meyers, M. A. and K. K. Chawla, *Mechanical Metallurgy Principles and Applications*. Englewood Cliffs, N.J., 1984.

[36] Staker, M.R. Un-published research. U. S. Army Materials Technology Laboratory, Watertown, MA 1983-1987.

[37] Bhansali, J. Un-published research. U. S. Army Materials Technology Laboratory, Watertown, MA 1987-1988.

[38] Chinella, J.F. Un-published research. U.S. Army Materials Technology Laboratory. Watertown. MA, 1985-1988.

[39] Dieter, G. E. *Mechanical Metallurgy* 2nd ed. New York, New York: McGraw-Hill, 1976.

[40] *Metallography and Microstructure*. Metals Handbook, Vol. 9. Ninth Ed. Metals Park, Ohio: ASM, 1985.

[41] Sastri, S. and R. Ray. Mössbauer studies on aging of highly deformed Hadfield's manganese steel. Met. Trans., 1974, *5*: 1501-1502.

[42] Woodward, R. L. A rational basis for the selection of armour. J. Austr. Inst. Met., 1977, *22*:167-170.

[43] Yellop, J. M. and R. L. Woodward. Investigations into the prevention of adiabatic shear failure in high strength armor materials. Res Mech., 1980, *1*: 41-57.

[44] Garde, A. M., E. Aigeltinger, and R. E. Reed-Hill. Relationship between deformation twinning and the stress-strain behavior of polycrystalline titanium and zirconium at 77 K Met. Trans., 1973, *4*: 2461-2468.

[45] Keshavan, M. K., G. Sargent, and H. Conrad with R. E. Reed-Hill, J. R. Donoso, and A. M. Garde. Communications-Discussion of "Relationship between deformation twinning and the stress-strain behavior of polycrystalline titanium and zirconium at 77 K." Met Trans A., 1975, *6A*: 1291-1294.

[46] Porter, D. A. and K. E. Easterling. *Phase Transformations in Metals and Alloys*. Wokingham, Berkshire, England: Van Nostrand Reinhold (UK) Co. LTd, 1984.

[47] Green, L. M. and M. Cohen. Pseudotwinning and pseudoelasticity in β Fe-Be alloys. Acta Met., 1979, 27: 1523-1537.

[48] Magee, C.L., D. W. Hoffman, and R. G. Davies. The effect of interstitial solutes on the twinning stress of b.c.c. metals. Phil. Mag., 1971, *23*: 1531-1540.

[49] ASTM, *Internal Friction Damping and Cyclic Plasticity*, STP 378, Philadelphia, ASTM, 1964.

Appendix

1.0A *Introduction to Martensitic and* Twinning Transformations

Because of the commercial importance and readily recognizable effects of the martensitic transformation in steels, martensitic transformations have been thoroughly studied during modern metallurgical history [7]. In contrast, deformation twinning in fcc alloys in particular was unrecognized until Blewitt's discovery of twinning in copper at 4.2 °K in 1957 [9,34].

Since Blewitt's discovery, fcc twinning has also been observed and studied in many alloys both at low and ambient temperatures. Mahajan and Williams [17], have reviewed deformation twinning (including fcc twinning) and Remy [9] has reviewed slip-twin interaction and the influence of twinning on the mechanical behavior behavior of fcc metals and alloys. According to Remy, the importance of twinning in many fcc commercial alloys is often misconceived as irrelevant in the common understanding of fcc deformation behavior. Reed-Hill has reviewed the role of deformation twinning on slip and plastic flow behavior in reviews [14], in experimental studies with Garde [44], and in controversial communications [45]. Adler [4] has demonstrated that the role of deformation twinning in influencing slip and plastic flow behavior in Hadfield steel may be described by transformation plasticity effects of dynamic softening and static hardening.

Martensitic transformations and mechanical or deformation twinning are fundamentally similar in that both transformations involve coordinated diffusionless shear-like displacements of a finite volume of parent crystal into a product of different orientation [34]. The kind of growth mechanism of these transformations are also similar since deformation twin and martensitic growth occurs by particular kinds of coordinated dislocation movements and glide, through glissile interfaces [46] that shear parent lattice into product. The motion of the glissile interface is not dependent upon thermally activated motion of individual atoms so that growth can be insensitive to temperature over particular ranges of temperature, and the product interface growth or motion can be called athermal [46]. The glissile interface controlled martensitic and twinning transformation are referred to as *military transformation* [46], to emphasize the analogy of marching ranks of soldiers and coordinated motions of atoms crossing an interface.

Both martensitic and deformation twinning transformations are thus defined in how they are formed and grow, and not in their specific end structure or properties.

Whereas martensite products are a different phase from that of the parent matrix, mechanical twins that do not undergo a shape change during the twin shear are identical in phase as that of the twin crystal.

Martensitic and twinning transformations can both result from strain [9,14,15,20,24,26,31]. Both kinds of transformation are influenced by kinetics, through temperature and strain so that the rate and extent of transformation can influence deformation microstructure, dislocation slip, and therefore plastic flow behavior or mechanical properties [15,24-27,31]. Both kinds of transformations may share similar kinds of known contributing hardening mechanisms [7] or proposed hardening methods [4,30,47,48]. Either kind of transformation product can distort the surrounding matrix leading to accommodation by dislocation slip to influence deformation slip structure and plastic flow behavior [27,34,35,].

Both kinds of products are related to the parent matrix as in a Kurdjumov-Sachs (K-S) relation and habit plane-matrix orientation as in martensite or whether by a twinning plane and polar twin shear for mechanical twinning. These orientation relations to the parent phase can also influence dislocation slip and plastic flow behavior [14,31,44].

Adler, Olson, and Owen [4] suggested that because of close similarities between deformation twinning and martensitic transformation, constitutive flow models developed for the understanding and interpretation of martensitic transformation plasticity may provide a basis for a better understanding of the influence of twinning on Hadfield steel plastic flow behavior. One purpose of this literature review is therefore to provide a description of martensitic transformation plasticity on plastic flow behavior in tension of metastable austenitic steel, including recent proposed constitutive flow relations of martensitic transformation plasticity [20]. Another pupose of this review is to review deformation twinning hardening mechanisms and Adler, Olson, and Owen's [4] Hadfield steel study.

Martensitic strain induced bct transformation in metastable austenitic steels is well known to influence plastic flow behavior [24-28] in a manner dependent upon the extent and rate of transformation. In metastable austenitic steel thermomechanically processed to high yield strengths in the austenitic condition, the effect of subsequent strain induced martensitic transformation was studied by Zackay, Parker, Fahr, and Busch [24]. The unusual properties of high strength, enhanced ductility, and high toughness of these steels was described in part by Zackey et. al. through the acronym *TRIP* for *transformation induced plasticity*, that was proposed to be used to identify and describe the plastic flow behavior of these steels.

More recent efforts to describe the effects of strain induced transformation [26] have included the use of of constitutive flow relations between imposed strain and resultant flow stress through observations of the rate and extent of strain induced transformation. Resultant stress in these constitutive flow relations was described by flow hardening and softening, attributed to the operation of dislocation slip and martensitic transformation plasticity effectively serving as parallel and alternative deformation mechanisms under particular conditions of imposed strain and temperature.

2.0A Martensitic Stress Assisted and Strained Induced Transformation and Effects of Transformation Plasticity

2.1A Spontaneous, Stress, and Strain Induced Kinds of Martensitic Transformations

Martensitic transformation mechanisms have been distinguished by types of driving force that provide the required thermodynamic nucleation energy requirements for transformation. At the start of spontaneous transformation (M_S), chemical free energy alone is sufficient to initiate martensitic transformation. On increasing temperature above M_S, transformation is considered to be *stress assisted* ; that is the driving force for transformation now may be assisted by strain energy. At a temperature limit of M_σ^S, transformation changes from primarily elastic stress assisted to what is called plastic *strain induced* . At a temperature M_d, no further martensitic transformation occurs as a result of plastic strain.

In the stress induced region, the primary deformation mode may be considered the martensitic transformation and yielding may be considered to occur from the martensitic transformation strain at stresses below those expected for slip in a non-transforming austenitic alloy. A general positive temperature dependence of yield stress is observed in the stress induced region near M_σ^S.

In the strain induced region, the dominant deformation mechanism may be considered to be slip, and the strain induced transformation may be considered to occur significantly only after slip plastic flow. The yield stress decreases with increasing temperature in the strain induced transformation region.

Since the temperature dependence of yield stress has different slopes near M_σ^S, M_σ^S may be determined experimentally by the intersection of the two slopes of yield stress versus temperature. The two regions of transformation may also be determined by comparison of yield stress and the stress at which a detectable threshold amount, say one percent of martensite is observed.

2.2A Effects ot Kinetics During The Stress and Strain Induced Martensitic Transformation

The kinetics or the influence of temperature, time, or strain on the volume fraction (f) of martensite formed is shown in Figure (2) for solution treated 0.27 C, M_σ^S = -98 °C TRIP steel anc for warm rolled 0.27 C, M_σ^S = 40 °C metastable austenitic steel undergoing tensile deformation versus temperature [25]. The f - ε and the σ - ε curves indicate very similar behavior, so that it can be inferred that the rate of transformation imposed by strain and temperature has a very strong influence on the observed flow behavior. The general shape of the f - ε curves can be described as sigmoidal at temperatures near M_σ^S in the strain induced region, while at temperatures in the stress assisted region, a high rate of transformation occurs with strain and the f- ε curves are initially linear. At high temperatures near M_d, the f- ε curves are again linear but with a low rate of transformation with strain.

The plastic strain due to the stress assisted martensitic transformation itself, for example, the strain and softening observed at low temperatures and stresses, is called *transformation plasticity.* Transformation plasticity describes a unique condition of achievement of macroplastic strain observed in a variety of transformations during phase changes under stress [14,27]. Transformation plasticity can provide contributions of strain by flow softening and flow hardening.

In addition to the well recognized effects of hardening due to martensitic transformation in carbon steels, martensitic transformation plasticity during the γ to α' strain induced transformation in metastable austenitic steels result in volume shape change toughening, macroplastic strain, and softening. The determination of softening and hardening effects and mechanisms of strain induced martensitic transformation plasticity can be difficult since strain induced martensite can have a wide variety of microstructure and properties.

For diffusional allotropic phase transformations [14,27], the interactions of the transformation and deformation occur microscopically as a result of applied resolved stress biasing around transforming particles during the transformation volume change. This stress biasing provides an assist to shape change and contributes to transformation plasticity strain through a bias in volumetric strain and accommodation strain. This volumetric strain from transformation may also contribute to the well known toughening due to transformation plasticity.

An example of allotropic phase transformation plasticity is shown by the changes in length of polycrystalline iron as a function of stress while undergoing the α to γ and γ to α transformation for one complete cycle of heating and cooling [14]. Whereas the transformation yields zero net strain with no applied stress, for heating or cooling to the equilibrium structure through the allotrope temperature, the combined interaction of an applied stress, with magnitude below the yield stress of a non-transforming structure, and the transformation itself results in a net strain, called transformation plasticity. Repeated cycling through the allotropic transformation with applied stress can lead to large uniform elongations.

Transformation plasticity also serves as an alternative or parallel deformation mechanism, so that a softening contribution to strain can be provided quite different from the hardening behavior usually observed in the plastic flow or rheology of most materials. An example of softening through transformation plasticity can be shown by an experimental wireless drawing process [14]. This process uses a narrow induction heated zone passed along a cylindrical rod towards toward a fixed end with velocity V_1. The rod is drawn at constant velocity V_2 in the opposite direction for cross sectional reductions up to 50 % per pass. A significant reduction in drawing force can be achieved, since the transformation plasticity strain occurs at a stress below the normal yield stress of the material.

2.3A A Softening and Hardening Mechanism During the Strain Induced Martensitic Transformation

An unambiguous example of the softening effect associated with the martensitic transformation under stress was provided by T. Suzuki et. al. [31] in a study of the α' transformation in 18Cr-8Ni stainless steel. Suzuki investigated the cause of anomalous strain hardening in this alloy at low temperatures by the observation of easy deformation in the early stage of deformation and rapid hardening in the later stage of deformation.

Suzuki found by transmission electron microscopy study that α' formed in only a few crystallographic orientations with the Kurdjumov-Sachs (K-S) orientation relationship $\{111\}_\gamma \parallel \{110\}_\alpha$ and $\langle 110\rangle_\gamma \parallel \langle 111\rangle_\alpha$ during the early easy deformation stage on primary slip planes at slip band intersections. It was also found that in most cases, the $\langle 110 \rangle_\gamma$ direction and the direction of the intersection of the two slip bands were parallel to one another in the early easy deformation stage.

Suzuki interpreted this behavior such that when dislocations piled up against a barrier; in this case an intersecting slip band, the high local stresses could induce a martensitic transformation along their path and the martensite thus formed could act as a window for the gliding dislocations to penetrate through by the occurrence of the transformation, and by the orientation of the slip systems of the K-S γ - α' orientation relation which can allow the fcc austenite to easily pass dislocations to and through the bct martensite. Ductility can be enhanced and softening can occur by the avoidance of the inhibition of slip during the shear band intersection transformation.

At high strains, significant numbers of other variants or crystallographic orientations were observed in the rapid hardening stage. Suzuki suggested that since the martensites formed are transparent only for gliding dislocations on the slip plane parallel to the planes which satisfy the K-S relations, a net softening effect occurs during early deformation when slip takes place only on the most active slip planes with nearly a single variant. At higher strains, Suzuki suggested that hardening commences when slip and transformation forms large numbers of other variants along additional and more increasingly active slip bands.

At higher temperatures, Suzuki's data suggested α' martensites formed at higher strains later during the deformation and easy slope behavior associated with the most active slip bands and transparent slip for enhanced ductility would be displaced to later deformation stages.

Suzuki has thus shown that the martensitic transformation acting in a parallel or an alternative deformation mechanism to slip can act as both a softening and hardening entity during deformation.

2.4A Constitutive Flow Equations For The Strain Induced Martensitic Transformation In Metastable, Austenitic Steels

Constitutive relations described below from Lazan [49] have been used in mechanics, materials and other fields to model complex system behavior on the basis of a forcing function (F), a system of materials or structure defined by a law or environment (S), and an output response behavior or reaction (R). In materials and mechanics applications, the output response of stress is usually related to rheological type behavior through deformation flow, creep, relaxation, damping, and, in the case of strain induced transformations, also by microstructure in the form of volume fraction of transformation product. Responses or outputs can also be re-applied to the system input for purposes of simplification during relational modeling of behavior for imposed

conditions. The system relations can be linear or non-linear, and should include all terms that are able to predict all details of output in order to be general. The general constitutive equation may be complicated, so a simplified or idealized form may be used that includes a limited number of easily determined relevant variables.

Narutani, Olson and Cohen [26] have applied constitutive modeling to the flow behavior of metastable austenitic steels *during* the strain induced transformation combined with slip. Narutani has determined that the system flow behavior can be modeled with excellent results by the major contributions of strain induced transformation plasticity through terms of softening and hardening called *dynamic softening* and *static hardening*, similar to the softening and hardening effects observed by Suzuki [31].

Transformation plasticity leading to macroplastic strain during the martensitic transformation occurs as a result of stress biasing [25,27]. During stress assisted martensitic transformation, imposed loading may favor or bias resolved stress on planes and directions in favor of variant orientations where the maximum thermodynamic assist of strain energy driving force is provided for transformation dilatation and shear.

In a metastable austenitic steel undergoing the strain induced transformation, macroplastic strain arises from slip accommodation of the martensitic dilatation and deviatoric strains along favored slip planes and favored directions of applied maximum resolved shear stress.

A greater net strain is observed during the strain induced transformation from the strain contribution of the martensitic shape change itself in initially ausformed rather than solution treated metastable austenitic steels. This greater net strain in ausformed or warm rolled conditions is due to a stronger martensitic crystallographic orientation bias from the warm rolled deformed structure. These ausform treatments that lead to the additional strain also contribute pronounced early softening during the early deformation stage in the stress assisted region, so that yield stress may be observed at low temperatures at values less than those observed from yielding by slip alone at higher temperatures.

In summary, martensitic transformation plasticity *during deformation* can contribute effects of softening and hardening, for enhanced ductility. At low strains slip inhibition is avoided and contributions of softening occur by strain induced transformation at shear band intersections. This softening contribution to stress may increase ductility by lowering work hardening rates for a given fracture stress. At high strains the work hardening and flow stress is high as transformation rate

decreases. The greater work hardening rates at high strains may enhance ductility by maintaining a high work hardening rate at high flow stress.

The macroplastic martensitic strain contributes to the observed strain from bias of slip accommodation and the shape change of the transformation itself due to a bias in variant orientation. Enhanced toughness is bestowed from the accommodation strain and from high localized strain hardening that inhibits incipient plastic instabilities of microcracking and void nucleation leading to fracture. The combined softening at low strains and hardening at high strains with high toughness can lead to strain hardening to high levels of strength at large strains, unlike the usual inverse strength-ductility relation of quenched and tempered steels.

Metastable austenitic steels that have been specially processed to obtain combinations of strength and high ductility. One class of these steels have been given the acronym *TRIP* [24] from the wo ds *transformation induced plasticity* to distinguish their unique characteristics of deformation and mechanical behavior.

The strain induced martensitic transformation is complicated and not fully understood, but even more complex behavior is found during deformation by combined slip and martensitic transformation during strain induced martensitic transformation. Because of the complexity of the strain induced transformation in austenitic metastable steels undergoing deformation, it is difficult to predict flow behavior by modeling in these steels. One approach used for understanding and modeling the plastic flow behavior of metastable austenitic steels during the strain induced transformation has been through the use of constitutive equations or relations.

The mechanical properties of TRIP steels may be better understood from constitutive relations based upon continuum plasticity and plastic flow instability conditions [27], and from constitutive flow models of strength based upon imposed strain and temperature dependent volume fraction of transformation [26,27]. Continuum plasticity theory plastic flow instability is determined both from physical requirements of maximum load and mathematically by $df = d(\sigma A) = \sigma dA + Ad\sigma = 0$, with the strain increment $d\varepsilon = dA/A$ resulting in $d\sigma/d\varepsilon = \sigma$. Therefore stable plastic flow requires ($dp > 0$) and

$$(5) \qquad d\sigma/d\varepsilon > \sigma.$$

Equation (5) specifies that the minimum strain hardening required at all strains in order to prevent plastic flow instability must be greater than the instantaneous stress. The corresponding work hardening curve for minimal work hardening to prevent

necking and fracture [27] is the solution of the differential equation of $d\sigma/d\varepsilon = \sigma$ and is the exponential function shown in Equation 6.

$$(6) \qquad \sigma = \sigma_0 \exp(\varepsilon).$$

The derivative or the work hardening rate of Equation (6) is $d\sigma/d\varepsilon = \sigma_0 \exp(\varepsilon)$ again is the original function itself, so for exponential plasticity, work hardening increases along with strain with increasing upward curvature, unlike the downward curvature associated with dislocation structural hardening and recovery type plasticity [28] often modeled by the power law as in equation 7.

$$(7) \qquad \sigma = K \varepsilon^{n}.$$

According to Olson [27], the onset of necking during power law hardening of equation (7) is usually interpreted with too small of local hardening, and that to increase uniform ductility, the strain hardening exponent should be increased. Olson suggested, that an alternative approach to increase uniform ductility for a given fracture stress would be to lower the initial hardening rate by a softening mechanism as in exponential flow hardening of Equation 6. The softening mechanism associated with transformation plasticity can serve to contribute this enhanced plastic flow stability in the lower strains, where the power law curve rises above the exponential hardening curve. At higher strains, transformation plasticity can contribute needed hardening and upward curvature from a lower rate of transformation and an increased rate of hardening from a high final volume fraction of transformed martensite.

An important conclusion of the power law and exponential law hardening behavior comparison is that softening can be as potentially important as high strain hardening in promoting the stability of plastic flow. Furthermore, if ideal exponential hardening occurs by early softening and later hardening, necking will not occur and and the resulting uniform ductility will be controlled by material properties and fracture. It has been shown [27] that the stress-strain curves of maximum uniform ductility in TRIP steels may closely approximate ideal exponential hardening.

An early attempt by Gerberich et. al.to model constitutive flow σ - ε behavior of TRIP steels [25] used a rule of mixtures (ROM) approach as in Equation (8) :

(8) $$\sigma = \sigma_\gamma + f(\Delta\sigma)$$

where

$\sigma = \gamma$ flow stress

f = volume fraction martensite

$\Delta\sigma$ = strength difference between γ and α' phases.

Olson and Azrin [25] found that the above equation does not accurately describe observed hardening behavior since Equation (8) requires that the flow stress of the two phase mixture always be above the austenite flow stress. The ROM approach of Equation (8) clearly neglects the softening contribution at low strains. At lower temperatures correlating to high rates of transformation, a great error in flow stress from Equation (8) is clearly seen from the softening contribution of the transformation.

Another constitutive flow relation for modeling strain induced martensitic transformation σ - ε behavior was proposed by Narutani, Olson, and Cohen [26] that considered two distinct deformation mechanisms during deformation; that is slip and transformation plasticity. Deformation by combined slip and transformation plasticity in the Narutani model included transformation plasticity effects of *static hardening* associated with slip in a austenitic-martensitic two phase rule of mixtures and *dynamic softening* associated from the operation of the martensitic transformation as a parallel or alternative deformation mechanism as discussed by Suzuki [31].

The Narutani model determined that the static hardening and dynamic softening contributions of transformation plasticity can accurately describe flow behavior of a transforming material during deformation from knowledge of volume fraction transformed martensite versus strain curves (f vs ε) and from knowledge of the flow properties (σ vs ε) of the two phases of constituent martensite and austenite.

Narutani's study shows results of σ vs ε curves of constituent austenite, martensite and transforming experimental alloy, and a transformation curve of f (α') vs ε . Material used for the metastable austenite (alloy A) was a 14Cr-7Ni-2Cu-1Mn-0.5Si-0.12C commercial high formability austenitic stainless steel. A stable austenitic steel was derived from Alloy A by increasing the Cr and Mn contents to 4.8% and 17.8% in order to maintain a constant intrinsic stacking fault energy. A martensitic composition was obtained from A by reducing the Cr content to 6.9%.

Stress strain curves and volume fraction curves were used to predict contributions of static hardening and dynamic softening to flow stress. The $\sigma_{\alpha'}$ martensite curves obtained by Narutani exhibited a uniform elongation of less than 4% and were extended by use of a power law fit from the low strain and local necking measurements. The

metastable austenitic experimental (σ_{exp}) σ - ε curves and f - ε curves exhibited normal negative temperature dependence of yield stress and sigmoidal transformation curves indicative of strain induced transformation. The measured σ_γ curves were shifted upwards slightly in order to compensate for a small 27 MPa difference in the yield stress between the metastable austenite and austenite curves.

An initial estimate of static hardening contribution to flow behavior was made by an approach of rule of mixtures static hardening contributions from equivalent hardness of α' and γ based on the f - ε curves of martensite and based on σ - ε curves of austenite and of martensite. This initial estimate determined the hardening effect based on rule of mixtures (RM) composition of martensite and austenite with the assumption that the strain in both α' and γ phases was equal to the macroplastic or observed experimental strain. Narutani noted this assumption was made from results of ausforming studies that indicated austenitic substructure was inherited by martensite, and that the strengthening contributions of deformation and transformation superimpose. Under these conditions, Narutani concluded the strengthening contributions of deformed and freshly formed martensite of deformed austenite at equivalent strain are comparable.

A second estimate of the static hardening contribution to flow stress was made in which the effective strain due to slip in both phases was not assumed to be equal to the macroplastic strain or imposed strain, since the macroplastic strain was now considered by Narutani to arise in part from stress biasing and orientation of the martensitic shape change which did not contribute to the working of either phase. To correct for the transformation plasticity contribution to macroplastic strain, the total imposed macroplastic strain (ε) less transformation strain (ε_t), was related to the plastic slip strain of the phases. The amount of imposed transformation strain was related to the amount of transformation with $\varepsilon_t = \alpha$ f. This strain corrected rule of mixtures (SCRM) then predicted the *static flow stress* (σ_S) from the slip contribution of deformation arising from the two phase rule of mixtures hardening of austenite and of martensite as shown in Equation (9):

(9) $$SCRM = \sigma_S = [\,1 - f\,]\sigma_\gamma(\,\varepsilon - \alpha f\,) + f(\sigma_{\alpha'})(\varepsilon - \alpha f\,)$$ where

f = volume fraction of α' martensite

ε = macroplastic or observed strain

σ = flow stress of austenite (σ_γ) or martensite ($\sigma_{\alpha'}$) at equivalent macroplastic strain

α = strain correction coef. = max upper limit of 0.12 at -196 ° C from slope (ε/f) of linear f vs ε curve.

The static flow stress σ_S was also estimated experimentally from yield strengths attributed to slip yielding at high temperatures where no transformation plasticity could occur as at 63 °C. These yield strength values of static hardness without transformation plasticity were corrected by temperature dependence of flow stress and corrected by aging contributions to hardening for comparison to lower temperature estimates by the theoretical RM and SCRM models. The static flow stress estimated by this direct elevated temperature method without transformation plasticity was in general agreement with the theoretical SCRM model.

By the SCRM model comparison to σ_{exp}, Narutani observed that experimental flow stress of the transforming alloy occurred at a significant lower stress than that of the SCRM model, which indicated a substantial dynamic softening increment associated with the separate transformation plasticity deformation mechanism. Narutani suggested that the true stress of the transforming material could be expressed as :

(10) $\sigma = \sigma_S - \Delta\sigma_d$ where

$\Delta\sigma_d$ = dynamic softening increment from the avoidance of slip inhibition through a parallel deformation mechanism of transformation plasticity.

Narutani found that results of temperature dependent f vs ε in prestrain tests suggested that the dynamic softening increment for a fixed prestrain was proportional to $df/d\varepsilon$ with a proportionality constant that increased with increasing σ_S and $df/d\varepsilon$. An example of this softening behavior with was provided by Narutani in describing flow in the stress assisted region at low temperatures where the flow stress and $df/d\varepsilon$ determined by transformation plasticity is initially constant versus imposed strain and so an increase in the static hardening by the strain corrected rule of mixtures must be accompanied by a linearly related increase in $\Delta\sigma_d$.

A plot of $\Delta\sigma_d/(df/d\varepsilon)$ vs σ_S was given with data based on the SCRM curves and by data representing the RM and prestrain-experiment studies estimates, was found by Narutani to result in a linear plot that defined a relation dependent on σ_S, independent of temperature and strain rate over the range examined. Narutani concluded therefore a relation for $\Delta\sigma_d$ could be obtained as:

(11) $\Delta\sigma_d = \beta\frac{df}{d\varepsilon}\sigma_S$ with the slope of $\beta = 5.3(10)^{-2}$.

Narutani combined equations (9) to (11) for a complete constitutive relation for the plastic flow of a metastable austenitic steel undergoing a strain induced martensitic transformation:

$$(12) \qquad \sigma = \{ [\, 1 - f \,]\sigma_\gamma(\varepsilon - \alpha f) + f \sigma_{\alpha'}(\varepsilon - \alpha f) \} \, [1- \beta \frac{df}{d\varepsilon}].$$

Calculated σ - ε curves from Equation (12) were compared against the experimental curves. Narutani concluded that the curves showed excellent agreement.

The authors noted from their results, that flow curves of σ_γ and $\sigma_{\alpha'}$ are rather weakly temperature dependent in comparison to large changes in the transforming metastable alloy f - ε and σ - ε curves so that the σ - ε curve behavior must be dominated by the f - ε kinetics of the transformation.

In conclusion, the authors stated that flow curves of metastable transforming austenite (σ_{exp}), α' and γ, allowed a separation of static hardening and dynamic softening contributions to the flow behavior of metastable austenite. The flow stress of the static hardening two phase mixture, σ_S was described by a strain corrected rule of mixtures. The dynamic softening effect of the transformation as a parallel deformation mechanism $\Delta\sigma_d$, was proportional to df/dε and σ_S. The combined effects of static hardening and dynamic softening were related in a constitutive relation that predicted flow stress for metastable austenites determined by the strain induced transformation kinetics and the flow properties of the two constituent phases.

3.0 Deformation Twinning With Combined Slip In Face Centered Cubic Metals

3.1A Introduction

Deformation twinning is not well recognized and is often considered to be of minor importance in the deformation of fcc metals and alloys. In contrast to this common belief, Remy [9] has pointed out in a recent review that since Blewitt's discovery in 1957 of twinning in pure copper, deformation twinning has been shown to occur in a number of fcc industrial Cu, Co, and Fe base alloys. According to Remy, the misconception that fcc deformation twinning is of minor importance to fcc deformation behavior may be due to the fact that deformation mechanism studies have often been restricted to single crystals of pure metals of high stacking fault energy (SFE) that do not twin readily at low temperatures. A general review of deformation twinning in metals and alloys has been written by Mahajan and Williams [17]. Another recent review by Remy [15], modeled deformation twinning and its relationship to stress strain behavior based upon fcc twinning kinetics.

The roles or influence that deformation twinning may have on slip for softening and hardening have been reviewed by Reed-Hill [14], and experimentally investigated and discussed by Garde, Aigeltinger, and Reed-Hill [44]. The controversy of the role twinning may provide to work hardening during combined slip and twinning has been exemplified by the Communications, of Keshavan,Sargent and Conrad and Author's Reply, of Reed - Hill, Donoso, and Garde [45], in regard to [44].

It is known that twinning, in comparison to slip, cannot alone provide strains of the large magnitudes observed for mixed slip twinning deformation. A single fcc crystal originally oriented so as to have the maximum resolved shear stress applied to it, may have a first order twinning contribution of strain in tension of approximately 0.40 [14]. Thus, crystals that undergo high strains by twinning and slip must undergo a large strain contribution by slip deformation. The slip contribution may be provided by slip bands, twin accommodation dislocations, and shear bands of highly active and localized slip bands.

The exact details of fcc deformation twinning are not completely understood in regard to the nucleation, propagation,and growth steps of twinning. One of the most recent theories of fcc twin nucleation is due to Mahajan and Chin [18]. Mahajan has proposed that twin nuclei can form by three layer microtwins by dislocation interactions of:

$$(13) \qquad \frac{1}{2}\langle 110\rangle + \frac{1}{2}\langle 101\rangle \dashrightarrow 3 \times \frac{1}{6}\langle 211\rangle.$$

3.2A Kinetics of fcc Deformation Twinning

Remy [15] considered the Mahajan model in his study of the relationship of deformation twinning with combined slip to the stress-strain behavior in fcc Co-33Ni. The Mahajan model implies that the number of macroscopic twins which form can be assumed to be proportional to the number of twin nuclei present as a result of plastic strain and the overall dislocation density. Remy assumed that the production of twin nuclei by Equation (13) was possible only for a suitable stress level, equivalent to a critical strain level (ε_C) in the case of a polycrystalline specimen.

Remy's twin kinetics curves and work hardening curves of true stress - strain (σ - ε) and twin volume fraction-true strain (f-ε) show sigmoidal, parabolic and linear shapes at ambient to high temperatures. In comparison to martensitic f -ε curves, the twin curves saturate at much lower volume fractions of transformation product. The twin kinetics curves also show that twinning started after only a critical strain (ε_C) which increased with increased temperature. Most importantly, the similarity of Remy's f-ε curve and σ -ε curve shapes at a given deformation temperature suggests that twinning kinetics strongly influence flow behavior in a somewhat similar manner to that observed for the strain induced γ to α' transformation in TRIP steels.

Remy concluded from his twin kinetics study of polycrystalline Co-33Ni that the critical shear twinning stress was an increasing function of temperature as a consequence of a temperature dependence of twinning stress on stacking fault energy which in the simplest approximate form is $\Delta G^{\varepsilon-\gamma}$.

3.3A Strain Hardening by FCC Deformation Twinning
Hall-Petch Structural Refinement

Two ways in which fcc deformation twinning have been most often previously accepted as contributing to strain hardening are by orientation or geometric hardening, and grain subdivision or Hall-Petch type substructure refinement.

Grain subdivision deformation twin hardening has been described by Mahajan and Chin [16] for fcc Co-8Fe, by Raghavan [11] for fcc Hadfield steel, and by Remy [9,15] for fcc metals and alloys and Co-33Ni. In general, the research on this mechanism of strain hardening agrees that in order for a dislocation to penetrate into an obstacle twin acting as a coherent boundary, the incident dislocation in most cases must dissociate into a slip dislocation in the twin and into a partial dislocation left at the boundary. The dislocation dissociation reactions required for this cross slip have been shown to be energetically unfavorable by the above studies so that stress concentrations from pile up of incident slip or twinning dislocations on twin boundaries occur before the incident dislocations penetrate the twin barriers. This increased stress required for penetration of twin barriers results in extra work hardening analogous to Hall-Petch hardening due to grain size refinement.

In addition to deformation twins serving as obstacles to undissociated dislocations, deformation twins have also been shown [9,11,16] to be structural barriers to other deformation twins and also stacking fault dislocations.

Remy [15] considered the development of a Hall-Petch law by defining (ε_m) and (σ_m) as average strain and flow stress at a temperature were an alloy deforms by both slip and twinning. Before twinning onset, the applied strain (ε_p) equaled the average or macroscopic strain (ε_m), and the overall flow stress (σ_p) equaled the average or macroscopic stress (σ_m).

When the applied strain ε_p was higher than the critical twinning strain (ε_c), the macroscopic or applied strain (ε_p) was considered to result from both the average strain in the matrix due to slip (ε_m) plus the shear due to twinning (ε_t). Similarly the overall flow stress σ_p was now due to the average slip flow stress of the matrix (σ_m) and an additional hardening increment due to Hall-Petch twin-slip interaction ($K_t x^{-r}$). The overall flow stress (σ_p) was written as :

(14) $\sigma_p(\varepsilon_p) = \sigma_m(\varepsilon_m) + K_t x^{-r}$ where $r = +1$, K = constant,

x = average distance between twins.

Remy obtained the average distance between twins from the method of Fullman's volumetric analysis for a distribution of fine disks:

$$(15)\quad N_L = \frac{1}{x} = \frac{1}{2t}\,\frac{f}{1 - f}$$

where

x = distance between neighboring twins
NL = number of twins line intersected per unit length
t = thickness of twins
f = volume fraction of twins.

Remy then substituted Equation (14) into (15) to obtain:

$$(16)\quad \sigma_p(\varepsilon_p) = \sigma_m(\varepsilon_m) + K_T(2t)^{-r}\left(\frac{f}{1 - f}\right)^r.$$

Remy found very good agreement with experimental results for r = 1 using Equation (16).

3.4A Strain Hardening by Texture Development or Geometric Hardening

The orientation factor hardening may contribute to hardening in fcc alloys undergoing combined slip and twinning as shown by Chin, Mammel and Dolan [29].

Chin et. al. computer modeled a Taylor least work analysis that considered both fcc {111} <110> slip and {111} <112> fcc deformation twinning during axisymmetric (restricted slip) tension and compression. Chin's model assumed equal critical resolved stresses for all respective slip or twinning systems, and assumed that slip and twinning compete to allow axisymmetric or constrained deformation. In order to maintain polycrystalline shape compatibility, a total of five slip or twinning systems were required per crystal from among the possible twelve slip systems and twelve twin systems. It is of interest that the assumption of competing deformation systems of slip and twinning may provide a contribution to softening, such that alternative, and

parallel deformation mechanisms are available. Chin's combined fcc slip-twinning Taylor model are given in Equations (17) and (18):

$$(17) \qquad W = \sigma_X \varepsilon_X = \tau_S \sum_i s_i + \tau_t \sum_i t_i$$

where

W = least work done

σ_X = applied stress

ε_X = axial strain

τ_S = the critical resolved shear (CRSS)stress for slip

τ_t = the CRSS for twinning

σ_i ,t_i = corresponding minimal shears from an ith system for slip and twinning, and therefore if

$\alpha = \frac{\tau_t}{\tau_S}$ = is defined as the ratio of the stresses for twinning vs slip, for $\alpha < 1.00$, twinning is favored.

then

$$(18) \qquad M = \frac{\sigma_X}{\tau_S} = \frac{1}{\varepsilon_X}\left(\sum_i s_i + a \sum_i t_i\right).$$

Results of Chin's model were given as plots of the Taylor factor $M = \frac{\sigma_X}{\tau_S}$ for crystallographic orientations and for ratios of critical resolved stress for twinning and slip $\alpha = \frac{\tau_t}{\tau_S}$.

To gain a basic understanding of Chin's Taylor analysis, Backofen [28] showed that a full analysis of a combined Taylor analysis as in Equation (18) was not necessary, but rather only required the individual Schmid factors m_S and m_t for a few orientations.

The kind of deformation within a crystal potentially occurring as fcc slip, mixed slip and twinning, or twinning, was shown by Backofen to be dependent upon the state of applied stress and upon the crystallographic orientation. This dependence of kind of deformation upon state of stress and orientation was also determined by the ratio (α) of Schmid factors ($m = 1/M$) of twinning to slip on {111} planes such that for $\alpha < 1$, twinning becomes favored as a kind of deformation mechanism.

Whereas slip is unidirectional with equal Schmid factors in tension or compression, deformation twinning is polar and has different Schmid factors in tension and compression. Chin, Mammel and Dolan, and Backofen demonstrated that as deformation becomes dominated by twinning, differences in the Schmid factors for tension or compression may contribute to anisotropic hardening or increased differences in Taylor factors among the crystal orientations, and from this anisotropic hardening, texture development may result. In particular it was shown for fcc combined slip and deformation twinning, that compression deformation may lead to increased anisotropy and hardening during texture development, but that deformation in tension may lead to a reduction of anisotropy during texture development.

Following is some of the approach that Backofen used in his discussion of Chin, Mammel and Dolan's Taylor analysis.

Direction cosines are convenient to find Schmid factors for the determination of the limits of pure twinning and pure slip in regard to α, and for determination of critical resolved shear stress in Equation (19).

$$\tau = \sigma_y \cos(\phi)\cos(\lambda) = \frac{\sigma_y}{M} = \sigma_y m \qquad \text{where} \tag{19}$$

σ_y = measured value of tensile stress σ_x at yielding
ϕ = angle between slip plane normal and σ_x
λ = angle between slip direction and σ_x
$m = \cos(\phi)\cos(\lambda)$ = Schmid factor for yielding in single crystals
M = reciprocal of Schmid factor

Critical resolved shear stress and Schmid factors in Equation 19 may be determined using direction cosines by the formula **V**/v where $\mathbf{V} = a\mathbf{i} + b\mathbf{j} + c\mathbf{k}$ and $v = \sqrt{a^2 + b^2 + c^2}$. This direction cosine formula may be applied to a cubic crystal to obtain the direction cosine normal **n** of a slip or twin plane (hkl), the direction cosine normal for a slip or twin direction **s** of the slip or slip or twin direction [uvw], and the direction cosine normal for load direction **x** of the load axis (h'k'l'). After the determination of the direction cosine unit vectors **n**, **s**, and **x**, the scalar product values of $\cos(\phi) = \mathbf{n}\cdot\mathbf{x}$ and $\cos(\lambda) = \mathbf{s}\cdot\mathbf{x}$ may be then easily determined by the dot product of the two respective unit vectors and the respective Schmid factors for slip and twinning in Equation (19) may be obtained.

Backofen predicted that different kinds of deformation would be possible by slip only, by mixed slip and twinning and by twinning only. These predictions were made by equating equal applied stresses σ_y to the different Schmid factors of twinning and slip by the relation $\tau = \sigma_y m$ in Equation (19) as in Equation (20) $\sigma_y = \tau_t/m_t = \tau_s/m_s$.

By comparison of Schmid factors of twinning and of slip m_t and m_s in Equation 20, Backofen showed that for [111], [110], and [001] load orientations, the largest or the most favorable stress resolution for twinning, is in compression along [001] and that to prevent twinning in all orientations, twinning must be prevented here. In order to prevent twinning in this most favorable [001] axial orientation, Backofen showed $\frac{\tau_t}{\tau_s} > \frac{m_t}{m_s} > \frac{2}{\sqrt{3}}$ which is the upper limit of the ratio of resolved stresses determined by the respective Schmid factors to prevent twinning in any orientation.

Backofen also showed that the smallest m_t, or least favorable stress resolution for twinning is in compression along [111], and to allow crystals of all orientations in a polycrystalline specimen to deform by twinning, twinning must be allowed here. This required $\frac{\tau_t}{\tau_s} < \frac{1}{\sqrt{3}}$ as the lower limit of resolved stresses before slip is suppressed totally in favor of twinning .

From the above two cases, Backofen concluded that slip and twinning would be mixed for values of $\alpha = \frac{\tau_t}{\tau_s}$ in the range $\frac{1}{\sqrt{3}} < \alpha < \frac{2}{\sqrt{3}}$ and for α smaller than $1/\sqrt{3})$, there would be twinning without slip; for α larger than $\frac{2}{\sqrt{3}}$, there would be slip without twinning. For $\alpha < 1$, twinning becomes dominant.

The most significant effect of mixed slip and twinning results from the polar symmetry of mechanical twinning in comparison to slip as shown in Figure (33) for [111] and [001] crystal orientations. In contrast to slip, for twinning there is a different Schmid factor in compression and tension, and as α is varied from $\frac{2}{\sqrt{3}}$ to $\frac{1}{\sqrt{3}}$ corresponding with diminishing slip and the onset of twinning to pure twinning, the corresponding variations in the Taylor factor are predicted to change. From Chin's Taylor analysis, Backofen showed this change in kind of deformation from slip to twinning, in tension acts to lower the strength anisotropy or lower the M range over all orientations in a polycrystal, but in compression, the anisotropy is increased, leading to increased hardening. These predictions have been observed by Chin, Hosford , and Mendorf for fcc Co-8Fe [28] and by Adler, Olson, and Owen [4] for fcc Hadfield steel reviewed in this present study.

The polarity of twinning systems in compression and tension, and distinct differences of the Schmid factors of twin systems in tension or compression could also imply that deformation twins may possibly contribute to deformation twin texture hardening during processing, where twinned microstructures formed originally in compression could serve as barriers for twinning systems developed later during tensile deformation.

4.0A Adler, P.H., G.B. Olson and W.S. Owen.

Strain Hardening of Hadfield manganese steel [4]

4.1A Introduction

The most recent study of Hadfield steel was completed in 1986 by Adler, Olson, and Owen [4]. This study of the strain hardening mechanisms of solution treated Hadfield steel included a brief review of other previous recent investigations and suggested most recent studies [10,11] have associated high strain hardening with deformation twinning except the recent study of Dastur and Leslie [21]. Dastur and Leslie concluded on the basis of a deformation study at low strains, that dynamic strain aging, and not deformation twinning, was the cause of the high work hardening in Hadfield steel. Adler also concluded that the possibility of strain induced martensitic transformation has been ruled out by recent investigations including White and Honeycombe [6] who showed that bct and hcp martensites are observed to form in only Fe-Mn-C austenites of lower carbon and manganese contents than that of the Hadfield composition.

Adler suggested that because of the close similarities between deformation twins and strain induced martensite, constitutive flow models developed for transformation plasticity in austenitic steels may provide a theoretical basis for the understanding of the influence of twinning on the flow behavior of Hadfield steel.

Transformation plasticity constitutive flow models [26,27] referred to by Adler have provided a quantitative description of two phenomena: a *dynamic softening* effect of the transformation as a parallel or alternative deformation mechanism to slip and a *static hardening* effect of the transformation product. These two effects have been observed to be dependent upon transformation kinetics with the result that softening dominates during high rates of transformation at low to medium strains, while static hardening dominates at later stages of deformation when the transformation nears completion or saturation. The resulting stress strain curves curve shape with the combined effects of dynamic softening and static hardening show upward exponential curvature stain hardening in contrast to the downward curvature normally associated with slip controlled plasticity and power law hardening [26].

Adler's constitutive model study approach examined stress-strain curve shape results during imposed deformations by tension and compression at varied temperatures in order to identify influences of deformation twinning or of slip on plastic flow. Slip dominated flow results were related to power law hardening and downward σ -ε curvature associated with metals that harden at a diminishing rate,

attributed to dynamic recovery of a rapidly growing population of dislocations. Transformation plasticity (twinning) dominated plastic flow results were related to exponential type hardening with upward σ -ε curvature associated with the effects of dynamic softening and static hardening arising from an ever growing population of transformed twins. Stress-strain flow behavior and strain hardening behavior of Hadfield steel were also compared under similar test conditions to two alloys of different composition having well understood deformation mechanisms of slip and of combined slip and twinning in order to detect any unique differences in plastic flow behavior and hardening of Hadfield steel. Strain dependent microstructures were examined for evidence of qualitative and quantitative amounts of twinning at different test temperatures in compression and tension. Texture effects were evaluated by X-ray diffraction and then compared to theoretical Taylor analysis predictions of anisotropic hardening and texture development predicted in tension and compression for combined slip and twinning deformation.

4.2A Materials and Procedure

The experimental method included high temperature solution treatment of Hadfield steel bar stock so that a large grain size of about 220 μ suitable for optical metallography was obtained. Decarburization and manganese loss was prevented during solution treatment by argon atmosphere quartz tube encapsulation with metal chips of cast iron and an Fe-17Mn-0.5C alloy.

Round tensile specimens were ground and compression specimens machined into 4:1 and 2.5 length to diameter ratios. Measured loads and and cross-head speeds displacements were converted to true stress and true strain by the method of Lee and Hart. Accuracy of the curve conversion was verified by comparison with results obtained by a one inch extensometer. Large deformation strains to 0.30 were made when possible.

Metallographic specimens of tensile and compression specimens were carefully polished in the final preparation steps by mechanical-chemical polishing followed by electropolishing in order to avoid the introduction of deformation twin artifacts that can be easily introduced by mechanical polishing.

X-ray diffraction scans of metallographic specimens were performed to examine both texture and phase content.

4.3A Results

Results of true stress, true strain curves were found to be in general agreement with those of Doepkin [3] for tensile deformations and with Raghavan [11] for compressive deformations on material of finer grain size. Adler described the true stress, true strain curves as having a near linear strain hardening behavior with slopes weakly dependent on temperature in comparison to the temperature dependence of yield stress.

A plot of temperature dependence of flow stress, determined by equivalent plastic strains versus deformation temperature, showed that Hadfield steel exhibited a normal negative temperature dependence of flow stress at strains of 0.24, 0.16, 0.08, .04, and 0.002 with increasing slope at low temperatures of less than -40 °C. Results similar to Doepkin's were obtained at 0.002 strain.

From metallographic results, the dependence of deformation twin content with plastic strains of 0.06, 0.18, 0.26, and at temperatures of -100 °C, 20 °C, and 250 °C was observed to increase progressively with plastic strain and weakly decrease dependent on deformation temperature over the strain range examined. A comparison of twin content versus plastic strain at -100 °C and 250 °C at higher magnification showed a slight increase in the rate of twin formation versus strain at the lower temperature. Adler suggested that this weak temperature influence on twinning kinetics correlated with the weak temperature dependence of work hardening observed in the stress-strain curves. No significant difference in twin content or twin appearance was observed between microstructures following deformation in tension or compression at 20 °C.

Results of X-ray diffraction of specimens deformed at 20 °C to 0.30 strain in tension, and at -100 °C to 0.25 strain in compression, showed strong texture effects in comparison to solution treated material. A [100] texture was observed in transverse x-ray scans of solution treated material which decomposed to a [111] fiber texture after deformation in tension and a [110] fiber texture after deformation in compression.

4.4A Discussion

Adler's discussion of the Hadfield steel strain hardening behavior restated that an important role of deformation twinning in Hadfield steel was suggested by the correlation of a low temperature sensitivity of the twinned microstructure with the

overall strain hardening behavior that was nearly linear and only mildly temperature dependent.

Close examination of strain hardening versus strain plots revealed significant similarities with martensitic transformation plasticity. Examination of a plastic strain hardening increment in tension versus strain behavior ($\sigma - \sigma_o$ vs ε_p) was made by the measurement of the difference between plastic flow stress (σ)and the yield stress (σ_o) vs equivalent plastic strain (ε_p). On the plastic strain hardening increment versus plastic strain plot, an inflection point was observed to change negative curvature to positive curvature ($d^2\sigma/d\varepsilon^2$) at lower strains as temperature was lowered.

This inflection point shift to lower strains at lower temperatures was suggested to be analogous to plastic flow influenced by kinetics of transformation plasticity and by combined effects of dynamic softening and static hardening. At lower temperatures and low strains, an increased rate of twinning provides a greater contribution of softening relative to slip hardening, such that the initial slip dominated work hardening and negative curvature power law hardening transitions at relatively low plastic strains to plastic flow determined by transformation plasticity upward curvature.

The observed change in curvature was shown more clearly by local tensile strain hardening ($d\sigma/d\varepsilon$) versus plastic strain ε_p. On this plot of local strain hardening, the observed $d^2\sigma/d\varepsilon^2$ inflection points of curvature corresponded to minima in $d\sigma/d\varepsilon$ and these minima were clearly observed to move to progressively lower strains with decreasing temperature.

Adler concluded the stress versus strain curve shapes and the associated temperature and strain dependent inflections were analogous to σ-ε behavior observed from effects of martensitic transformation plasticity as given by Narutani, Olson and Cohen [26] where a dominant role of martensitic transformation plasticity during deformation of a transforming metastable austenitic steel was found to be related to transformation kinetics through imposed strain and temperature.

The work hardening inflections of Hadfield steel were consistent with this known constitutive flow behavior of transformation plasticity, including the combined dynamic softening and static hardening phenomena modeled by Narutani [26], or Olson [27], where dynamic softening dominated above low strains where strain induced transformation becomes a dominant deformation mechanism and static hardening dominated at high strains as the transformation neared completion or saturation and slip dominated deformation was reasserted.

Adler concluded that the combined softening and hardening defined a σ-ε region of upward strain hardening curvature $d^2\sigma/d\varepsilon^2$ defined by two inflection points in the flow curves of Hadfield steel. The first inflection to positive curvature at low or early strains would correlate with initiation of deformation behavior dominated or influenced by twinning and transformation plasticity over the initial yielding and plastic flow by influenced by slip. The second inflection re-establishing negative curvature would correlate to a decreased rate of twinning and transformation plasticity at high strains, and would correlate to an increased influence of slip deformation and a large contribution of hardening provided by a high volume fraction of transformed twins.

Between the inflection points, the stress-strain curves showed upward curvature unique to transformation plasticity from combined deformation by twinning and slip with related effects of dynamic softening and static hardening.

Adler briefly reviewed the experimental derivation and significance of the martensitic transformation plasticity constitutive flow equation of the Narutani study. After this review, Adler concluded the Hadfield steel strain hardening increment curves of σ -σ_o versus ε, that showed temperature and strain dependent inflections, were consistent with transformation plasticity dynamic softening and static hardening dependence on transformation kinetics. This similarity to martensitic transformation plasticity and deformation twinning transformation plasticity was related to softening and hardening effects that result from increased rates or from decreased rates of twinning. Increased twinning rates would reduce strain hardening at low strains due to a high contribution of dynamic softening associated with twinning as a parallel deformation mechanism. At high strains and low twinning rates, strain hardening rates would increase as the transformation neared completion and slip re-established influence of plastic flow by a static hardening contribution due to austenite flow stress and due to the high volume fraction of product twins.

The strain hardening increment versus plastic strain ($\sigma - \sigma_o$ vs ε_p) curves at different temperatures, were replotted as strain hardening increment $\sigma - \sigma_o$ versus deformation temperature by plots determined by increments of strain. This latter plot of strain hardening was determined by strain increments of 0.002 to 0.04, 0.08, 0.16, and to 0.24 . Plastic flow strain hardening curvature that occurred at each strain increment and deformation temperature was also included. Positive and negative strain hardening curvature $d^2\sigma/d\varepsilon^2$ observed were related to temperature-strain regions of plastic flow dominated by deformation mechanisms of twinning or slip, so that this plot served as a deformation map or constitutive relation plot.

This deformation mechanism map or constitutive relation plot also related the extent of strain hardening dependence upon type of dominant deformation mechanism as a function of temperature and strain. Several distinct regions of behaviors of strain hardening curvature were observed.

At high temperatures and low strains, Adler suggested the constitutive flow behavior was characteristic of slip dominant plastic σ -ε curves with downward curvature $d^2\sigma/d\varepsilon^2$ related to power law hardening. At lower temperatures, twinning was interpreted as influencing flow behavior at progressively lower strains with a reduction in the initial strain hardening at low strains, and increased hardening at high strains in agreement with the upward rising σ -ε curves observed by Adler and by Doepkin. At high strains and low temperatures, a second inflection region of downward curvature was observed that Adler suggested may be due to the approach of twinning saturation or the near completion of twinning transformation in the later stage of deformation. At small strains and at the lowest temperatures less than -196 °C, a small region of downward curvature was observed that Adler suggested may be due to a reversal of slip and twinning kinetics similar to that observed in stress assisted isothermal martensitic transformations [27].

The strain hardening increment results were reported to be similar for 0.04 - 0.002 strain increments reported Dastur and Leslie, but whereas Dastur and Leslie included 0.04 - 0.002 strain increments, Adler included a wider range of temperatures and strain increments. Adler concluded that work hardening increments and inflections were similar to those reported by Dastur and Leslie with the 0.04 – 0.002 strain increment, but Adler's constitutive behavior and work hardening behavior was examined over a wider range of strains and temperatures, so that some significant differences from Dastur and Leslie's results were observed.

Dastur and Leslie observed a maximum strain hardening increment from a 0.04 - 0.002 strain increment from -25 °C to 300 °C and observed a dynamic strain aging mechanism at temperatures from -25 °C to 290 °C that was associated with a special interaction between carbon and manganese atoms. Dastur and Leslie therefore concluded on the basis the low strain hardening increments of 0.04 - 0.002 that strain hardening in Hadfield steel diminished above temperatures of 300 °C and below temperatures of -25 °C from the cessation of dynamic strain aging.

Adler's more extensive constitutive behavior plot of work hardening increments versus deformation temperature for strain increments between 0.002 to 0.04, 0.08, 0.16, and 0.24 indicated that the hardening behavior observed over a wide range of strains of interest, particularly at low temperatures, was consistent with effects of

transformation plasticity contributions of dynamic softening and static hardening. The low work hardening increment observed at low temperatures and at low strain increments was reported by Adler to be consistent with an earlier onset of plastic flow dominated by deformation twinning and by softening from twinning as a parallel deformation mechanism.

Adler's constitutive behavior plot also showed that for low deformation temperatures, anomalous strain softening and hardening occurred at temperatures less than -40 °C (233 K), where no dynamic strain aging mechanism could operate, such that reduced hardening occurred at low strains of 0 04, and increased hardening occurred at higher strains of 0.16 and 0.24 . This anomalous hardening was consistent with transformation plasticity effects of softening and hardening where increased rates of twinning provides an increased softening contribution to flow stress at low strains, and increased hardening contributions are provided at higher strains as the rate of twinning decreases and slip is re-established.

The observed [111] textures developed in tension and the [110] texture developed in compression were identified by Adler as similar to textures developed in 70-30 brass which also deforms by combined slip and twinning. The similar behavior of brass and Hadfield deformation textures was suggested to infer an important role of twinning during deformation of these two materials.

To compare hardening behaviors during deformation in compression and tension, Adler plotted a differential strength increment from the difference in strain hardening observed during compression and tension versus plastic stain ($\sigma_c - \sigma_t$ vs ε_p). In this σ_c-σ_t vs ε_p plot, the strength increment versus ε was observed to have been of a few percent of the flow stress at small strains where the $\sigma - \varepsilon$ curves had downward curvature and where slip was related to the dominant deformation mechanism. At high strains, the observed $\sigma_c - \sigma_t$ strength differential increased substantially where the curves had upward curvature and where twinning was related to the dominate deformation mechanism. Adler concluded that since the observed extent of twinning in tension and compression was not significantly different, the difference in flow behavior may have been due to the effect of twins in a role of texture development.

In order to explain how texture effects may relate to the observed differential strain hardening during tensile and compressive deformation, Adler referred to a modified Taylor analysis for axisymmetric deformation by combined fcc slip and twinning, from Chin, Mammel, and Dolan [29]. As discussed before, the combined {111}<112> twinning and {111}<110> slip Taylor analysis for axisymmetric flow by Chin et. al.assumed the existence of critical resolved stresses for both respective

slip(τ_S) and twinning(τ_t) shears, that the respective resolved shear stresses are equal for all respective slip and twin systems, and that slip and twinning compete on basis of Schmid factors to provide deformation. In the Chin-Taylor analysis, in order to maintain polycrystalline shape compatibility while undergoing minimal shear strains for minimal work, five slip or twinning systems are required per crystal, among a total of twenty four systems, from twelve slip systems and twelve twinning systems. It is of interest to also note that Chin's assumption of competing deformation mechanisms for the slip-twin Taylor analysis is consistent with a role of dynamic softening in transformation plasticity.

The ratio $\alpha = \left(\frac{\tau_t}{\tau_S}\right)$ used in Formula (18) determines the extent of twinning or slip for a given crystal orientation such that for values of a less than one, twinning is favored as opposed to slip. Chin's Taylor analysis predicted that as α decreased below one correlating to plastic flow dominated by twinning, that increased anisotropy or increased differences in orientation dependent Taylor factors would occur during compression, but that a decrease of anisotropic hardening would occur in tension.

Adler examined the observed strain hardening differences observed between compression and tension in comparison to anisotropic hardening effects predicted by Chin's Taylor analysis under conditions where twinning began to influence plastic flow for both tension and compression as in Equation (18). Adler showed by Chin's Taylor analysis, that in conditions that favored deformation by twinning ($\alpha \leq 1.00$), Chin's predicted Taylor factors as in the observed [110] texture developed in compression were greater than those predicted Taylor factors as in the observed [111] texture developed in tension. Adler also noted that $\frac{M[110]}{M[001]}$ and $\frac{M[111]}{M[001]}$ ratios of Chin's Taylor factors as in to the [110] experimental textures developed in compression, and as in the [111] experimental textures developed in tension, correlated to the observed hardening behavior of weak texture hardening in tension but strong texture hardening in compression.

In order to provide further evidence of the importance of twinning, alloy composition effects were investigated by Adler in order to establish a correlation between strain hardening and predicted stacking fault energy as previously suggested by White-Honeycombe [6]. Since stacking faults are precursors to twins, and also may be considered to be the thinnest possible twins, Adler used a model developed for hcp martensitic nucleation that included chemical free energy between parent and product phases, a strain energy, and a surface energy. This nucleation theory approach

considered the nucleation of a second phase embryo with volume and surface free energy. The chemical free energy was obtained by the use of a regular solution model with interaction parameters for FeMn and FeC, but the MnC interaction parameter was neglected due to the small mole fractions of Mn and C.

A plot of the calculated values of free energy and stacking fault energy versus manganese content at a constant 1.15% carbon content was made along with strain hardening by a 20% reduction by cold rolling. Adler noted that a minimum intrinsic stacking fault energy (γ) was predicted at a manganese content in the vicinity of the Hadfield composition, and that the 20% reduction data of White and Honeycombe's [6] also showed a maximum strain hardening increment at this same manganese content for a fixed 1.15% carbon composition. Adler concluded that the plots suggested that the optimal 12% to 14% Mn Hadfield content may correlate to a minimum fault energy, a maximum rate of deformation twinning and a maximum in work hardening.

A strain hardening study was made by Adler using combined slip - deformation twinning Hadfield steel, a high carbon Fe-Ni-C alloy that undergoes deformation by slip alone, and a low carbon Co -Ni alloy that undergoes combined slip and fcc deformation twinning in order to determine any differences in plastic flow behavior.

The comparative strain hardening study was begun by Adler by first identifying the twinning kinetics of Hadfield steel versus strain under similar conditions to that of another fcc material that deforms by combined slip and twinning; Co-33Ni-0.02C, studied by Remy [15]. Three volume fractions of Hadfield twins at strains at 0.06, 0.18 and 0.30 were determined by point counting using 4000 points for tensile deformation at 20 °C. The twinned volume fractions of Hadfield steel were plotted versus strain along with similar data obtained by Remy for Co-33Ni-0.02C, which was also deformed in tension at 20 °C. The f-ε twinning kinetics of the Hadfield steel and Co-33Ni-0.02C were observed to be nearly identical.

To examine Hadfield strain hardening behavior in comparison to a high carbon austenitic alloy that deforms by slip, which should therefore exhibit constitutive flow behavior of downward curvature, as in power law hardening, an Fe-20.6Ni-1.04C alloy was identically heat treated and then tested in tension under the same conditions as was the Hadfield steel.

Adler plotted the $\sigma - \sigma_o$ plastic strain hardening increments versus plastic strains in tension ε_p at 20 °C for the Hadfield steel, Co-33Ni-0.02C and Fe-20.6Ni-1.04C alloys. No modulus correction was required since the alloys had very similar elastic constants. Three distinctive regions of strain hardening behavior were observed among the alloys at plastic strains of: $\varepsilon_p \leq 0.05$, $0.06 < \varepsilon_p < 0.22$, and $0.22 < \varepsilon_p < 0.30$.

At low strains of ε_p <0.05, the observed strain hardening of all alloys was identical with negative curvature characteristic of slip strain hardening. From the comparison of the high carbon Fe-Mn-C alloy with the high carbon Fe-Ni-C alloy, Adler concluded that there was no special role of a Hadfield steel Mn-C interaction in determining plastic flow during slip strain hardening as proposed by Dastur and Leslie [21]. Adler also concluded that the identical strain hardening of the low carbon Co-33Ni-0.02 C with the other alloys implied that there was no special role of carbon in strain hardening at low strains and at 20 °C during deformation by slip.

At higher strains of 0.06< ε_p < 0.22 the strain hardening curves of the two materials that deform by combined slip and twinning fell below the slip controlled Fe-Ni-C alloy and Adler concluded this behavior was consistent with the dynamic softening effect of deformation twinning. The Hadfield steel had upward curvature within this region of strain hardening but the curvature of the other alloys were negative, with downward curvature. Adler also noted the Hadfield $\sigma - \sigma_y$ curve was above the Co-Ni curve in this region and that the Hadfield steel plastic work hardening curve eventually crossed the Fe-Ni-C curve at ε_p = 0.22. At ε_p = 0.30, the Hadfield curve continued upward curvature to e_p = 0.50 while the curvature of the other alloys continued downward.

Adler suggested that because the twinning kinetics of the Hadfield steel and Co-33Ni-0.02 C would imply a very similar softening contribution due to twinning, the observed difference in strain hardening of the twinning alloys was more likely due to a difference in a static hardening contribution of the Hadfield twins. Adler suggested that any additional strengthening effect of texture development could be excluded from contributing to the strain hardening of Hadfield steel from the previous observations of results from the Chin-Taylor analysis which implied textures developed during slip-twinning tensile deformation would either lower, or have little effect on strain hardening.

In order to discuss and to further examine the observed difference in strain hardening behavior between Hadfield steel and the Co-33Ni-0.02 C alloy which had identical twinning kinetics, Adler first compared Hadfield's steel and the Co-33Ni-0.02C alloy's potential for static hardening by a contribution from Hall-Petch substructural hardening determined by the volume fraction of twins as determined by Remy [15] in Equation (20) :

Equation (20) $$\Delta\sigma_S = K_T(2t)^{-1}\left(\frac{f}{1 - f}\right)$$

where

$\Delta\sigma_S$ = the static hardening increment due to twin boundaries as slip obstacles

K_T = an experimentally determined constant

t = average twin thickness

f = volume fraction of twins.

For comparison of the Hadfield and the Co-33Ni-0.02C strain hardening increment predicted by Equation (20), twin dimensions of the respective alloys and twinned volume fractions were determined by Fullman's method as shown in Equation (15). Adler found the average twin dimensions roughly scaled with the grain size such that for the Hadfield steel with an average grain size of 220 μ, the average twin thickness was 5.4 μ, while the Co-33Ni-0.02C alloy with an average grain size of 80 μ had an average twin thickness of 1.9 μ.. Adler concluded that the thicker twins of the Hadfield steel should predict a lower strain hardening increment in the Hadfield steel than that observed in the C0-33Ni-0.02C alloy contrary to the observed results; furthermore, since the twinning kinetics were equal, the unusually high strain hardening of the Hadfield steel indicated that an anomalous hardening effect was associated with deformation twins in Hadfield steel.

In order to account for the anomalous high strain hardening in the Hadfield steel beyond that expected from substructure refinement alone, Adler proposed there was reason to believe that a fcc twinning shear in Hadfield steel should not produce a true twin crystal, but rather what has been called a *pseudotwin* [30] which could possess properties similar to bct Fe-C martensites.

Adler's explanation of pseudotwinning during the fcc twin shear was dependent upon conditions of the diffusionless shear of atoms of close packed planes from positions above normally unoccupied fcc tetrahedral sites to positions above normally occupied fcc octahedral interstitial sites. Carbon atoms trapped in the newly created tetrahedral sites, could distort the lattice. Adler noted that although the distortion would be expected to be isotropic for a random solution of carbon in fcc Fe, any non-randomness of the solution would cause asymmetry of distortion as discussed by Cahn [30]. Mössbauer spectroscopy [41] of high carbon Fe-C austenites has indicated a structure

of a non-random carbon solid solution indicative of C-C repulsion interaction in Hadfield steel.

Adler proposed that the carbon induced distortions from the fcc twinning shear in a non-random high carbon solution would produce a body-centered orthorhombic lattice, and that these distortions would likely produce a strengthening effect analogous to that of the tetragonal distortion of bct Fe-C martensites (dipole distortion-dislocation interaction [7]). Adler also suggested additional analogous strengthening behavior contributions of the proposed pseudotwins in Hadfield steel to bct martensites by suggesting that there was evidence from Mössbauer spectroscopy, that prior plastic deformation may enhance carbon clustering behavior for aging contributions in Hadfield steel. Lastly, a non-random solution of manganese was suggested by Adler to also possibly contribute to lattice distortion, especially if a strong Mn-C attraction as proposed by Dastur and Leslie would help to retain carbon in distorted tetrahedral sites. Adler suggested that microdiffraction experiments would have to be conducted in order to test the pseudotwin hypothesis.

Adler stated that the observed strain hardening behavior of Hadfield steel and the effect of proposed pseudotwinning would suggest an amended constitutive model of transformation plasticity including effects of static hardening and dynamic softening from the Narutani study [26]. The Hadfield steel transformation plasticity constitutive model of Equation 21 and Equation 22 was therefore obtained by including static hardening effects of fcc combined slip and deformation twinning, with the proposed intrinsic strength increase of the proposed pseudotwin phase, with the structural hardening effects of deformation twins from Remy model (Equation 20), and by the austenite flow stress corrected for the amount of macroplastic strain arising from twinning. Dynamic softening effects of the amended Hadfield steel transformation plasticity model included deformation twinning as an alternative, parallel deformation mechanism to deformation slip, for enhancement of ductility by the avoidance of slip inhibition and by a negative contribution to flow stress.

$$(21) \quad \sigma = \sigma_S \left(1 - \beta \frac{d f}{d\varepsilon} \right)$$

with

$$(22) \quad \sigma_S = \sigma_\gamma(\varepsilon - \alpha f) + K_t (2t)^{-1} \left(\frac{f}{1 - f} \right) + \Delta\sigma_0 f$$

f = volume fraction twins

α = Remy coefficient of 0.231 for fcc twinning

β = dynamic softening coefficient similar to gamma to alpha prime transformation.

$\sigma_\gamma(\varepsilon - \alpha f)$ = austenite flow stress correction as a function of macroscopic strain and f twins

$K_t (2t)^{-1} \left(\frac{f}{1 - f} \right)$ = Remy model for twin boundary strengthening

$\Delta\sigma_0$ = Intrinsic strength difference between austenite and pseudotwin phase independent of strain and dependent upon carbon content.

Adler noted that if the difference in twin thickness between the Hadfield steel and the Co-33Ni alloy was neglected, the $\Delta\sigma_0$ term became the only significant contribution to the difference in $\sigma - \sigma_0$ of Co -Ni and Hadfield steel, which together with the measured twin volume fraction, defined a $\Delta\sigma_0$ value of 620 MPa. Adler noted that this pseudotwin strength increment was high in comparison to the strength of the austenitic phase, but the pseudotwin strengthening was relatively small in comparison to bct martensites of high carbon content.

4.5A Conclusions

In summary, Adler concluded that plastic flow behavior of Hadfield steel in uniaxial tension and compression showed $\sigma - \varepsilon$ curve shapes that indicated effects of transformation plasticity softening and hardening with curve shapes that correlated with temperature, strain and the observed extent and rate of twinning. The $\sigma - \varepsilon$ curve shapes were consistent with the softening effect of twinning as a parallel deformation mechanism to slip and were consistent with a hardening effect of the twinned microstructure. The combined effect of the softening and hardening give upward exponential curvature to the $\sigma - \varepsilon$ curves in contrast to downward power law curvature

indicative of slip controlled plasticity. Higher strain hardening observed in compression compared to that in tension was consistent with observed texture development, consistent with a previous Taylor analysis for combined slip and fcc twinning by Chin, Mammel, and Dolan. A computed dependence of stacking fault energy with Mn content at a constant carbon content correlated with a previously observed dependence of strain hardening versus percent manganese determined by White and Honeycombe, and this correlation suggested the Hadfield composition corresponded to an optimum composition for a maximum rate of deformation twinning at a constant carbon content. Comparison of Hadfield steel with a Co-33Ni-0.02 C alloy with identical twinning kinetics and with a Fe-20.6Ni-1.04C alloy that deforms by slip demonstrated no differences in strain hardening at low strains where deformation was controlled by slip, but that at large strains, unusual strain hardening was observed and associated with Hadfield steel twin formation. The consideration of a fcc twinning process in a non-random solid solution suggested the occurrence of pseudotwinning for which the product is a distorted phase with orthorhombic symmetry. The high hardness of the pseudotwin phase would account for the unusual anomalous high hardening of the Hadfield steel.

DISTRIBUTION LIST

No. of Copies	To
	Commander, U.S. Army Laboratory Command, 2800 Powder Mill Road, Adelphi, MD 20783-1145
1	ATTN: AMSLC-IM-TL
1	AMSLC-CT
	Commander, Defense Technical Information Center, Cameron Station, Building 5, 5010 Duke Street, Alexandria, VA 22304-6145
2	ATTN: DTIC-FDAC
	Commander, U.S. Army Materiel Command, 5001 Eisenhower Avenue, Alexandria, VA 22333
1	ATTN: AMCLD
	Commander, U.S. Army Missile Command, Redstone Scientific Information Center, Redstone Arsenal, AL 35898-5241
1	ATTN: AMSMI-RD-CS-R/Doc
1	AMSMI-RLM
	Commander, U.S. Army Tank-Automotive Command, Warren, MI 48397-5000
1	ATTN: AMSTA-ZSK
2	AMSTA-TSL, Technical Library
	Director, U.S. Army Ballistic Research Laboratory, Aberdeen Proving Ground, MD 21005
1	ATTN: SLCBR-TSB-S (STINFO)
	Director, Benet Weapons Laboratory, LCWSL, USA AMCCOM, Watervliet, NY 12189
1	ATTN: AMSMC-LCB-TL
1	AMSMC-LCB-R
1	AMSMC-LCB-RM
1	AMSMC-LCB-RP
	Naval Research Laboratory, Washington, DC 20375
1	ATTN: Code 5830
2	Dr. G. R. Yoder - Code 6384
	Commander, U.S. Air Force Wright Research & Development Center, Wright-Patterson Air Force Base, OH 45433-6523
1	ATTN: WRDC/MLC
1	WRDC/MLLP, M. Forney, Jr.
1	WRDC/MLBC, Mr. Stanley Schulman
	Wyman-Gordon Company, Worcester, MA 01601
1	ATTN: Technical Library
	General Dynamics, Convair Aerospace Division, P.O. Box 748, Fort Worth, TX 76101
1	ATTN: Mfg. Engineering Technical Library

No. of Copies	To
	Worcester Polytechnic Institute, Mechanical Engineering Department, 100 Institute Road, Worcester, MA 01609
1	ATTN: Dr. F. Tuler
	Northwestern University, Department of Materials Science and Engineering, Evanston, IL 60208
1	ATTN: Dr. G. Olson
	Lockheed Missiles and Space Company, Inc., 1111 Lockheed Way, Sunnyvale, CA 94086
1	ATTN: G. Hopple, O/48-92 B/195B
1	B. Boggs, O/48/92 B/195B
1	K. Massarat, O/81-22 B/157
	Los Alamos National Laboratory, MS G730, Los Alamos, NM 87545
1	ATTN: M. Stevens
	University of California, San Diego, Department of Applied Mechanics and Engineering Sciences, La Jolla, CA 92093
1	ATTN: Professor S. Nemat-Nasser
1	Professor M. Meyers
1	Professor R. Asaro
	Director, U.S. Army Materials Technology Laboratory, Watertown, MA 02172-0001
2	ATTN: SLCMT-TML
1	Author

U.S. Army Materials Technology Laboratory,
Watertown, Massachusetts 02172-0001
PROCESSING AND CHARACTERIZATION OF
HIGH STRENGTH, HIGH DUCTILITY
HADFIELD STEEL -
John F. Chinella

Technical Report MTL TR 90-21, April 1990, 132 pp - illus-Tables

AD

UNCLASSIFIED
UNLIMITED DISTRIBUTION

Key Words

Austenitic steels
Microstructure
Thermomechanical processing

Hadfield steel plastic flow behavior is known by strain hardening without necking to high levels of strength and strain, and is described by upward curvature strain hardening with near-constant, near-linear strain hardening rates over large ranges of deformation temperature. This plastic flow behavior is valued for severe service applications, but Hadfield steel yield stress is low. The purpose of this experimental study is to warm roll solution treated, Fe-12.5Mn-2.01Mo-1.15C Hadfield steel to high yield strength and to retain the valued characteristics of Hadfield steel plastic flow behavior. The objective of the study is to determine the effects of warm rolling on plastic flow behavior and microstructure of Hadfield steel. Experimental plastic flow behavior is evaluated in tension from both engineering and true stress-strain behavior. The purpose of the study is met by material thermomechanically processed to provide high yield stress, moderate rates of increasing load or strain hardening, high true uniform strain and ultrahigh true uniform stress. The experimental stress-strain curves and microstructures suggest an influence of Hadfield steel deformation twins on plastic flow.

U.S. Army Materials Technology Laboratory,
Watertown, Massachusetts 02172-0001
PROCESSING AND CHARACTERIZATION OF
HIGH STRENGTH, HIGH DUCTILITY
HADFIELD STEEL -
John F. Chinella

Technical Report MTL TR 90-21, April 1990, 132 pp - illus-Tables

AD

UNCLASSIFIED
UNLIMITED DISTRIBUTION

Key Words

Austenitic steels
Microstructure
Thermomechanical processing

Hadfield steel plastic flow behavior is known by strain hardening without necking to high levels of strength and strain, and is described by upward curvature strain hardening with near-constant, near-linear strain hardening rates over large ranges of deformation temperature. This plastic flow behavior is valued for severe service applications, but Hadfield steel yield stress is low. The purpose of this experimental study is to warm roll solution treated, Fe-12.5Mn-2.01Mo-1.15C Hadfield steel to high yield strength and to retain the valued characteristics of Hadfield steel plastic flow behavior. The objective of the study is to determine the effects of warm rolling on plastic flow behavior and microstructure of Hadfield steel. Experimental plastic flow behavior is evaluated in tension from both engineering and true stress-strain behavior. The purpose of the study is met by material thermomechanically processed to provide high yield stress, moderate rates of increasing load or strain hardening, high true uniform strain and ultrahigh true uniform stress. The experimental stress-strain curves and microstructures suggest an influence of Hadfield steel deformation twins on plastic flow.

U.S. Army Materials Technology Laboratory,
Watertown, Massachusetts 02172-0001
PROCESSING AND CHARACTERIZATION OF
HIGH STRENGTH, HIGH DUCTILITY
HADFIELD STEEL -
John F. Chinella

Technical Report MTL TR 90-21, April 1990, 132 pp - illus-Tables

AD

UNCLASSIFIED
UNLIMITED DISTRIBUTION

Key Words

Austenitic steels
Microstructure
Thermomechanical processing

Hadfield steel plastic flow behavior is known by strain hardening without necking to high levels of strength and strain, and is described by upward curvature strain hardening with near-constant, near-linear strain hardening rates over large ranges of deformation temperature. This plastic flow behavior is valued for severe service applications, but Hadfield steel yield stress is low. The purpose of this experimental study is to warm roll solution treated, Fe-12.5Mn-2.01Mo-1.15C Hadfield steel to high yield strength and to retain the valued characteristics of Hadfield steel plastic flow behavior. The objective of the study is to determine the effects of warm rolling on plastic flow behavior and microstructure of Hadfield steel. Experimental plastic flow behavior is evaluated in tension from both engineering and true stress-strain behavior. The purpose of the study is met by material thermomechanically processed to provide high yield stress, moderate rates of increasing load or strain hardening, high t uniform strain and ultrahigh true uniform stress. The experimental stress-strain curves and microstructures suggest an influence of Hadfield steel deformation twins on plastic flow.

U.S. Army Materials Technology Laboratory,
Watertown, Massachusetts 02172-0001
PROCESSING AND CHARACTERIZATION OF
HIGH STRENGTH, HIGH DUCTILITY
HADFIELD STEEL -
John F. Chinella

Technical Report MTL TR 90-21, April 1990, 132 pp - illus-Tables

AD

UNCLASSIFIED
UNLIMITED DISTRIBUTION

Key Words

Austenitic steels
Microstructure
Thermomechanical processing

Hadfield steel plastic flow behavior is known by strain hardening without necking to high levels of strength and strain, and is described by upward curvature strain hardening with near-constant, near-linear strain hardening rates over large ranges of deformation temperature. This plastic flow behavior is valued for severe service applications, but Hadfield steel yield stress is low. The purpose of this experimental study is to warm roll solution treated, Fe-12.5Mn-2.01Mo-1.15C Hadfield steel to high yield strength and to retain the valued characteristics of Hadfield steel plastic flow behavior. The objective of the study is to determine the effects of warm rolling on plastic flow behavior and microstructure of Hadfield steel. Experimental plastic flow behavior is evaluated in tension from both engineering and true stress-strain behavior. The purpose of the study is met by material thermomechanically processed to provide high yield stress, moderate rates of increasing load or strain hardening, high true uniform strain and ultrahigh true uniform stress. The experimental stress-strain curves and microstructures suggest an influence of Hadfield steel deformation twins on plastic flow.